


ARTICLE

PPM1F controls integrin activity via a conserved phospho-switch

Tanja M. Grimm^{1,2*}, Nina I. Dierdorf^{1,2*}, Karin Betz^{2,3}, Christoph Paone^{1,2}, and Christof R. Hauck^{1,2} 

Control of integrin activity is vital during development and tissue homeostasis, while derailment of integrin function contributes to pathophysiological processes. Phosphorylation of a conserved threonine motif (T788/T789) in the integrin β cytoplasmic domain increases integrin activity. Here, we report that T788/T789 functions as a phospho-switch, which determines the association with either talin and kindlin-2, the major integrin activators, or filaminA, an integrin activity suppressor. A genetic screen identifies the phosphatase PPM1F as the critical enzyme, which selectively and directly dephosphorylates the T788/T789 motif. PPM1F-deficient cell lines show constitutive integrin phosphorylation, exaggerated talin binding, increased integrin activity, and enhanced cell adhesion. These gain-of-function phenotypes are reverted by reexpression of active PPM1F, but not a phosphatase-dead mutant. Disruption of the *ppm1f* gene in mice results in early embryonic death at day E10.5. Together, PPM1F controls the T788/T789 phospho-switch in the integrin β 1 cytoplasmic tail and constitutes a novel target to modulate integrin activity.

Introduction

Integrins are essential heterodimeric cell surface receptors that mediate extracellular matrix adhesion and instruct animal cells about the chemical and mechanical properties of their micro-environment (Gahmberg et al., 2009; Hynes, 2002; Morse et al., 2014). Accordingly, integrins are instrumental for cell adhesion during development, tissue regeneration, or leukocyte extravasation, but also contribute to pathological processes such as cancer cell invasion and metastasis (Bökel and Brown, 2002; Hamidi and Ivaska, 2018; Nieswandt et al., 2009; Sekine et al., 2012; Vestweber, 2002; Winograd-Katz et al., 2014).

A major regulatory principle of integrins involves an extensive conformational change, which has been termed integrin activation (Calderwood, 2004; Sims et al., 1991; Vinogradova et al., 2002). The active conformation of integrins can be stabilized either by the presence of an extracellular ligand (outside-in activation) or by a characteristic intracellular binding event of the scaffold protein talin to the cytoplasmic tail of the integrin β subunit (inside-out activation; Hughes et al., 1996; Shattil et al., 2010; Vinogradova et al., 2002; Wegener et al., 2007). During inside-out activation, the globular head of talin binds to a conserved NPxY amino acid sequence, thereby spatially separating the α and β subunits and forcing the extracellular domains into the extended, active conformation (Anthis et al., 2009; Calderwood et al., 2002; Wegener et al., 2007). This active

conformation is a prerequisite for proper integrin-mediated cell attachment to the extracellular matrix (Harburger and Calderwood, 2009; Moser et al., 2009). Cell adhesion can be further promoted by integrin clustering (Bunch, 2010; Cluzel et al., 2005; van Kooyk and Figdor, 2000), which is supported by kindlin (Li et al., 2017; Ye et al., 2013), an additional binding partner of the integrin β subunit (Bledzka et al., 2012; Harburger et al., 2009; Li et al., 2017). Together, talin and kindlin initiate the formation of large, heteromeric protein complexes at integrin cytoplasmic tails, which are termed focal adhesion sites. These structures can comprise several hundred distinct proteins, the so-called integrin adhesome (Horton et al., 2015; Zaidel-Bar and Geiger, 2010; Zaidel-Bar et al., 2007).

Besides talin and kindlin as positive regulators of integrin function, several negative regulators of integrin activity such as filaminA, Dok1, Sharpin, or ICAP-1 have been described (Bouvard et al., 2003; Kiema et al., 2006; Liu et al., 2015; Oxley et al., 2008; Rantala et al., 2011). These nonenzymatic proteins are thought to act by competitive binding to the integrin β subunit, where they displace positive regulators of integrin activity. For example, filaminA and talin have overlapping binding sites in the leukocyte-specific integrin subunits β 2 and β 7, which they occupy in a mutually exclusive manner (Kiema et al., 2006; Takala et al., 2008). Interestingly, an evolutionary conserved

¹Lehrstuhl Zellbiologie, Fachbereich Biologie, Universität Konstanz, Konstanz, Germany; ²Konstanz Research School Chemical Biology, Universität Konstanz, Konstanz, Germany; ³Lehrstuhl Zelluläre Chemie, Fachbereich Chemie, Universität Konstanz, Konstanz, Germany.

*T.M. Grimm and N.I. Dierdorf contributed equally to this paper; Correspondence to Christof R. Hauck: christof.hauck@uni-konstanz.de.

© 2020 Grimm et al. This article is distributed under the terms of an Attribution-Noncommercial-Share Alike-No Mirror Sites license for the first six months after the publication date (see <http://www.rupress.org/terms/>). After six months it is available under a Creative Commons License (Attribution-Noncommercial-Share Alike 4.0 International license, as described at <https://creativecommons.org/licenses/by-nc-sa/4.0/>).

threonine motif within the context of the filaminA and talin core binding sites is located in the cytoplasmic tails of most integrin β subunits (T788/T789 in the human integrin β 1; Fig. 1 A and Fig. S1 A; García-Alvarez et al., 2003; Gingras et al., 2009; Kiema et al., 2006; Liu et al., 2015; Wegener et al., 2007). Upon cell stimulation, these threonine residues are phosphorylated (Buyon et al., 1990; Chatila et al., 1989; Craig et al., 2009; Hibbs et al., 1991; Hilden et al., 2003), and mutations mimicking Ser/Thr phosphorylation lead to enhanced integrin activity and integrin-based cell adhesion in vitro (Craig et al., 2009; Nilsson et al., 2006). In contrast, alanine substitution of this particular threonine motif severely compromises integrin function, leading to impaired integrin activation and abrogation of cell-matrix adhesion (Fagerholm et al., 2005; Hibbs et al., 1991; Nilsson et al., 2006; Wennerberg et al., 1998). These prior findings indicate that the conserved T788/T789 residues could form a phospho-switch to regulate integrin affinity and, thereby, control integrin-mediated cellular processes. However, the enzymatic machinery operating this phospho-switch within the cell is currently unknown.

Here we report that phosphorylation of the conserved threonine motif in the cytoplasmic tail of the integrin β 1 subunit dissociates filaminA to allow access of talin to its canonical NPxY binding site. Using a focused genetic screen, we identify a member of the metal-dependent protein phosphatase (PPM) family, the serine/threonine phosphatase PPM1F, as the critical enzyme responsible for dephosphorylating the threonine motif. Our results uncover the mechanistic details of integrin activity regulation by this conserved phospho-switch and identify the underlying enzymatic machinery, thereby providing a novel access point to modulate integrin activity.

Results

The integrin β 1 T788/T789 motif constitutes a conserved phospho-switch to regulate integrin activity

The T788/T789 motif of the β 1 integrin cytoplasmic tail, which is located within the context of talin, kindlin, and filaminA binding sites, is highly conserved across species and within different human β subunits (Fig. 1 A and Fig. S1 A). Previous studies using the leukocyte-specific integrins β 2 and β 7 already suggested that these threonine residues could operate as a phospho-switch to control binding of talin versus filaminA (Kiema et al., 2006; Takala et al., 2008). To evaluate the consequences of integrin β 1 T788/T789 phosphorylation for filaminA or talin binding in vitro, we produced recombinant cytoplasmic domains mimicking T788 or T788/T789 phosphorylation (T/D or TT/DD) or harboring nonphosphorylatable alanine residues (TT/AA; Fig. S1, B and C). We also generated a Y783A mutant in the NPxY motif, which impairs talin and filaminA association, and mutated a tyrosine residue outside of the talin or filamin core binding sites to alanine (Y795A; Calderwood et al., 1999; Pfaff et al., 1998). Pull-down experiments with the various integrin cytoplasmic domains showed that His-Small Ubiquitin-Related Modifier (SUMO)-tagged yeast enolase as irrelevant control protein did not associate with any of the integrin β 1 cytoplasmic domains (Fig. 1 B). The recombinant His-SUMO-tagged integrin

binding domains of filaminA (Ig domain 19–21 of filaminA) and talin (F3 lobe of the talin head domain) bound the integrin β 1 WT and TT/AA variants, but not the Y783A variant (Fig. 1 B), in line with previous reports (Calderwood et al., 1999; O'Toole et al., 1995; Pfaff et al., 1998; Tadokoro et al., 2003). Importantly, talin also showed unaltered association with the pseudo-phosphorylated integrin β 1 variants T/D and TT/DD, while filaminA binding was reduced (T/D) or completely absent (TT/DD), indicating that filaminA–integrin interaction is controlled by the phosphorylation state of the T788/T789 motif (Fig. 1 B). Similar results were obtained by solid phase binding assays, where one of the binding partners was immobilized (Fig. 1 C). Again, the pseudo-phosphorylation of T788/T789 led to a complete loss of filaminA binding (Fig. 1 C). Furthermore, pull-down assays with biotinylated, synthetic peptides covering residues 762–798 of integrin β 1 in either the unphosphorylated or the phosphorylated (pT788/pT789) form confirmed that phosphothreonine residues at these positions impede filaminA binding (Fig. 1 D). Modeling of the pT788/pT789 β 1A integrin peptide based on known structures of the filaminA/integrin β 7 complex (PDB2BRQ; Fig. 1 E) or the talin/integrin β 1D complex (PDB3G9W; Fig. 1 F) suggested that phosphorylation of T788 and T789 not only sterically obstructs the binding interface with filaminA but also leads to charge repulsion. In contrast, integrin β 1 pT788/pT789 phosphate groups do not interfere with the binding interface to talin (Fig. 1 E). These structural models are in line with data reported previously for β 2 and β 7 (Kiema et al., 2006; Takala et al., 2008) and strongly support our conclusion that phosphorylation of the integrin β 1 T788/T789 motif disrupts filaminA binding, but does not impact talin association.

The integrin β 1 T788/T789 phospho-switch regulates talin versus filaminA binding in intact cells

To validate our in vitro findings in the cellular context, we performed Opa-protein-triggered integrin clustering (OPTIC) assays (Baade et al., 2019; assay scheme, Fig. S1 D; construct expression, Fig. S1 E). Clustering of the WT integrin β 1 cytoplasmic domain at the plasma membrane led to a strong recruitment of GFP-talin, while GFP alone was not enriched (Fig. 2 A). Furthermore, talin was equally well recruited to the pseudo-phosphorylated TT/DD and, to a slightly lesser extent, to the TT/AA variant (Fig. 2 A). Only disruption of the NPxY core binding motif (integrin Y783A) abolished talin recruitment (Fig. 2 A). In contrast, the filaminA integrin binding domain was only recruited in the case of the TT/AA mutant, where phosphorylation of this motif is impossible, while clustering of the WT integrin as well as the phospho-mimicking TT/DD variant did not support filaminA recruitment in the intact cell (Fig. 2 B). These results demonstrated that the phosphorylation status of the integrin β 1 T788/T789 motif dictates the association with integrin activity regulators in intact cells. Moreover, these findings also suggested that filamin can only occupy the talin binding site if the T788/T789 motif in the integrin tail is dephosphorylated. To test this idea, we performed in vitro competition assays with recombinant talin, filaminA, and integrin β 1 cytoplasmic domains (Fig. 2 C). While talin was not able to displace filaminA from integrin β 1 (Fig. S1 F), increasing levels of

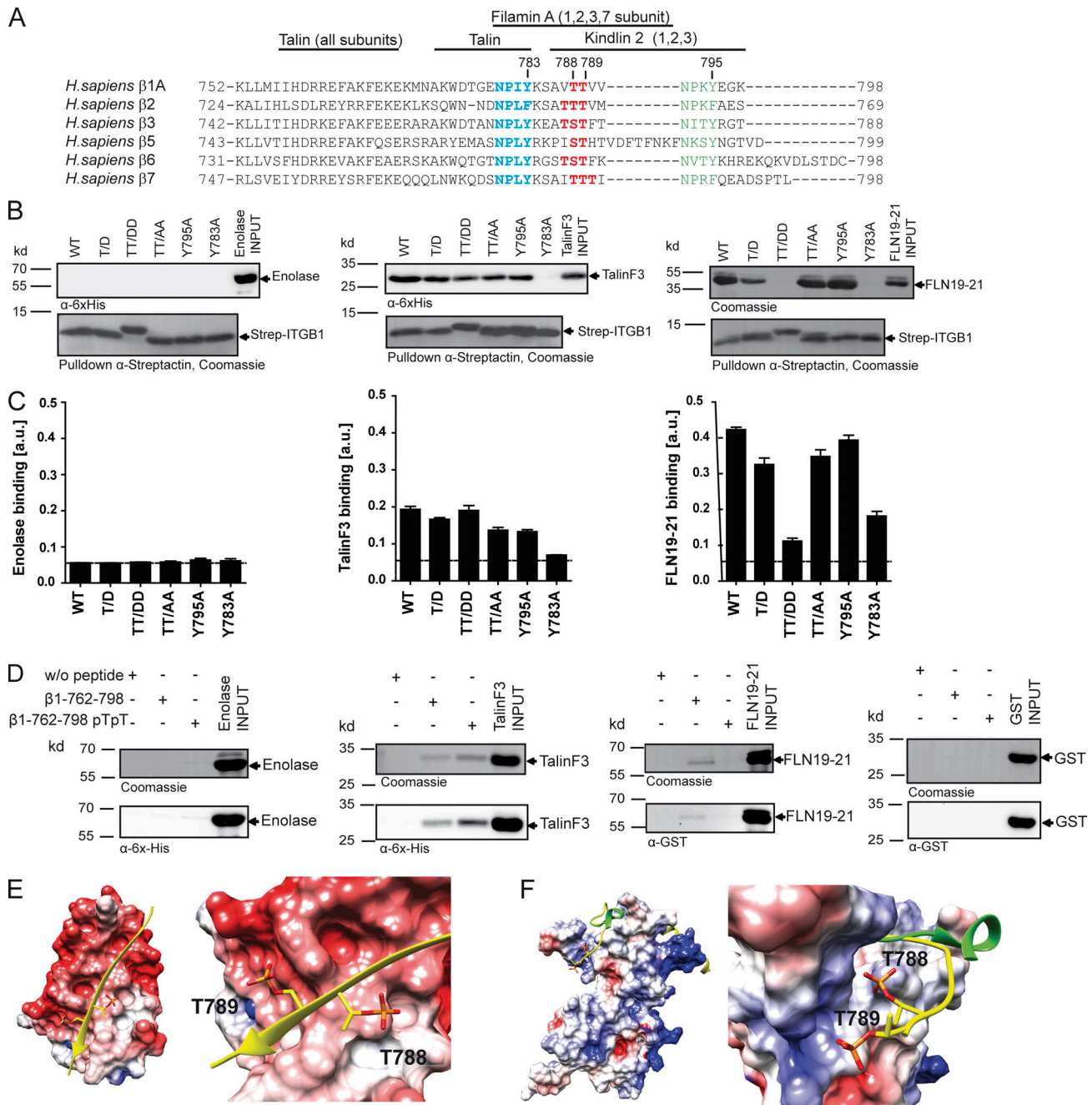


Figure 1. The integrin β1 T788/T789 motif constitutes a conserved phospho-switch to regulate integrin activity. (A) Alignment of cytoplasmic amino acid residues of human integrin β subunits. The conserved threonine motif (red), the proximal NPXY motif (blue), the distal NPXY motif (green), and the binding sites of talin, kindlin-2, and filaminA are marked. (B) Strep-tag-integrin β1 (Strep-ITGB1) cytoplasmic domains in the WT form, with modifications of the T788/T789 motif (T/D, TT/DD, TT/AA), alanine mutation of Tyr-795 (Y795A), or of Tyr-783 (Y783A) were incubated with His-tagged enolase, FLN19-21, or talin-F3. Upon streptactin pull-down, bound His-tagged proteins were detected by WB with α-His antibody or Coomassie staining. 50% of His-tagged proteins were directly loaded (input) for comparison. (C) His-tagged proteins as in B were immobilized in triplicate wells and incubated with the indicated Strep-ITGB1 variants at 4°C. After washing, binding was detected by incubation with streptactin-HRP. Bars represent mean ± SEM of triplicates from a representative experiment. (D) Biotinylated integrin β1 peptides in the nonphosphorylated form (β1-762-798) or phosphorylated at T788/T789 (β1-762-798 pTpT) were bound to streptavidin-agarose (0.5 mg/ml beads) before being incubated with His-tagged enolase, His-talin-F3, GST, or GST-tagged FLN19-21. Beads without peptide loading were used as negative control. Upon pull-down, bound His- and GST-tagged proteins were detected by WB with α-His or α-GST antibody and Coomassie staining. 50% protein amount was directly loaded as input. (E and F) Structural models of filaminA-Ig21 domain (E) and talin-F3 domain (F) with phosphorylated integrin β1A based on the known structures of filaminA Ig21/integrin β7 complex (PDB2BRQ) or talin/integrin β1D complex (PDB3G9W). The phosphorylated β1A T788/T789 motif was generated in Coot. The electrostatic surfaces of filaminA-Ig21 and talin-F3 are depicted in red (negative charge, value -5) and blue (positive charge, value 5), β1 is shown in yellow; the phosphorylated threonine residues are shown in ball and stick representation. See also Fig. S1. Coot, Crystallographic object-oriented toolkit; *H. sapiens*, *Homo sapiens*; w/o, without.

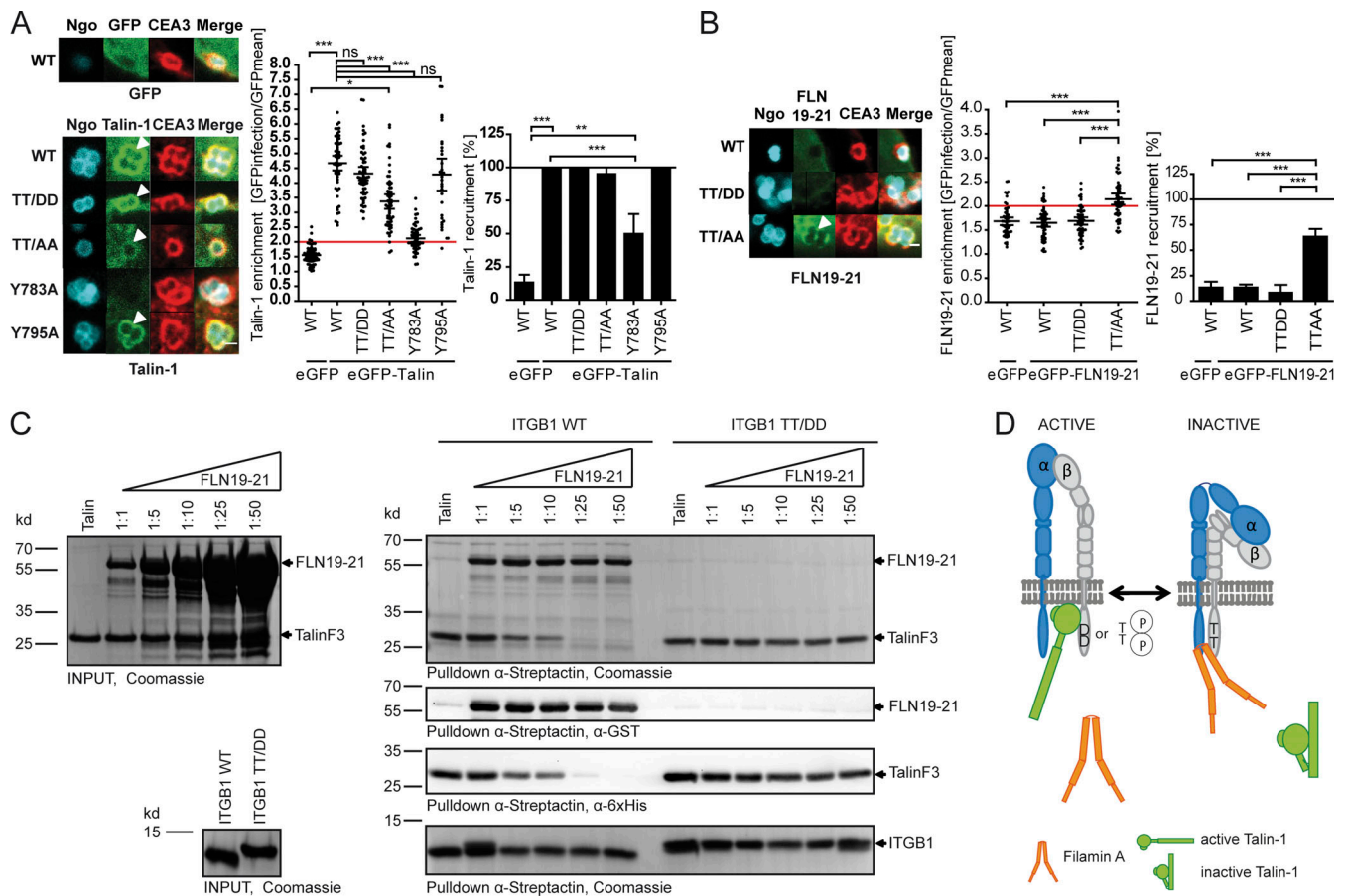


Figure 2. The integrin $\beta 1$ T788/T789 phospho-switch regulates talin versus filaminA binding in intact cells. (A) 293T cells were cotransfected with indicated CEA3-integrin $\beta 1$ cytoplasmic tail fusion proteins together with GFP or GFP-talin-1. After 48 h, cells were infected with CEACAM-binding bacteria (Ngo) for 1 h, fixed, and stained for CEACAM3. Micrographs (left panel) show representative infection sites of bacterial attachment (blue) and CEA3-integrin $\beta 1$ clustering (red). Recruitment of GFP-talin (green) to clustered integrin cytoplasmic tails is indicated (white arrowhead). Scale bar, 1 μ m. Talin recruitment was quantified with the enrichment ratio (ER) indicating the -fold enrichment of GFP-intensity at bacterial attachment sites versus the overall cellular GFP level (middle panel). Dots represent individual ERs of 30–60 recruitment sites from $n \geq 2$ independent experiments. Horizontal lines indicate mean values and 95% confidence intervals (whiskers). The red line indicates the threshold of positive recruitment. The bar graph (right panel) depicts the percentage of cells showing an ER of talin-1 recruitment ≥ 2 . Statistically significant differences were evaluated using one-way ANOVA, followed by Bonferroni post hoc test (***, $P < 0.001$; **, $P < 0.01$; *, $P < 0.05$). (B) Cells transfected with the indicated CEA3-integrin $\beta 1$ cytoplasmic tail fusion proteins together with GFP-FLN19-21 were evaluated as in A. (C) His-talinF3 and Strep-ITGB1 WT or Strep-ITGB1 TT/DD were incubated with increasing amounts of GST-FLN19-21. Left panels show the input proteins. Upon streptactin pulldown, proteins bound to ITGB1 WT or ITGB1 TT/DD were visualized by Coomassie staining (right; top panel), WB with α -GST antibody to detect FLN19-21 (second panel), or with α -His to detect talinF3 (third panel). Coomassie staining also verified similar amounts of precipitated Strep-ITGB1 WT and TT/DD (lowest panel). (D) Schematic view of talin versus filaminA association with the integrin $\beta 1$ cytoplasmic tail depending on T788/T789 (pseudo-)phosphorylation. See also Fig. S1. D, aspartate; T, threonine; P, phospho-.

filaminA led to a sharp drop in talin association with the WT integrin $\beta 1$ tail (Fig. 2 C). However, in the case of the pseudo-phosphorylated integrin $\beta 1$ tail, even a large excess of filaminA was not able to outcompete talin (Fig. 2 C). Identical results were obtained by solid phase binding assays (Fig. S1 G). These biochemical findings support the idea that dephosphorylation of integrin $\beta 1$, and in particular of the T788/T789 motif, is a prerequisite to allow filaminA to displace talin and to inactivate integrins (Fig. 2 D).

The phosphatase PPM1F regulates integrin activity and integrin-dependent cell adhesion

Based on the observations that a phosphorylated T788/T789 motif impedes filamin binding and that the pseudophosphorylated integrin $\beta 1$ T788D promotes cell adhesion (Craig et al.,

2009; Nilsson et al., 2006), we hypothesized that an integrin-directed protein phosphatase(s) counteracts integrin activation. Accordingly, deletion of such a putative protein phosphatase should lead to a gain of function with regard to integrin-based cell-matrix adhesion. Therefore, we performed a focused genetic knock-down screen with shRNAs individually targeting all protein phosphatases reported in the integrin adhesome (Zaidel-Bar et al., 2007; Fig. S2 A). As the cellular system, we deliberately chose 293T cells, a human cell line exhibiting weak adhesion to extracellular matrix proteins under tissue culture conditions. Stable knock-down cells were plated on the integrin ligands fibronectin or collagen or on poly-L-lysine, to which cells attach independently of integrins (Fig. 3 A). Compared with control cells, depletion of the protein tyrosine phosphatases (PTPs)

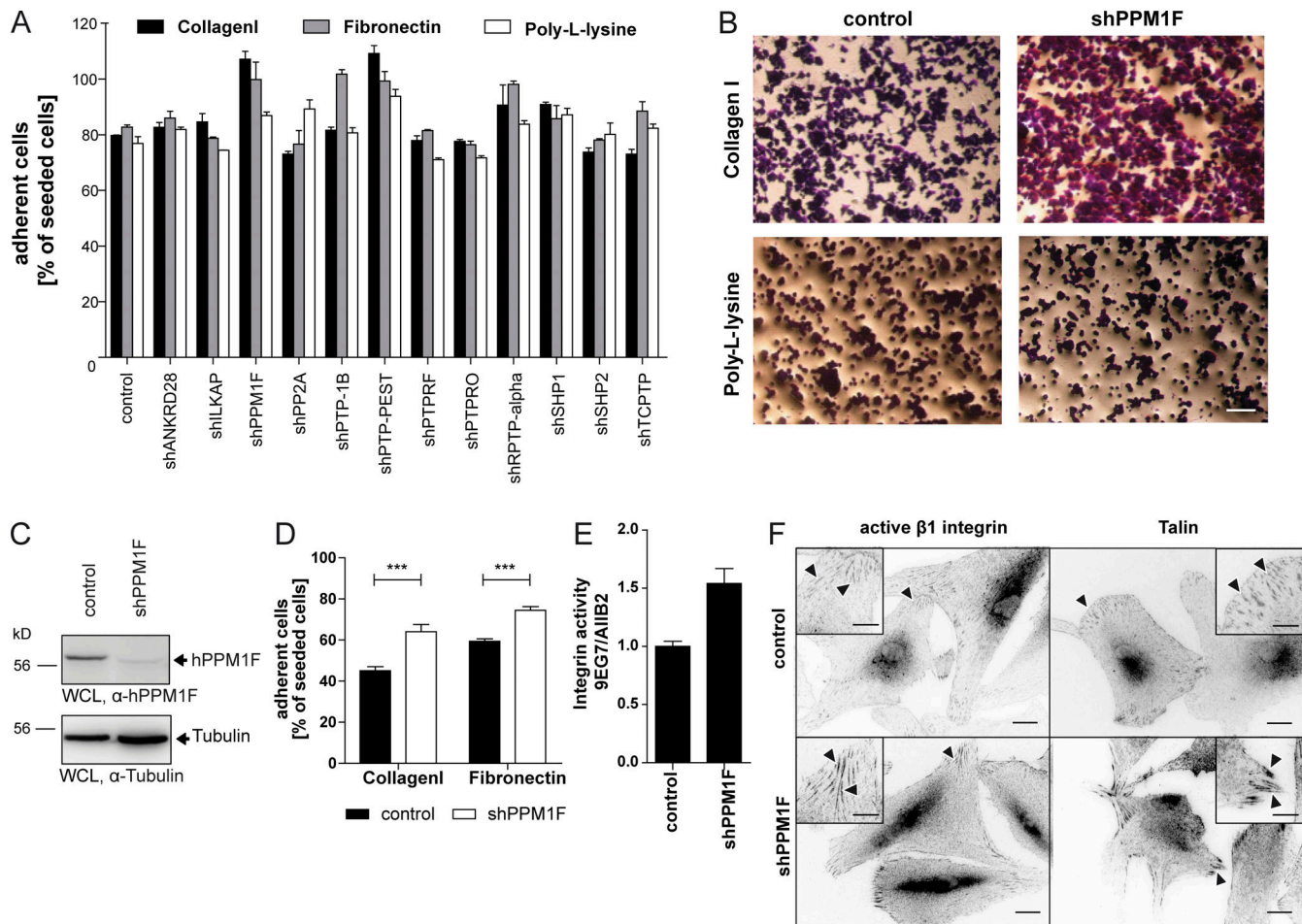


Figure 3. The phosphatase PPM1F regulates integrin activity and integrin-dependent cell adhesion. (A) 293T cells were transduced with lentiviral particles encoding shRNA directed against the indicated protein phosphatases. Stable knock-down cells were plated for 40 min on 1 μ g/ml collagen I, 0.8 μ g/ml FN_{III9-11}, or 10 μ g/ml poly-L-lysine and washed, and adherent cells were fixed and stained with crystal violet. In parallel, cells were plated for 3 h, fixed, and stained without washing (total seeded cells). Crystal violet staining was quantified and normalized to total seeded cells; control = lentivirus without shRNA; bars represent mean \pm SD of three wells. Shown is a representative result repeated twice with comparable results. (B) Representative micrographs from A showing shPPM1F-transduced and control cells on collagen I and poly-L-lysine; scale bar, 150 μ m. (C) NHDFs were transduced with lentiviral particles encoding shRNA targeting PPM1F or without shRNA (control). Knock-down was confirmed by WB of WCL with α -hPPM1F and α -tubulin antibody as loading control. (D) Control and PPM1F knock-down NHDFs were subjected to adhesion assays (1 μ g/ml collagen I, 0.8 μ g/ml FN_{III9-12}). Values were normalized to total seeded cells. Bars represent mean \pm SEM of three independent experiments, each done in triplicate; unpaired *t* test, ***, *P* < 0.001. (E) NHDFs as in D were seeded onto fibronectin-coated dishes for 40 min, fixed, and stained for active integrin β 1 (9EG7) or total integrin β 1 (AIB2). Graphs show the ratio of active integrin β 1 to total integrin β 1. Bars represent mean \pm SEM of triplicates from one representative experiment. (F) NHDFs as in D were seeded for 2 h onto 1 μ g/ml FN_{III9-11}-coated coverslips. Fixed cells were stained as indicated. Arrowheads point to active integrin β 1/talin enrichment; scale bar, 20 μ m. Insets: Higher magnification of boxed area; scale bar, 10 μ m. See also Fig. S2.

PTP-1B, PTP-PEST, and RPTP α as well as depletion of the serine/threonine phosphatase PPM1F (also known as POPX2 [Koh et al., 2002], Ca²⁺/calmodulin-dependent protein kinase phosphatase [CaMKP; Ishida et al., 2008], and hFEM2 [Tan et al., 2001]) resulted in enhanced cell adhesion to collagen and/or fibronectin, but not poly-L-lysine (Fig. 3, A and B). PTP-1B, PTP-PEST, and RPTP α dephosphorylate the focal adhesion proteins paxillin, p130^{CAS}, and c-Src, respectively, which could indirectly affect integrin-mediated adhesion (Arias-Salgado et al., 2005; Garton et al., 1996; Shen et al., 2000). As PPM1F, a member of the PPM (Moorhead et al., 2009), dephosphorylates serine/threonine residues and has not been implicated in cell adhesion, we decided to focus on this enzyme. Western blotting (WB) confirmed the depletion of the phosphatase in knock-down cells and

demonstrated that levels of several key focal adhesion proteins such as integrin β 1, talin, filamin, kindlin-2, focal adhesion kinase, paxillin, vinculin, zyxin, integrin-linked kinase (ILK), ezrin, or α -actinin were not altered (Fig. S2 B). These results indicated that reduction of PPM1F is directly connected to increased integrin-mediated cell adhesion.

PPM1F knock-down in normal human dermal fibroblasts (NHDF) recapitulated the phenotype observed in 293T cells leading to enhanced cell adhesion on integrin ligands (Fig. 3, C and D). Depletion of PPM1F did not affect expression of integrin subunits or other cytosolic focal adhesion proteins (Fig. S2, C and D), suggesting that the increased adhesion might be due to alterations in integrin activity. Indeed, PPM1F knock-down NHDFs exhibited elevated levels of active integrin β 1 (Fig. 3 E),

and the active receptor was enriched at peripheral focal adhesions, where prominent recruitment of talin was observed (Fig. 3 F). Similar levels of active integrin $\beta 1$ and strong recruitment of talin were also seen in NHDF cells with knock-down of filaminA, while knock-down of integrin $\beta 1$ eliminated the integrin staining and confirmed the specificity of the used integrin antibody (Fig. S2, E–G). Together, reduction of PPM1F results in elevated levels of active integrin accompanied by increased accumulation of talin phenocopying the depletion of the negative integrin regulator filaminA.

PPM1F knock-out (KO) results in constitutive integrin activity and an exaggerated cell adhesion phenotype

PPM1F is ubiquitously expressed, but with high levels in neuronal cells (Ishida et al., 2018). To confirm the phenotype of PPM1F knock-down cells, we disrupted the *Ppm1f* gene in human glioblastoma A172 cells by CRISPR/Cas9. Compared with A172 WT cells and A172 control cells, which were transduced with a vector lacking the PPM1F sgRNA, the derived A172 PPM1F KO cells completely lacked expression of PPM1F (Fig. 4 A). Expression of focal adhesion proteins was unaltered and surface expression of different integrin subunits was not increased in A172 PPM1F KO cells (Fig. S3, A and B). Similar to PPM1F knock-down 293T and NHDF cells, the A172 PPM1F KO cells showed a 1.5–2-fold increase in cell adhesion compared with A172 WT or control cells at different time points after plating on substrates coated with low, medium, or high concentrations of extracellular matrix ligands (Fig. 4 B; and Fig. S3, C and D). Furthermore, A172 PPM1F KO cells displayed elevated levels of active integrin $\beta 1$ (Fig. 4 C) and exhibited a prominent increase of active integrin $\beta 1$ in the form of a peripheral “active integrin belt” (Fig. 4 D), which colocalized with enlarged clusters of talin (Fig. 4 D and Fig. S3 E). This phenotype was seen in around 80–90% of A172 PPM1F KO cells during the first 1–2 h of spreading (Fig. 4 E and Fig. S3 F). In general, PPM1F KO cells did not spread as fast as A172 WT cells and, therefore, covered a smaller area (Fig. 4, F and G; and Fig. S3 G), suggesting that cell spreading might be compromised due to intensified integrin–matrix interaction. This observation also indicates that other PPM1F substrates such as p21-activated kinase (PAK) or mammalian Diaphanous-related formin 1 (mDial), which promote actin-based cell protrusions and which are negatively regulated by PPM1F, might not be responsible for the spreading defect of PPM1F KO cells (Koh et al., 2002; Parrini et al., 2009; Xie et al., 2008). To further confirm that the increased cell adhesion of PPM1F-deficient cells is connected to filamin-dependent activity regulation of integrins, we performed epistasis experiments. Therefore, A172 control cells and PPM1F KO cells received either a control shRNA or shRNA targeting human filaminA (Fig. 4 H). Similar to the KO of PPM1F and consistent with the known inhibitory role of filaminA (Liu et al., 2015; Takala et al., 2008; Waldt et al., 2018), shRNA-mediated knock-down of filaminA in A172 control cells increased cell adhesion, reduced cell spreading, and elevated integrin activity (Fig. 4, I and J; and Fig. S4, A–D). However, depletion of filaminA in PPM1F KO cells did not further elevate the increased integrin-dependent adhesion or the enhanced integrin activity in these cells, nor did it further

reduce cell spreading (Fig. 4, I and J; and Fig. S4, A–D). The results of these epistasis experiments highlight the strong similarities in the phenotype of PPM1F KO cells and filaminA knock-down cells and suggest that PPM1F and filaminA work together in the same pathway controlling integrin activity (Fig. S4 E). Together, the absence of PPM1F results in a gain of function with regard to integrin-based cell adhesion due to enhanced integrin activity, elevated talin recruitment, and reduced filaminA association with integrin $\beta 1$.

The phosphatase PPM1F regulates the phosphorylation state of the integrin T788/T789 motif

Association of filaminA and talin with the integrin β subunit as well as integrin activity are regulated by phosphorylation of the T788/T789 motif. Therefore, we wondered about the phosphorylation status of these residues in PPM1F-deficient cells. Interestingly, while suspended A172 WT cells showed low levels of integrin $\beta 1$ T788/T789 phosphorylation, KO of PPM1F resulted in constitutively elevated levels of pT788/pT789 (Fig. 5 A). Upon seeding onto fibronectin, the level of pT788/pT789 increased transiently in WT A172 cells during the initial attachment phase up to 45 min (Fig. 5 B). In contrast, PPM1F KO cells permanently exhibited substantially elevated T788/T789 phosphorylation (Fig. 5 C). Quantification of multiple blots demonstrated a four- to fivefold higher phosphorylation level of integrin $\beta 1$ T788/T789 in A172 PPM1F KO cells compared with WT cells (Fig. 5 D). To rigorously demonstrate that this phenotype is due to the lack of PPM1F activity, we complemented the PPM1F KO A172 cells with either WT monomeric (m)Kate-PPM1F or the phosphatase-dead mutant mKate-PPM1F D360A (Fig. S3 H). As seen before, expression of core focal adhesion proteins or surface expression of integrin subunits was not altered by this genetic manipulation (Fig. S3, A and B). However, expression of PPM1F WT, but not expression of PPM1F D360A, reverted the increased phosphorylation of integrin $\beta 1$ T788/T789 back to levels seen in WT A172 cells (Fig. 5 D). The increased integrin T788/T789 phosphorylation seen in the PPM1F KO cells correlated well with the elevated integrin activity and enhanced cell adhesion to integrin ligands, which was also reverted back to basic levels upon re-expression of WT PPM1F, but not PPM1F D360A (Fig. 5, E–G). Together, these findings are consistent with the idea that PPM1F regulates the phosphorylation state of the T788/T789 motif, thereby controlling association of talin versus filaminA with the cytoplasmic tail of integrin $\beta 1$ and determining cell–matrix adhesion strength (Fig. 5 H). The uniform phenotype of enhanced integrin activity observed upon depletion or disruption of PPM1F in multiple cell types also indicated that PPM1F might act directly on the integrin $\beta 1$ subunit.

Recombinant PPM1F dephosphorylates the conserved T788/T789 motif in the integrin $\beta 1$ cytoplasmic domain

To test the ability of PPM1F to directly dephosphorylate pT788/pT789 of integrin $\beta 1$, human PPM1F WT and PPM1F D360A were produced in *Escherichia coli* (Fig. 6 A). Using the generic phosphatase substrate 4-methylumbelliferylphosphate (4-MUP), maximum velocity (V_{\max}) and Michaelis constant (K_m) values of PPM1F were comparable to other Ser/Thr phosphatases (Gee

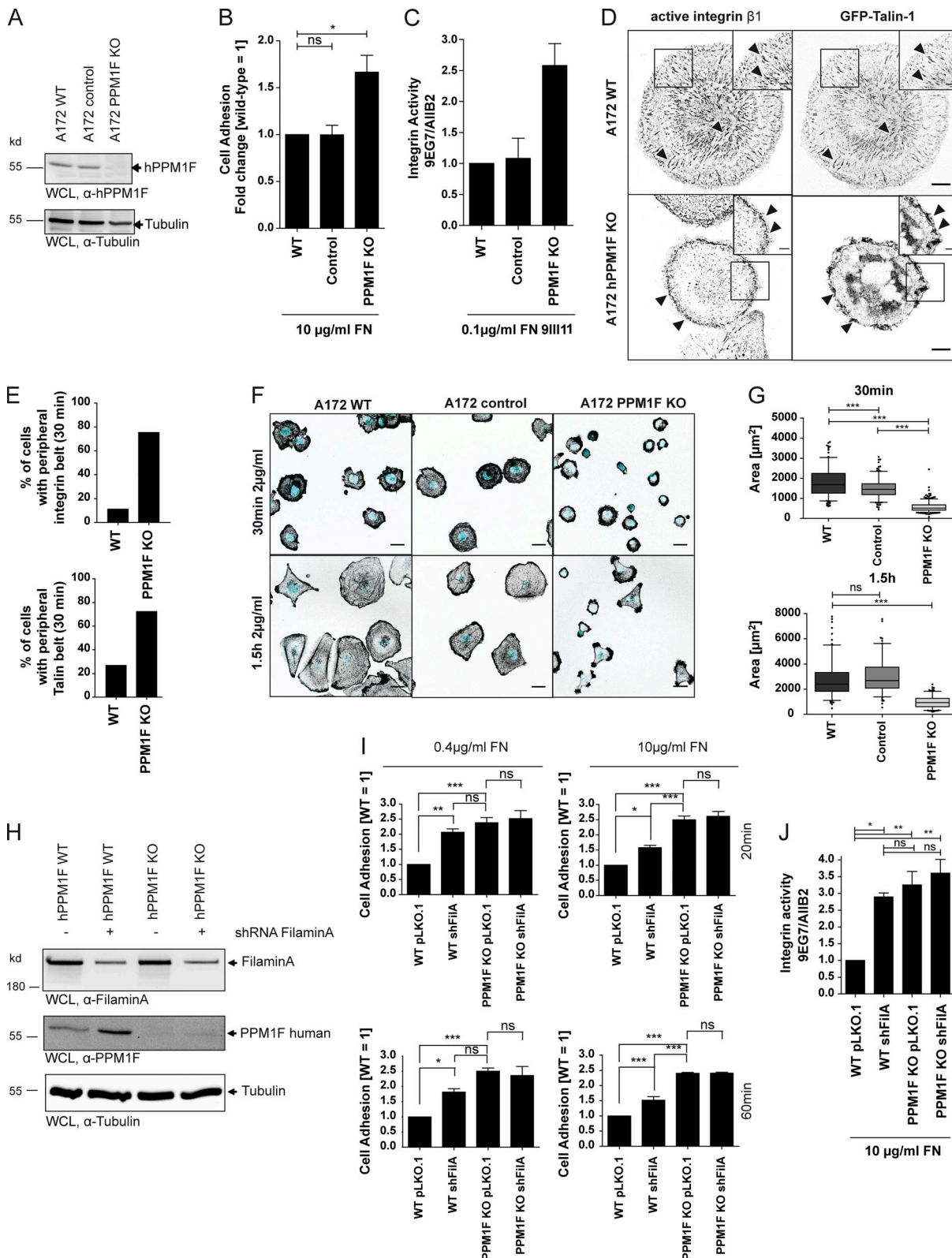


Figure 4. PPM1F KO results in constitutive integrin activity and an exaggerated cell adhesion phenotype. (A) A172 cells expressing Cerulean (WT) were treated with sgRNA against Cerulean (control) or sgRNA against Cerulean and PPM1F (PPM1F KO) combined with Cas9. Clonal cell lines were derived and analyzed by WB with polyclonal α-PPM1F (upper panel) or α-tubulin (lower panel) antibodies. (B) Cells from A were seeded onto 10 µg/ml FN₁₁₉₋₁₁ for 30 min in triplicate. Cell adhesion was measured as in A. Adhesion of A172 WT cells was used as reference. Bars represent mean ± SEM from three independent experiments. Statistics was calculated using one-way ANOVA, followed by Bonferroni post hoc test (*, P < 0.05). (C) Cells from A were replated onto 0.1 µg/ml FN₁₁₉₋₁₁-coated 96-well plates for 40 min. Samples were stained for active integrin β1 (9EG7), total integrin β1 (AIIB2), or with secondary antibody only as a

control. The graph shows the ratio of active integrin $\beta 1$ versus total integrin $\beta 1$ after background subtraction. Bars represent mean \pm SEM from a representative experiment done in triplicate. **(D)** Cells transfected with GFP-talin were seeded onto FN₁₁₉₋₁₁ for 30 min. Cells were fixed, stained with antibodies against active integrin $\beta 1$, and analyzed by confocal microscopy; scale bar, 10 μ m. Arrowheads point to active integrin $\beta 1$ /talin enrichment. Insets: Higher magnification of boxed area; scale bar, 5 μ m. **(E)** Quantification of peripheral belt formation by active integrin (upper graph) or talin-1 (lower graph) in A172 WT and PPM1F KO cells. Data are shown in percentages of all cells analyzed; $n \geq 30$ derived from ≥ 2 independent experiments. **(F)** A172 WT, control, and PPM1F KO cells were seeded onto 2 μ g/ml FN₁₁₉₋₁₁-coated coverslips for 30 min or 1.5 h before fixation and staining with DAPI and phalloidin-Cy5. Representative pictures are shown; scale bar, 25 μ m. **(G)** Quantification of cell area from cells in F; $n \geq 100$ cells from two or more independent experiments; mean values and 95% confidence intervals are shown, outliers are represented in dots, and statistics was performed using one-way ANOVA with post hoc Bonferroni test (***, $P < 0.001$). **(H)** A172 WT and PPM1F KO cells were transduced with lentiviral particles harboring shRNA against human filaminA or empty pLKO.1 vector as a control. After puromycin selection, lysates were prepared and subjected to WB analysis using indicated antibodies. **(I)** Cell adhesion assays were performed with starved A172 cells from H for 20 or 60 min using 0.4 or 10 μ g/ml FN₁₁₉₋₁₁ as integrin-dependent matrix. After a washing step, adherent cells were fixed and stained with crystal violet. Staining was quantified and normalized to the total number of seeded cells. Bar graphs show mean \pm SEM of four independent experiments done in triplicate referenced to WT cell adhesion (= 1); one-way ANOVA and Bonferroni post hoc test (***, $P < 0.001$; **, $P < 0.01$; *, $P < 0.05$). **(J)** Cell lines from H were kept in suspension for 45 min and incubated for 15 min with 10 μ g/ml FN₁₁₉₋₁₁ before staining for total (A1B2) or active integrin $\beta 1$ (9EG7). Samples were analyzed by flow cytometry, 10,000 counts; unstained cells and an IgG-matched irrelevant antibody served as negative controls. The mean fluorescence intensity (MFI) ratio of active to total integrin $\beta 1$ was calculated and normalized to the WT sample (= 1). Bars represent mean MFI \pm SEM of three independent experiments; one-way ANOVA and Bonferroni post hoc test (**, $P < 0.01$; *, $P < 0.05$). See also Fig. S3 and Fig. S4. FN, FN₁₁₉₋₁₁.

et al., 1999), while PPM1F D360A was inactive (Fig. 6 B). PPM1F also dephosphorylated synthetic peptides spanning the integrin $\beta 1$ T788/T789 motif (Fig. 6, C and D). Though the doubly phosphorylated peptide ($\beta 1$ -pT788/pT789) served as a suitable substrate for PPM1F, dephosphorylation was more effective with the mono-phosphorylated integrin $\beta 1$ peptides $\beta 1$ -pT788 or $\beta 1$ -pT789 (Fig. 6 D). PPM1F acted specifically on integrin pT788/pT789, since a phospho-peptide derived from myosin light chain (MLC; pMLC) was not dephosphorylated (Fig. 6, C and D). In a complementary approach, PPM1F was overexpressed and purified from human cells. Again, we observed dephosphorylation of synthetic integrin phospho-peptides by WT GST-PPM1F isolated from human cells, but not by GST-PPM1F D360A (Fig. S5, A-E). In a further approach, we used purified Ca²⁺/calmodulin-dependent kinase II (CaMKII) β , which has been reported as a potential kinase of integrin $\beta 1$ (Suzuki and Takahashi, 2003), to phosphorylate the recombinant cytoplasmic domain of integrin $\beta 1$ in the presence of ATP, Ca²⁺, and calmodulin. In contrast to WT integrin $\beta 1$, the T788A/T789A mutant was not phosphorylated, demonstrating that CamKII β selectively acts on the integrin $\beta 1$ T788/T789 motif in vitro (Fig. S5 F). Recombinant WT PPM1F, but not PPM1F D360A, dephosphorylated the resulting integrin $\beta 1$ pT788/pT789 (Fig. 6 E). To check if other protein phosphatases also act on the T788/T789 motif, we recombinantly expressed several enzymes, including integrin-linked kinase-associated protein (ILKAP, an additional member of the PPM family present at integrin adhesion sites; Leung-Hagesteijn et al., 2001), PP5, and PTP1B (Fig. 6 F), and verified the activity of the purified proteins with 4-MUP (Fig. S5 G). Next, PPM1F, ILKAP, PP5, and PTP1B were incubated with the doubly phosphorylated $\beta 1$ -pT788/pT789 peptide. While PTP1B, PP5, and ILKAP failed to dephosphorylate integrin $\beta 1$ pT788/pT789 to a significant extent, PPM1F was highly active (Fig. 6 F). Moreover, ILKAP did not dephosphorylate the GST- $\beta 1$ integrin cytoplasmic domain phosphorylated in vitro by CaMKII β , while PPM1F was active against this phospho-protein substrate (Fig. 6, G and H). Therefore, PPM1F is the integrin phosphatase that specifically controls the phosphorylation state of the conserved T788/T789 motif in the cytoplasmic domain of integrin β subunits.

Kindlin2 association with the phosphorylated integrin $\beta 1$ cytoplasmic tail requires the presence of talin

The T788/T789 motif is also at the core of the kindlin binding site in integrin $\beta 1$ (Fig. 1 A), and kindlin, together with talin, is the major positive regulator of integrin function (Harburger et al., 2009; Li et al., 2017; Theodosiou et al., 2016). Therefore, we wondered if the phosphorylation state of T788/T789 also influences kindlin association with integrin $\beta 1$. In vitro, recombinant kindlin2 bound the WT integrin $\beta 1$ cytoplasmic domain and the Y783A mutant with the corrupted NPxY talin binding motif, but not the Y795A variant, which disrupts the core NPKY kindlin binding motif (Li et al., 2017; Fig. 7 A). Kindlin2 also did not associate with the A788/A789 variant, which is in line with previous studies showing that the hydroxyl-groups of the conserved threonine residues are involved in H-bonds between kindlin and integrin $\beta 1$ (Li et al., 2017). Unexpectedly however, kindlin2 did not bind the pseudo-phosphorylated integrin $\beta 1$ variants T/D and TT/DD (Fig. 7 A), and the same results were obtained by solid phase binding assays (Fig. 7 B). Furthermore, pull-down assays with biotinylated, phosphorylated (pT788/pT789), or unphosphorylated integrin $\beta 1$ peptides confirmed that phosphorylation of these threonine residues prevents kindlin2 binding (Fig. 7 C). Similar to the situation with talin, kindlin2 was readily displaced from the integrin $\beta 1$ tail in vitro by the integrin-binding domain of filaminA (Fig. 7 D and Fig. S1 H). These puzzling results would imply that kindlin2 is outcompeted by filaminA, when the integrin $\beta 1$ tail is unphosphorylated, but kindlin2 could also not bind on its own, when the T788/T789 motif is phosphorylated. As kindlin2 cooperates with talin to modulate integrin function (Theodosiou et al., 2016; Ye et al., 2013), we wondered whether the capability of talin to associate with the phosphorylated integrin tail might enable binding of kindlin2. Therefore, recombinant full-length human kindlin2 and His-tagged talin F3 domain were employed in pull-down assays with various Twin-StrepII-tag (strep)-tagged integrin $\beta 1$ cytoplasmic domains (Fig. 7 E). As before, kindlin2 alone bound the unphosphorylated integrin $\beta 1$ cytoplasmic domain, but failed to associate with the pseudo-phosphorylated TT/DD variant (Fig. 7 F). Importantly, the presence of the recombinant

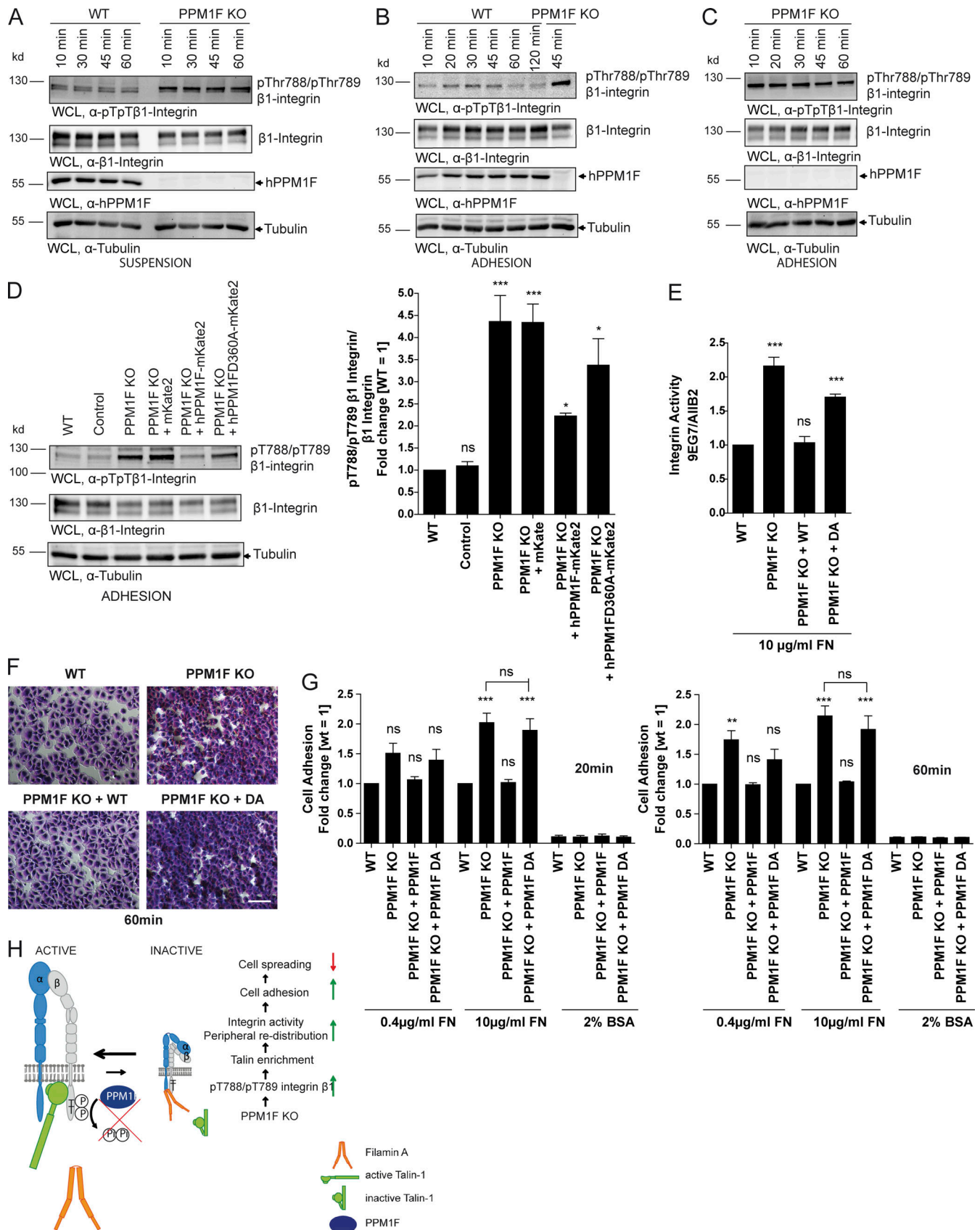


Figure 5. **The phosphatase PPM1F regulates the phosphorylation state of the integrin T788/T789 motif in intact cells.** (A) Starved A172 WT and PPM1F KO cells were kept in DMEM plus 0.25% BSA for the indicated time periods before WCLs were prepared and subjected to WB analysis with indicated antibodies. (B and C) Starved A172 WT (B) or PPM1F KO cells (C) were seeded onto 2 μg/ml FN₁₁₉₋₁₁ for the indicated time periods before being lysed and

analyzed by immunoblotting as in A; PPM1F KO cells were used as a control in B to directly compare integrin β 1 phosphorylation levels. **(D)** PPM1F KO cells were reconstituted with either WT human PPM1F (PPM1F KO + hPPM1F-mKate2) or the phosphatase-dead mutant PPM1F D360A (PPM1F KO + hPPM1FD360A-mKate2). Furthermore, PPM1F KO cells were stably transduced with mKate2 (PPM1F KO + mKate2). As a comparison, A172 WT cells and A172 cells transduced with a vector lacking the PPM1F sgRNA (control) were used. The cells were seeded onto 2 μ g/ml FN₁₁₉₋₁₁ for 45 min and WCLs subjected to WB with indicated antibodies (left panels). Bar graphs show densitometric quantification of band intensities from pT788/pT789- β 1 versus total β 1 integrin antibody signal for the indicated samples from three independent experiments; WT was set to 1 (right graph). Statistics was performed using one-way ANOVA, followed by Bonferroni post hoc test (*, $P < 0.05$; ***, $P < 0.001$). **(E)** Indicated A172 cell lines were kept in suspension for 45 min and incubated for 15 min with 10 μ g/ml FN₁₁₉₋₁₁ before being stained for total (AIB2) or active integrin β 1 (9EG7). Samples were analyzed by flow cytometry, 10,000 counts. The mean fluorescence intensity ratio of active to total integrin β 1 was calculated and normalized to the WT sample (= 1). Bars represent mean fluorescence intensity \pm SEM of four independent experiments; statistics was performed using one-way ANOVA and Bonferroni post hoc test (***, $P < 0.001$). **(F and G)** Cell adhesion assays were performed with starved A172 cell lines for 20 or 60 min using 0.4 or 10 μ g/ml FN₁₁₉₋₁₁; 2% BSA-coated wells were used as a negative control. After a washing step, adherent cells were fixed and stained with crystal violet. Staining was quantified and referenced to WT cell adhesion (= 1). **(F)** Representative pictures after 60 min adhesion on 10 μ g/ml FN₁₁₉₋₁₁; scale bar, 150 μ m. **(G)** Bar graphs show mean \pm SEM of four independent experiments pipetted in triplicate; statistics was performed using one-way ANOVA and Bonferroni post hoc test (***, $P < 0.001$; **, $P < 0.01$). **(H)** Model summarizing effects of PPM1F KO on integrin activity. In PPM1F KO cells, the balance between active and inactive integrins is shifted toward the active conformation by constitutive phosphorylation of integrin β 1 at T788/T789, thereby prohibiting filaminA binding, while promoting increased talin association and cell adhesion. DA, phosphatase-dead mutant of PPM1F D360A; FN, FN₁₁₉₋₁₁₂; P, phospho-; T, threonine.

talin F3 domain allowed the association of kindlin2 with integrin β 1 TT/DD (Fig. 7 F). Despite the presence of talin, binding of kindlin2 still required the intact membrane distal NPXY amino acid motif (Fig. 7 F), suggesting that talin and kindlin2 do not physically interact, as also observed by Bledzka et al. (2012). Rather, talin binding seems to reorient the integrin tail in a manner that allows kindlin2 association with the pseudo-phosphorylated integrin. Disruption of the talin binding site in the pseudo-phosphorylated integrin β 1 (TT/DD + Y783A) concomitantly abolished kindlin association (Fig. 7 F), confirming that kindlin2 binding to pseudo-phosphorylated integrin depended on the presence of talin.

To analyze if this cooperation is also true for phosphothreonine residues and if the cooperative binding with talin might allow kindlin2 to withstand the presence of filaminA, pull-down experiments with phospho-integrin peptide β 1-762-798 pTpT and with the unphosphorylated peptide (β 1-762-798) were performed (Fig. 7 G). Clearly, in the absence of filaminA, kindlin2 together with talin associated with the unphosphorylated as well as the phosphorylated integrin β 1 peptides (Fig. 7 G). Upon addition of filaminA, kindlin2 was readily displaced from the unphosphorylated integrin β 1 peptide, even though the talin F3 domain was present (Fig. 7 G). Importantly, this displacement was completely prevented by phosphorylation of the T788/T789 motif, which allowed not only talin but also kindlin2 to remain associated with the integrin β 1 cytoplasmic tail in the presence of filaminA (Fig. 7 G). These observations form the basis of a refined working model for integrin activity regulation by a phosphorylation-dependent displacement of the negative regulator filaminA and the cooperative binding of talin and kindlin2 under these circumstances (Fig. 7 H).

Kindlin2 and talin recruitment are dictated by integrin β 1 phosphorylation and PPM1F activity

To follow the consequences of integrin β 1 T788/T789 phosphorylation for kindlin2 recruitment in intact cells, we employed integrin β 1 chimeras and their phospho-mimicking mutants as well as deletion of PPM1F. In agreement with the in vitro binding data, GFP-kindlin2 clustered at WT integrin β 1 tails, but was not enriched at the integrin β 1 TT/AA or the integrin

β 1 Y795A variant (Fig. 8 A). However, in contrast to the situation with purified components, GFP-kindlin2 was also strongly enriched at pseudo-phosphorylated integrin β 1 in intact cells (Fig. 8 A). The recruitment of GFP-kindlin2 in this situation was critically dependent on talin binding, as mutation of the core talin binding site in the regular (Y783A) or in the pseudophosphorylated (TT/DD + Y783A) integrin β 1 tail abolished the increased association (Fig. 8, A and B).

The capability of kindlin2 to associate with full-length phosphorylated integrin β 1 was also reflected by the fact that PPM1F KO cells, which display elevated levels of pT788/pT789, showed not only a peripheral ring of active integrin but also accumulation of kindlin2 at these sites (Fig. 8 B). The accumulation of kindlin2 in these structures mimicked the accumulation seen for talin in the PPM1F KO cells (Fig. 8 B). Importantly, reexpression of active, WT PPM1F, which reduces the increased integrin β 1 T788/T789 phosphorylation, also prevented kindlin2 and talin accumulation, while in PPM1F KO cells reexpressing inactive PPM1F D360A, the massive peripheral ring of active integrin and the exaggerated presence of kindlin2 and talin persisted (Fig. 8 B). These data illustrate how phosphorylation of the integrin β 1 subunit enforces cooperation between the integrin activators talin and kindlin2 to overcome filamin-mediated inhibition of integrins. Moreover, these results point to the critical position of PPM1F during integrin activity regulation as the major protein phosphatase directed toward the conserved T788/T789 motif.

PPM1F activity determines the interaction of talin and filaminA with the integrin β 1 cytoplasmic tail in intact cells

To test whether PPM1F activity toward the conserved threonine motif in the integrin cytoplasmic tail dictates integrin activity, we again employed the chimeric receptor proteins in the unphosphorylated (WT) or pseudo-phosphorylated (T788D/T789D) forms. These integrin β 1 chimeras were coexpressed with PPM1F WT or PPM1F D360A and together with either GFP-talin (Fig. 8 C) or the GFP-tagged integrin binding domain of filamin (GFP-FLN19-21; Fig. 8 D). Upon PPM1F overexpression, talin recruitment to the clustered WT β 1 integrin tail was strongly impaired, while overexpression of inactive PPM1F D360A did

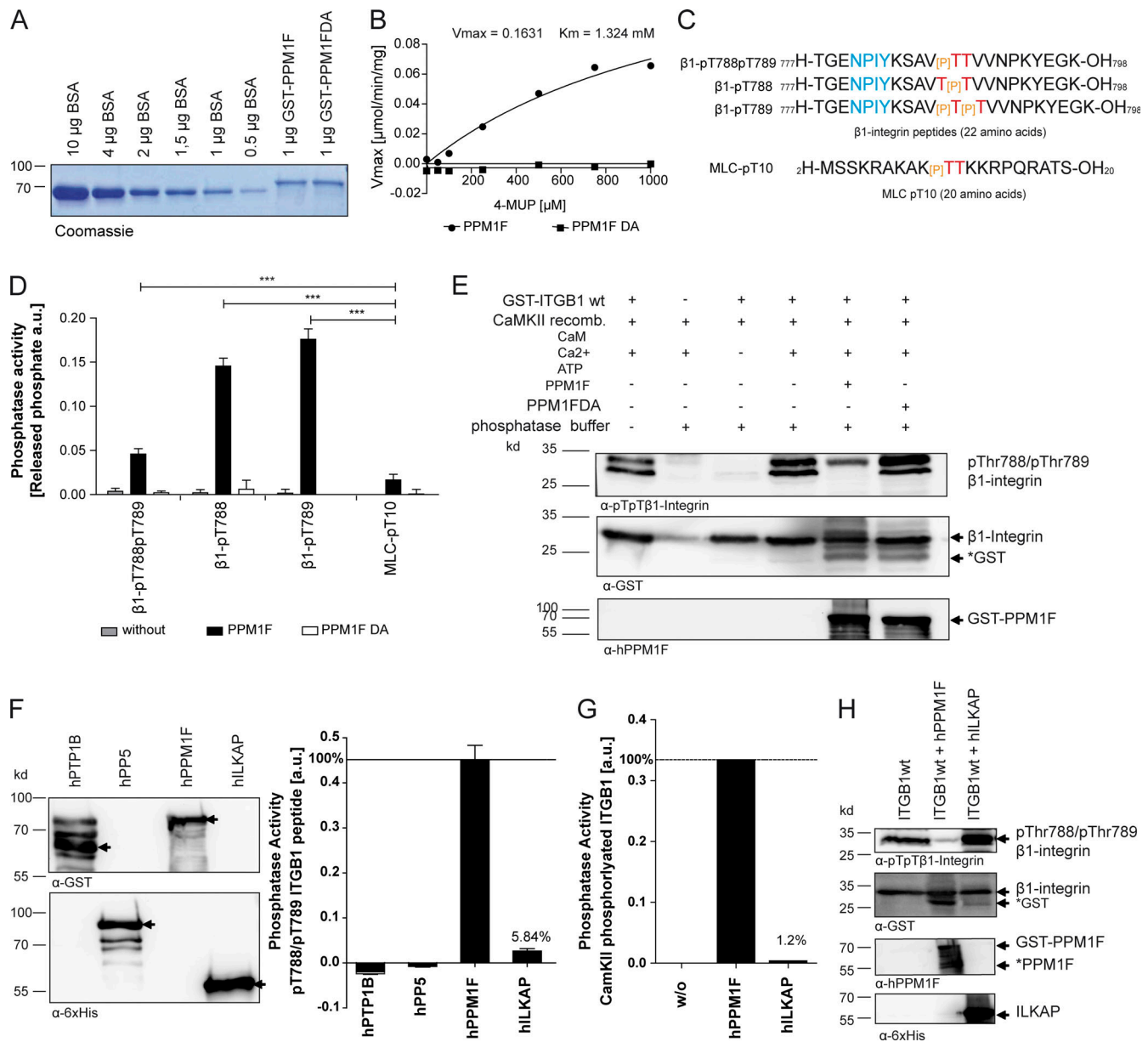


Figure 6. Recombinant PPM1F dephosphorylates the conserved 788/789 motif in the integrin $\beta 1$ cytoplasmic domain. (A) Recombinant GST-PPM1F and GST-PPM1F D360A (DA) were expressed in *E. coli*, purified, and analyzed via SDS-PAGE and Coomassie staining. A BSA standard was used to evaluate the protein content. (B) The activity of purified enzymes from A was determined using the fluorogenic substrate 4-MUP. Curves were obtained by a direct nonlinear fit of the data to the Michaelis–Menten equation, and V_{max} and K_m values for PPM1F were determined from one representative experiment. (C) Sequences of double or single phosphorylated integrin $\beta 1$ peptides and the single phosphorylated control peptide MLC2. (D) 500 ng GST-PPM1F or GST-PPM1F DA were incubated at 30°C with synthetic integrin $\beta 1$ peptides from C. Release of phosphate was measured after 60 min by malachite green. Bars depict mean \pm SD of three independent experiments performed in duplicate; unpaired t test (***, $P < 0.001$). (E) CaMKII β (120 ng) was incubated with GST-integrin $\beta 1$ cytoplasmic domain in the presence or absence of ATP/calmodulin/ $CaCl_2$. 2 μ g GST-PPM1F or GST-PPM1F DA were added as indicated, and samples were incubated for 60 min at 30°C. Reactions were stopped via addition of SDS sample buffer and subjected to WB with indicated antibodies; *GST is free GST cleaved off from PPM1F proteins. (F) 200 ng of the indicated recombinant phosphatases were separated by SDS-PAGE and probed with α -GST (hPTP1B; PPM1F) and α -His (hPP5; hILKAP) antibodies (left panels); 200 ng of the purified phosphatases were incubated at 30°C with $\beta 1$ -22pT788pT789 peptide. Phosphate release was measured after 60 min with malachite green. Bars depict mean \pm SEM of triplicates from a representative experiment. Blank (= no enzyme) values were subtracted from each sample. (G) Phosphatase assay as in F using purified GST-integrin $\beta 1$ cytoplasmic domain phosphorylated in vitro by CaMKII β as a substrate. (H) Assays conducted as in G were analyzed by WB using indicated antibodies; *PPM1F is free PPM1F released from GST. See also Fig. S5. CaMKII recomb., recombinant human Ca^{2+} /calmodulin-dependent protein kinase II; w/o, without.

not compromise talin association (Fig. 8 C). As predicted from the in vitro binding assays, talin also associated with integrin $\beta 1$ T788D/T789D, and this association could not be diminished by

overexpression of PPM1F (Fig. 8 C). Vice versa, GFP-filamina was only enriched around clustered WT integrin $\beta 1$ in situations where WT PPM1F, but not the D360A mutant, was

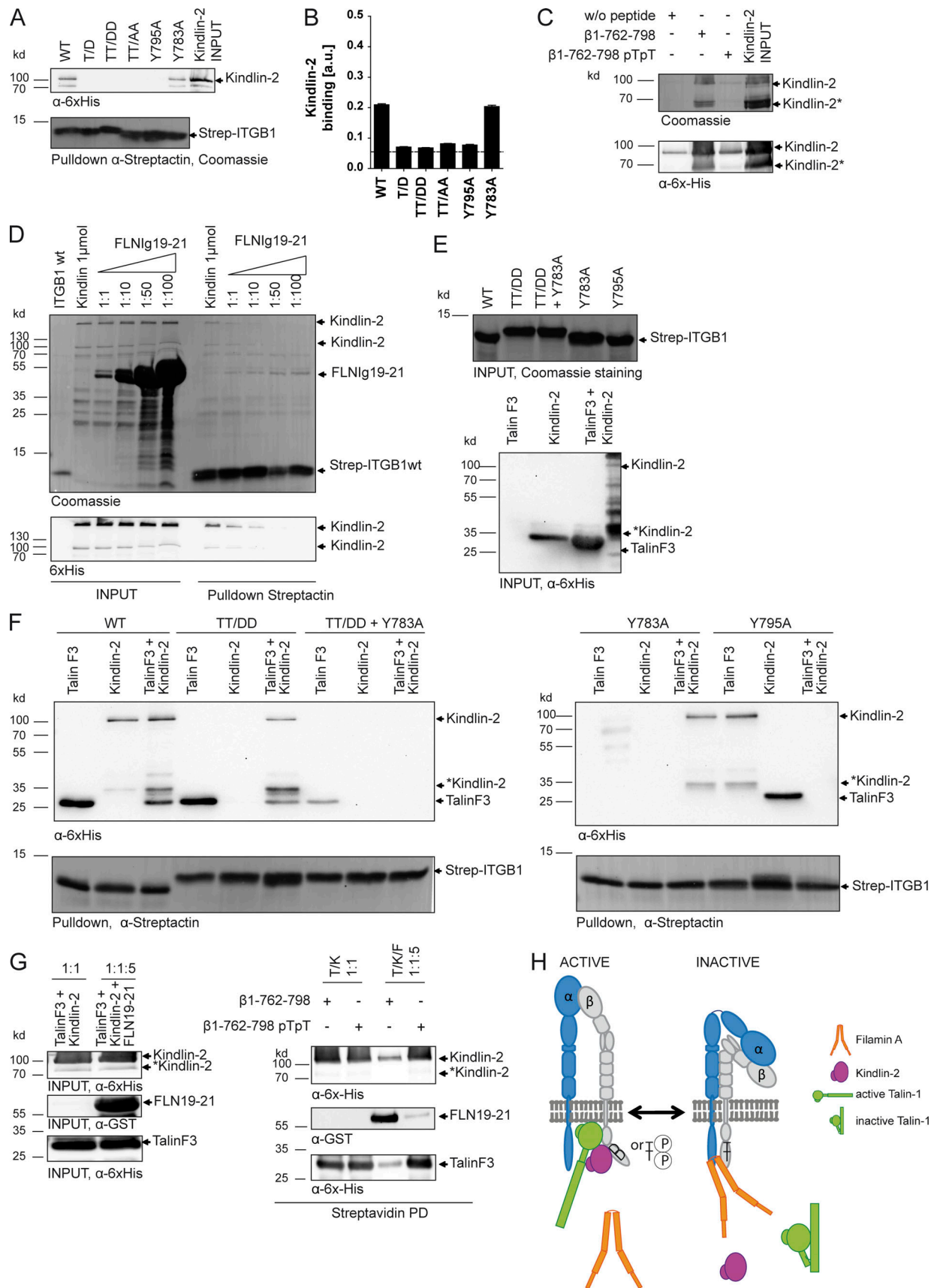


Figure 7. **Kindlin-2 association with the phosphorylated integrin β 1 cytoplasmic tail requires the presence of talin.** (A) Strep-tag-integrin β 1 (Strep-ITGB1) cytoplasmic domains in the WT form, with modifications of the T788/T789 motif (T/D, TT/DD, TT/AA), alanine mutation of Tyr-795 (Y795A), or of

Tyr-783 (Y783A) were incubated with His-kindlin-2. Upon streptactin pull-down, bound kindlin-2 was detected by WB with α -His antibody or Coomassie staining. 50% of His-kindlin-2 was directly loaded (input) for comparison. **(B)** His-tagged kindlin-2 was immobilized and incubated with the indicated Strep-ITGB1 variants at 4°C in triplicate wells. After washing, binding was detected by incubation with streptactin-HRP. Bars represent mean \pm SEM of triplicates from one representative experiment. **(C)** Biotinylated integrin β 1 peptides with or without phosphorylated T788/T789 were bound to streptavidin-agarose (0.5 mg/ml beads), before incubation with His-kindlin-2. Upon streptavidin pull-down, bound kindlin-2 was detected as in A. *Kindlin-2 is the N-terminal kindlin-2 fragment, which is also detected by α -His-antibody and interacts with integrin tails. **(D)** His-kindlin-2 and Strep-ITGB1 WT were incubated with increasing amounts of His-FLN19-21. Left panels show the input proteins, right panels protein visualization upon pull-down of ITGB1 by streptactin. Proteins were visualized by Coomassie staining (upper panel) and with α -His to detect bound kindlin-2 (lower panel). Coomassie staining also verified similar amounts of precipitated Strep-ITGB1 WT (lowest bands in the upper panel). **(E and F)** Strep-tag-integrin β 1 (Strep-ITGB1) cytoplasmic domains in the WT form, with modifications of the T788/T789 motif (T/D, TT/DD, TT/AA), alanine mutation of Tyr-795 (Y795A), or of Tyr-783 (Y783A) together with or without T788D/T789D mutation were incubated with kindlin-2 and talin-F3 alone or together in a 1:1 ratio. Upon streptactin pull-down, bound His-tagged proteins were detected by WB with α -His antibody or Coomassie staining. Input is shown in E, pull-down in F; *Kindlin-2 as in C. **(G)** Indicated biotinylated integrin β 1 peptides were bound to streptavidin-agarose (0.25 mg/ml beads) before incubation with His-tagged talin-F3 (1 \times) and kindlin-2 (1 \times) with or without GST-tagged FLN19-21 (5 \times molar amount). Upon streptavidin pull-down, bound His- and GST-tagged proteins were detected by WB using α -His or α -GST antibody and Coomassie staining (right panels); left panels show protein input (100%); *Kindlin-2 as in C. **(H)** Schematic view of talin and kindlin-2 versus filaminA association with the integrin β 1 cytoplasmic tail depending on T788/T789 (pseudo-)phosphorylation. See also Fig. S1. P, phospho-; T, threonine; w/o, without; wt, wild type.

overexpressed (Fig. 8 D). These results indicate that continuous activity of PPM1F toward the integrin β 1 T788/T789 motif is needed to enable filaminA association, which nicely explains the elevated integrin activity in PPM1F-deficient as well as filaminA-deficient cells. Together, these data illustrate the consequences of PPM1F activity on protein–protein interactions occurring at the integrin β 1 subunit in intact cells and suggest that this phosphatase holds a key position to set integrin activity levels.

Homozygous disruption of the *ppm1f* gene results in embryonic lethality, and *ppm1f*^{-/-} fibroblasts show constitutive T788/T789 phosphorylation, elevated integrin activity, and increased cell adhesion

Integrin β 1 and its key interaction partners, such as talin, kindlin, filaminA, paxillin, and focal adhesion kinase, are all essential for mammals (Fässler and Meyer, 1995; Ilić et al., 1995; Stephens et al., 1995; Monkley et al., 2000; Hagel et al., 2002; Feng et al., 2006; Montanez et al., 2008). Furthermore, compromising integrin activity regulation via targeted mutations in the integrin β 1 cytoplasmic domain abrogates integrin function in the intact tissue (Czuchra et al., 2006; Meves et al., 2013). Accordingly, if PPM1F indeed serves a critical function in integrin activity regulation, one would expect a severe phenotype upon inactivation of the *ppm1f* gene.

To test this prediction, we employed mice containing a gene-trap insertion in exon 4 of the *ppm1f* gene resulting in disruption of the *ppm1f* gene (Fig. 9 A). The genotype of the mice containing the disrupted *ppm1f* allele was verified by PCR (Fig. 9 B). While crosses between WT (*ppm1f*^{+/+}) and heterozygous (*ppm1f*^{+/-}) mice led to the expected 50:50 ratio of *ppm1f*^{+/+} and *ppm1f*^{+/-} offspring, crosses between heterozygous *ppm1f*^{+/-} animals yielded no homozygous *ppm1f*^{-/-} pups, suggesting that PPM1F-deficient embryos die in utero (Fig. 9 C). Timed matings showed that *ppm1f*^{-/-} embryos were not present at embryonic day (E) 12.5, E13.5, or E14.5 of development, but putative *ppm1f*^{-/-} embryos were detected at E10.5, when ~20% (9 out of 50 total) embryos showed retarded development (Fig. 9 D). These embryos were about half the size of the other embryos, displayed malformed forebrain structures, and showed reduced development of the branchial arches (Fig. 9 D). This observation suggested that

ppm1f^{-/-} embryos die before or around E10.5 in utero. To unambiguously determine their genotype, we isolated primary murine embryonic fibroblasts (MEFs) from E10.5 embryos. PCR on genomic DNA of isolated fibroblasts confirmed that the small malformed embryos harbor two dysfunctional PPM1F alleles (*ppm1f*^{-/-}), while the normal-sized embryos were either homozygous for the WT allele or heterozygous (*ppm1f*^{+/-}; Fig. 9 E). Primary fibroblasts from *ppm1f*^{-/-} mouse embryos and WT littermates were immortalized by retroviral transduction with SV40 largeT antigen, and WB with polyclonal anti-murine PPM1F (mPPM1F) antibodies demonstrated the absence of the full-length enzyme or any truncated *ppm1f* gene products in *ppm1f*^{-/-} KO fibroblasts (MEF PPM1F^{-/-}; Fig. 9 F). Already during regular cell culture, MEF PPM1F^{-/-} showed enhanced cell attachment to the culture dish, and it took longer to detach these cells during passaging. When placed onto fibronectin, the primary *ppm1f*^{-/-} cells showed pronounced accumulation of active integrin β 1 and talin at peripheral focal adhesion sites (Fig. 9 G). Most importantly, phosphorylation of the threonine motif in the integrin β 1 cytoplasmic tail was strongly elevated in the MEF PPM1F^{-/-} cells compared with the WT cells (Fig. 9 H). The enhanced integrin phosphorylation in MEF PPM1F^{-/-} cells correlated with elevated levels of active integrin β 1 (Fig. 9 I) and translated into increased adhesiveness on low (0.4 μ g/ml) and high (10 μ g/ml) concentrations of the integrin ligand fibronectin (Fig. 9 J). Furthermore, the enhanced integrin-mediated cell adhesion directly translated into reduced cell migration velocity and migration distance of MEF PPM1F^{-/-} cells (Fig. 9 K). These results highlight the severe consequences of PPM1F deletion on integrin function in primary cells. Together, our data further confirm a critical and nonredundant role of PPM1F as a negative regulator of integrin activity during embryonic development and during physiological integrin-dependent processes such as cell adhesion, spreading, and migration.

Discussion

Dynamic modulation of integrin activity is indispensable for the normal functioning of animal cells, especially with regard to cell attachment, spreading, and migration (Morse et al., 2014; Shattil et al., 2010). Integrin activity is controlled by protein–protein

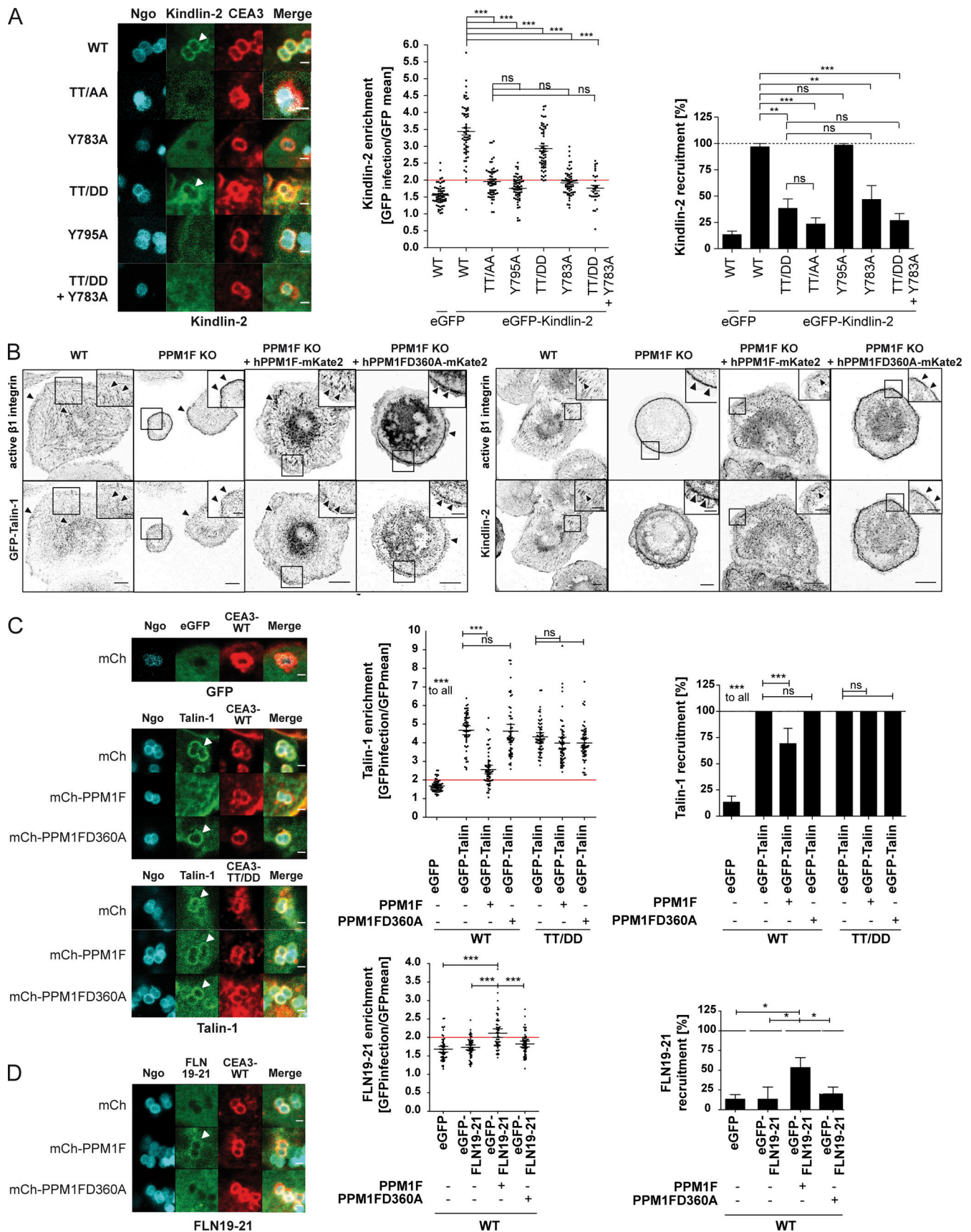


Figure 8. **Kindlin2 and talin versus filaminA recruitment are dictated by integrin $\beta 1$ phosphorylation and PPM1F activity in intact cells.** (A) 293T cells were cotransfected with indicated CEA3-integrin $\beta 1$ cytoplasmic tail fusion proteins together with GFP-kindlin-2. After 48 h, cells were infected with

CEACAM-binding bacteria (Ngo) for 1 h, fixed, and stained for CEACAM3. Micrographs (left panel) show representative infection sites of bacterial attachment (blue) and CEA3-integrin β 1 clustering (red). Recruitment of GFP-kindlin-2 (green) to clustered integrin cytoplasmic tails is indicated (white arrowhead). Scale bar, 1 μ m. Kindlin-2 recruitment was quantified with the enrichment ratio (ER) indicating the -fold enrichment of GFP intensity at bacterial attachment sites versus the overall cellular GFP level (middle panel). Data from GFP-transfected cells (Fig. 2 A) were used as negative control for statistical calculations. Dots represent individual ER values of 30–60 recruitment sites from $n \geq 2$ independent experiments. Horizontal lines indicate mean values and 95% confidence intervals (whiskers). The red line indicates the threshold of positive recruitment. The bar graph (right panel) depicts the percentage of cells showing a ratio of kindlin-2 recruitment ER ≥ 2 . Statistically significant differences were evaluated using one-way ANOVA, followed by Bonferroni post hoc test (***, $P < 0.001$; **, $P < 0.01$). (B) A172 WT, PPM1F KO, or PPM1F KO cells reexpressing mKate-tagged PPM1F or PPM1F D360A were seeded directly or 48 h after transfection with GFP-talin-1 onto 2 μ g/ml FN_{III9-11} for 1.5 h. Cells were fixed, stained with antibodies against active integrin β 1 (9EG7) and optionally against kindlin-2, and analyzed by confocal microscopy; scale bar, 10 μ m. Arrowheads point to active integrin β 1/talin or kindlin-2 enrichment. Insets: Higher magnification of boxed area; scale bar, 5 μ m. (C and D) 293T cells were cotransfected with indicated CEA3-integrin β 1 cytoplasmic tail fusion protein in the WT (CEA3-WT) or T788D/T789D (CEA3-TT/DD) form together with GFP, GFP-talin-1 (C), or GFP-FLN19-21 (D). After 48 h, cells were infected with CEACAM-binding bacteria (Ngo) for 1 h, fixed, and stained for CEACAM3. Micrographs (left panel) show representative infection sites of bacterial attachment (blue) and CEA3-integrin β 1 clustering (red). Recruitment of GFP proteins (green) to integrin cytoplasmic tails is indicated (white arrowhead). Scale bar, 1 μ m. Protein recruitment was quantified with the ER indicating the fold enrichment of GFP intensity at bacterial attachment sites versus the overall cellular level (middle panel). Dots represent individual ER values of 60 recruitment sites from three independent experiments. Horizontal lines indicate mean values and 95% CIs (whiskers). The red line indicates the threshold of positive recruitment. The bar graph (right panel) depicts the percentage of cells showing a ratio of protein recruitment ER ≥ 2 . Statistically significant differences were evaluated using one-way ANOVA, followed by Bonferroni post hoc test (***, $P < 0.001$; *, $P < 0.05$). See also Fig. S1.

interactions occurring at the cytoplasmic tail of the integrin β subunit, and the fine-tuning of cell adhesion requires regular transitions from talin/kindlin-bound active to filaminA-associated inactive integrin. Here we identify the molecular machinery that executes this integrin activity switch: the cytoplasmic metal-dependent protein phosphatase PPM1F. This serine/threonine phosphatase acts on a conserved threonine motif located in the cytoplasmic tail of most integrin β subunits and thereby controls filamin binding. Accordingly, this phosphatase represents the first enzyme known to directly regulate integrin activity.

PPM1F belongs to the PPMs, which, in contrast to the family of phospho-protein phosphatases, do not rely on regulatory subunits for subcellular localization and substrate recognition (Moorhead et al., 2009; Stern et al., 2007). Instead, these phosphatases harbor additional domains involved in protein-protein interaction and phosphatase activity regulation (Ishida et al., 2018). The tertiary structure of PPM1F is not known, but a PPM family member from *Caenorhabditis elegans* termed FEM-2 (sharing ~25% sequence identity with human PPM1F) has been crystallized (Zhang et al., 2013). Though the N-terminal domain of FEM-2 exhibits a large intramolecular binding interface with the C-terminal catalytic domain, in vitro experiments did not indicate a role of the N terminus in regulating phosphatase activity, but rather in mediating protein-protein interactions (Zhang et al., 2013). In this regard, PPM1F is known to bind the focal adhesion protein β -PIX and has been identified by unbiased mass spectrometry approaches as a constituent of focal adhesions (Schiller et al., 2011). PPM1F also functions as a negative regulator of the β -PIX-associated protein serine/threonine kinase PAK and of CaMKII (Harvey et al., 2004; Ishida et al., 1998; Koh et al., 2002). In both cases, PPM1F shows preference for phospho-threonine (pT) residues located in the activation loops of these kinases (Ishida et al., 2008). Interestingly, the amino acid sequences surrounding these known PPM1F target motifs in PAK and CaMKII (K/Rx₍₁₋₂₎TxV) are highly reminiscent of the sequence (Kx₂TTV) encompassing T788/T789 in integrin β 1. As such a motif occurs also in the cytoplasmic domains of human integrins β 2, β 3, β 5, β 6, and β 7, it can be envisioned

that this ubiquitously expressed threonine phosphatase controls a larger set of integrin heterodimers. It is important to note that PPM1F, but not the related PPM family member ILKAP, readily dephosphorylated the phospho-T788/T789 motif. In myoblasts, the phosphatase PP2A has been shown to associate with and dephosphorylate the T788/T789 motif on integrin β 1 (Kim et al., 2004). Striated muscle cells require stable, long-term adhesion for their physiological function. Therefore, PPM1F-mediated negative regulation of integrin activity might not be required to the same extent in this tissue, where PP2A could be involved in integrin regulation. Though additional enzymes might be able to dephosphorylate phospho-T788/T789 of integrin β 1, the prominent gain in integrin function in normal fibroblasts and glioma cells upon PPM1F depletion and the severe phenotype of homozygous deletion of PPM1F in the mouse strongly argue for a unique role of PPM1F. The idea that the integrin β 1 subunit is a major target of PPM1F is supported by the constitutive T788/T789 phosphorylation, the enhanced talin recruitment, and the exaggerated integrin β 1 activity seen in all examined PPM1F-deficient cells. The biochemical consequence of PPM1F action, namely filaminA binding to the T788/T789 motif, nicely explains how this phosphatase can have a direct impact on integrin activity.

The proposed phospho-switch mechanism in the integrin β 1 subunit and the role of filaminA in this context is in line with previous reports on the integrin β 7 and integrin β 2 subunits (Kiema et al., 2006; Takala et al., 2008). Structural modeling clearly indicates that sterical hindrance and charge repulsion will prohibit filaminA from binding to the phosphorylated T788/T789 motif in integrin β 1, and we experimentally confirm this binding pattern with pseudo-phosphorylated recombinant proteins as well as synthetic phospho-peptides. Intriguingly, our in vitro competition assays demonstrate that filaminA readily displaces the talin band 4.1, ezrin, radixin, moesin (FERM) domain as well as kindlin2 from the integrin β 1 tail, but can do so only in the absence of T788/T789 phosphorylation (Fig. 10 A). Phosphorylation of this conserved motif and the resulting dissociation of filamin grants talin access to the membrane proximal NPxY motif (Fig. 10, B and C). The binding of talin to the

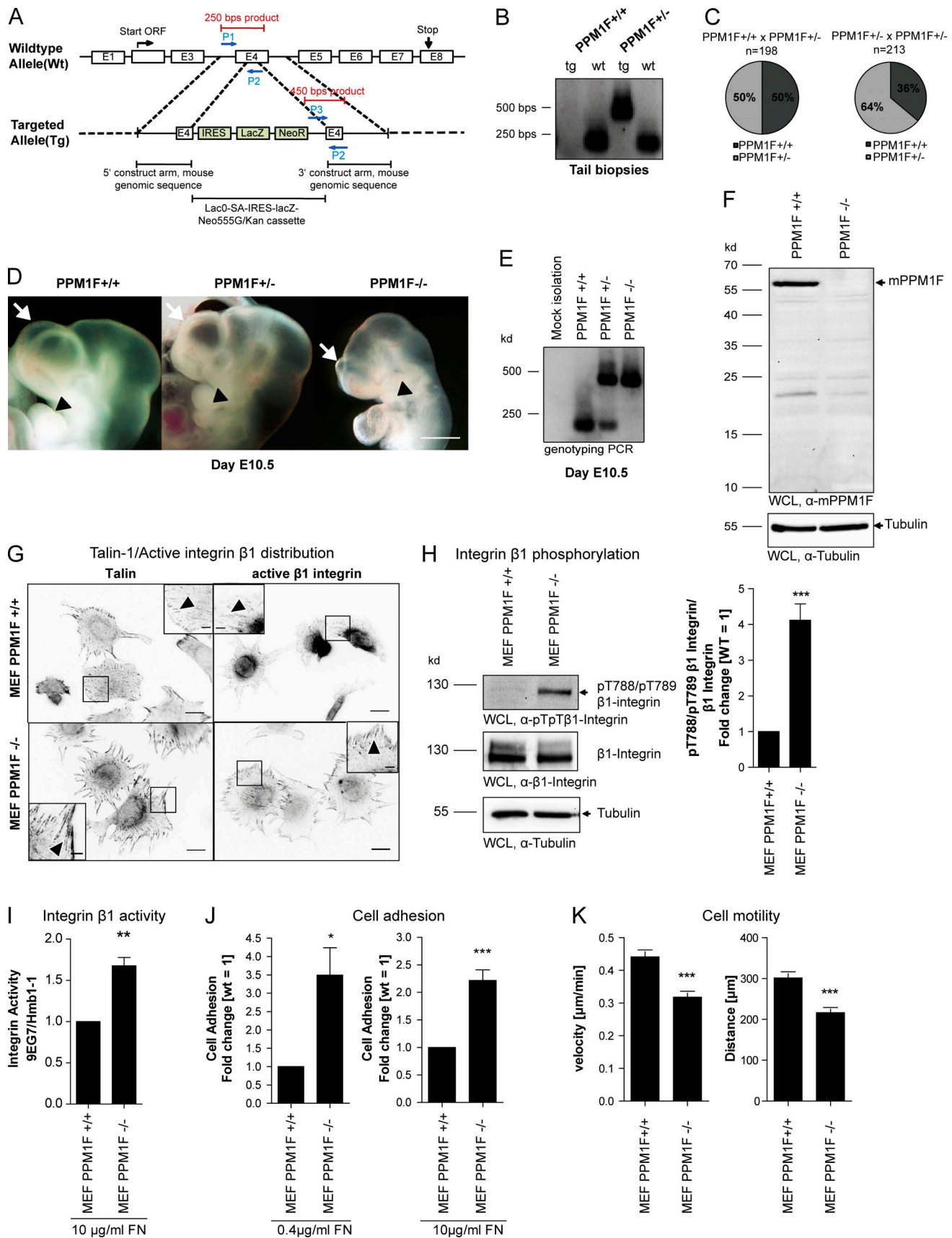


Figure 9. Homozygous disruption of the *ppm1f* gene results in embryonic lethality and *ppm1f*^{-/-} fibroblasts show constitutive T788/T789 phosphorylation, elevated integrin activity, and increased cell adhesion. (A) Schematic representation of the WT and targeted *ppm1f* locus. Insertion of a

lacZ-neomycin-resistance cassette into exon 4 resulted in gene disruption and expression of β -galactosidase under the control of the *ppm1f* gene promoter. The primers used for genotyping (blue) and the resulting PCR fragments (red) are shown. E, exon number; P1, gene specific primer forward; P2, gene specific primer reverse; P3, targeted primer forward. **(B)** DNA extracts from tail biopsies were genotyped by PCR using primers indicated in A to result in a 250-bps product (WT allele, P1, P2) or a 450-bps product (targeted allele, P2, P3). **(C)** *ppm1^{+/+}* and *ppm1^{-/-}* mice were mated as depicted, and the offspring was genotyped after weaning by PCR using DNA extracts from tail biopsies. **(D)** Close-up view of head morphology at E10.5 from WT, *ppm1^{+/+}*, and *ppm1^{-/-}* embryos. *Ppm1^{-/-}* embryos are smaller in size and exhibit a stunted telencephalon (white arrow) and reduced development of branchial arches (black arrowhead). Scale bars, 1 mm. **(E)** Two *ppm1^{-/-}* mice were mated, and genomic DNA was extracted from fibroblasts isolated from *ppm1^{+/+}* (WT), *ppm1^{-/-}* (heterozygous), and *ppm1^{-/-}* mouse embryos at E10.5 (MEFs). Genotyping PCR identified WT, heterozygous, and homozygous *ppm1* KO embryos. **(F)** WCLs from MEFs isolated from WT (PPM1F^{+/+}) or from *ppm1^{-/-}* embryos were probed with polyclonal α -mPPM1F antiserum (upper panel) or monoclonal α -tubulin (lower panel). PPM1F^{-/-} cells do not express truncated versions of PPM1F. **(G)** MEFs as in F were seeded onto 1 μ g/ml FN₁₁₉₋₁₂ for 2 h. Samples were fixed and stained for talin (left row) or the active integrin β 1 (right row) before analysis by confocal microscopy; scale bar, 20 μ m. Insets show higher magnification of boxed areas; scale bar, 5 μ m. Arrowheads point to active integrin β 1 or talin enrichment. **(H)** MEFs as in F were seeded onto 2 μ g/ml FN₁₁₉₋₁₂ for 45 min, and WCLs were subjected to WB with indicated antibodies (left panels). Bar graphs (right panels) show densitometric quantification of band intensities from pT788/pT789- β 1 versus total β 1 integrin antibody signal from four independent experiments; WT was set to 1. Statistics was performed using one-way ANOVA, followed by Bonferroni post hoc test (***, $P < 0.001$). **(I)** MEFs as in F were kept in suspension for 45 min and incubated for 15 min with 10 μ g/ml FN₁₁₉₋₁₂ (FN). Samples were stained for total (Hmb1-1) or active β 1 integrin (9EG7) and analyzed by flow cytometry, $\geq 10,000$ counts. The mean fluorescence intensity (MFI) ratio of active to total β 1 integrin was calculated and normalized to the WT sample (= 1). Bars represent mean MFI \pm SEM of three independent experiments; statistics was performed using unpaired Student's *t* test (**, $P < 0.01$). **(J)** MEFs as in F were seeded in triplicate onto fibronectin-coated wells for 20 min, and cell adhesion was quantified. Bars represent mean \pm SEM of five independent experiments performed in triplicate. Values were normalized to MEF WT cells (= 1). Statistics was performed using unpaired Student's *t* test (***, $P < 0.001$; *, $P < 0.05$). **(K)** Serum-starved MEFs were stimulated by addition of 10% FCS, and cell migration was monitored every 30 min for 12 h using time-lapse microscopy. Cell tracks were evaluated for velocity and covered distance. Bars show mean \pm SEM of three independent experiments. Samples were done in duplicate, each $n = 15$; unpaired *t* test (***, $P < 0.001$).

phosphorylated integrin tail unclasps the integrin α and β subunits and leads to extension of the bend extracellular domains (Fig. 10 C). In this situation, talin binding is required before kindlin2 can associate with the membrane distal NPxY motif, as the T788/T789 motif is phosphorylated (Fig. 10 D). Upon kindlin2 binding, the active conformation of integrins is further stabilized, and integrin-mediated adhesion is further promoted by receptor clustering (Fig. 10 D). The phosphorylation-guided cooperation between talin and kindlin, as suggested by our in vitro and in vivo data, could be a means to safeguard against a kindlin2-mediated inside-out activation of integrins in the absence of prior talin binding. In retrospect, these findings now provide a mechanistic explanation for the previously observed adhesion phenotype of integrin β 1 T789D and of integrin β 1 TT788/789AA-expressing cells, which appear locked in either the active or inactive situation (Nilsson et al., 2006; Wennerberg et al., 1998). Our novel observations also nicely combine with previous results in a coherent picture of integrin activity regulation from within the cell (inside-out signaling). It has been noted before that overexpression of the isolated talin FERM domain can trigger inside-out signaling of integrin β 1 and β 3, while kindlin overexpression on its own is not sufficient, but rather intensifies talin-initiated integrin activity (Harburger et al., 2009; Li et al., 2017; Ma et al., 2008; Ye et al., 2010). On the other hand, kindlin critically contributes to integrin activity when cells respond to an integrin ligand and reorganize their cytoskeleton during outside-in signaling (Böttcher et al., 2017; Montanez et al., 2008; Theodosiou et al., 2016).

Interestingly, clustering of the WT integrin β 1 chimera in intact cells, a situation mimicking the unclasped integrin, does not lead to filaminA recruitment. This finding could indicate that the threonine motif is mainly phosphorylated when the integrin β subunit is separated from the integrin α subunit. Intriguingly, upon overexpression of PPM1F, but not PPM1F D360A, filaminA accumulates at the WT integrin β 1 cytoplasmic tail. This observation suggests that the activity of the

overexpressed phosphatase can override a potential default phosphorylation of the threonine motif in the unclasped integrin β subunit to allow filaminA binding. It is interesting to speculate that a default phosphorylation of the conserved threonine motif in the isolated WT integrin β 1 tail would not only promote displacement of the negative regulator filamin but also prohibit kindlin2 from driving integrin inside-out signaling in the absence of talin. This scenario is in line with the observation that kindlin overexpression does not lead to integrin inside-out activation (Ma et al., 2008; Harburger et al., 2009; Ye et al., 2010; Li et al., 2017).

A major remaining question is where and when the conserved threonine motif in integrin β subunits is phosphorylated and which kinase(s) are involved in this regulatory step. Phosphorylation of the conserved integrin threonine motif has been most intensely studied for the integrin β 2 subunit, where T758/T759 form part of the Kx₂TTTV motif in the cytoplasmic tail. In this case, stimulation of G-protein-coupled receptors or the T cell receptor leads to phosphorylation of T758 in integrin β 2 and enhanced integrin-mediated cell attachment (Chatila et al., 1989; Fagerholm et al., 2005; Takala et al., 2008; Uotila et al., 2014; Valmu et al., 1991). Application of PKC inhibitors abrogates T758 phosphorylation, and the corresponding synthetic peptides of the integrin cytoplasmic domain are phosphorylated in vitro by conventional and unconventional PKC enzymes (Fagerholm et al., 2002). However, additional kinases such as CaMKII have been shown to associate with the integrin β 1 subunit in breast tumor cells (Takahashi, 2001), and inhibitors of CaMKII prevent the increase in T789 phosphorylation driven by constitutive active Ndr1 kinase, an abundant kinase in differentiating neurons (Rehberg et al., 2014). Our kinase assays with the purified integrin β 1 cytoplasmic domain now confirm that CaMKII is a bona fide integrin kinase. These studies indicate that multiple serine/threonine kinases can relay signaling inputs, eventually originating from different extracellular and/or intracellular cues, toward the integrin β 1 cytoplasmic domain.

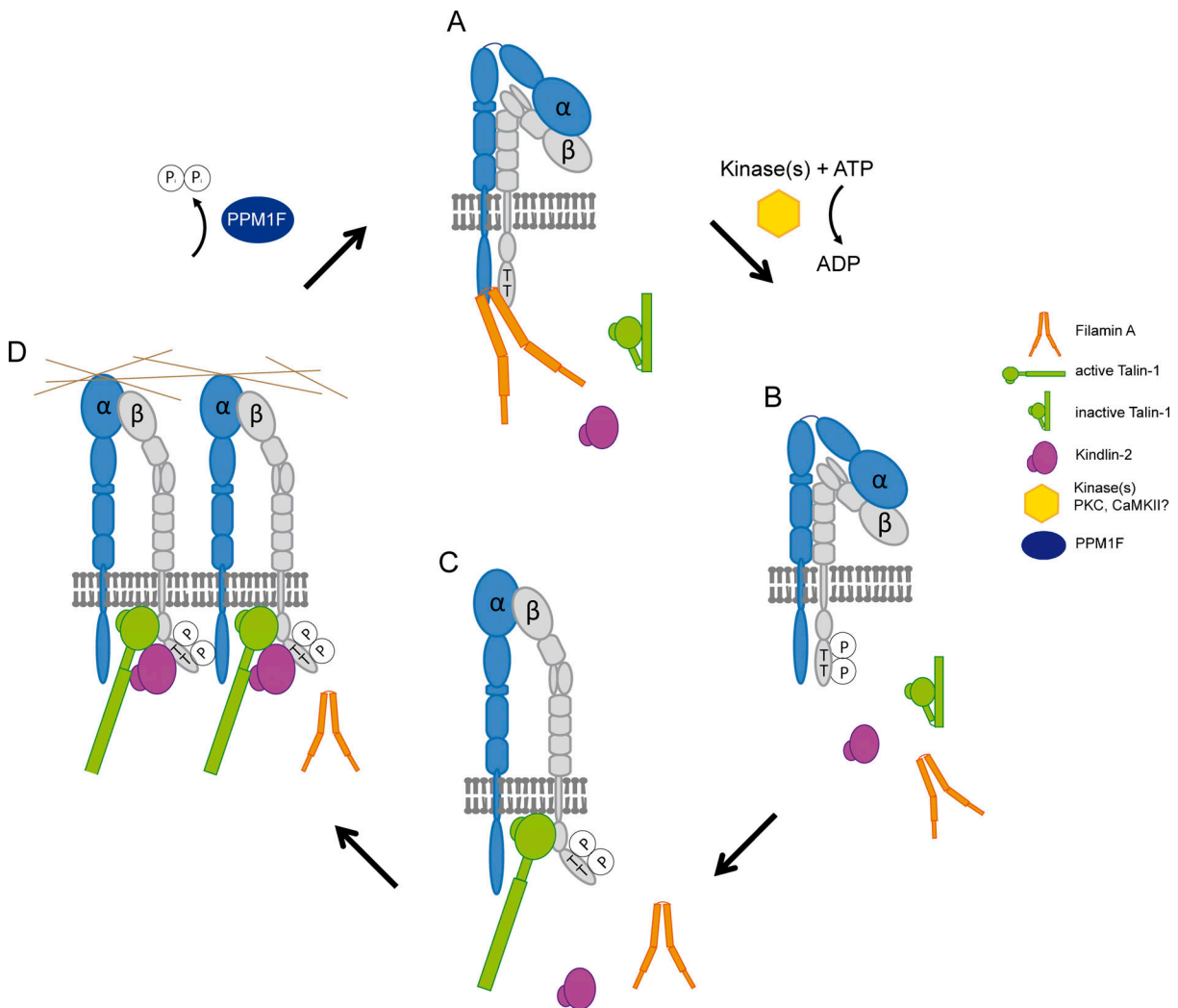


Figure 10. Phosphorylation and dephosphorylation of the conserved threonine motif in the integrin β tail orchestrate the regulation of integrin activity. (A) FilaminA stabilizes the inactive, clapsed low-affinity integrin conformation by outcompeting talin and kindlin-2 at the integrin β tail. (B and C) Upon phosphorylation of integrin β 1 at T788/T789 by integrin-targeted kinase(s), filaminA is displaced, and integrins are primed for (C) inside-out activation by talin, resulting in integrin tail separation and a conformational change to the active, unclapsed high-affinity integrin state. (D) Talin-initiated tail reorientation promotes cooperative kindlin association (sequentially or simultaneously), integrin clustering (with multivalent ligands), and further integrin downstream signaling. Counteracting these processes, PPM1F-mediated dephosphorylation of integrin β 1 T788/T789 allows (re)association of filaminA, which displaces talin and kindlin from the cytoplasmic tail and favors the closed integrin conformation. P, phospho-; T, threonine; w/o, without.

Our finding of a strong elevation of integrin phosphorylation upon deletion of a single phosphatase was therefore unexpected. However, in several distinct human cell types and in different scenarios, such as matrix-attached or suspended cells, PPM1F deficiency leads to constitutive T788/T789 phosphorylation. It has to be noted that apart from the integrin β 1 subunit, PPM1F acts on additional substrates such as kinases, cytoskeletal proteins, and apoptosis regulators (Zhang et al., 2013; Ishida et al., 2018). Therefore, it remains to be determined whether the abortion of embryonic development seen in PPM1F KO mice is a direct consequence of alterations in integrin activity and to what extent deregulation of other PPM1F substrates may play a role. However, the early embryonic lethality observed upon disruption of genes encoding integrin β 1, talin, kindlin, filaminA, and PPM1F in mammals and the functional interplay of these proteins in intact cells strongly argue for a

critical role of PPM1F-mediated integrin activity regulation *in vivo*.

It is easily conceivable that PPM1F is ideally suited to serve as key control for the T788/T789 phospho-switch, as it dephosphorylates the integrin β cytoplasmic domain, and this phosphatase is also able to reverse the auto-phosphorylation of CaMKII at Thr286 (Harvey et al., 2004; Ishida et al., 1998). Thus, PPM1F could shift the balance toward the unphosphorylated, inactive integrin by acting on both an integrin-directed serine/threonine kinase and the integrin T788/T789 motif itself. Taken together, our study identifies PPM1F as the enigmatic integrin phosphatase that acts on the highly conserved threonine motif in the integrin β cytoplasmic domain (Gahmberg et al., 2014). Thereby, this widely expressed protein phosphatase functions as an essential constituent of the integrin off-switch. In contrast to other negative regulators of integrins, such as ICAP-1 α , Sharnpin,

or Dok1, PPM1F has a defined enzymatic activity that can serve as a target for small molecule modulators. Given the important role of fine-tuning integrin activity in thrombus formation, immune cell motility, or wound healing, agonists as well as antagonists of PPM1F could provide novel access points to adjust integrin activation thresholds.

Materials and methods

Antibodies used

The following antibodies were used with the corresponding dilutions for WB, immunofluorescence (IF), immunohistochemistry, or integrin activity assay (IA): α -actinin (BM75.2; mouse anti-human/anti-mouse; Abcam; 1:1,000 WB), α_1 -integrin (TS2/7; mouse anti-human/anti-mouse; Abcam; 1:50 IF), α_2 -integrin (6F1; mouse anti-human/anti-mouse; DSHB; 1:60 IF), α_3 -integrin (PIB5; mouse anti-human/anti-mouse; DSHB; 1:60 IF), α_5 -integrin (BIIG2; rat anti-human; DSHB; 1:10 IF; and MFR5; rat anti-mouse; BD Pharmingen; 1:300 IF), α_v -integrin (PE-P2W7; mouse anti-human/anti-mouse; sc-9969; 1:300 IF), β_1 -integrin (AIIB2; IgG₁, rat anti-human; DSHB; 1:600 IA; and HM β 1-1, armenian hamster anti-mouse; BioLegend; 1:300 IF/IA; and D2E5; rabbit anti-human; Cell Signaling; 1:1,000 WB), active β_1 -integrin (9EG7; G₁, rat anti-human/anti-mouse; generous gift of D. Vestweber, Max-Planck-Institut for Molecular Medicine, Münster, Germany; 1:300 IA/IF), pT788/789 β_1 -integrin (44-872G; rabbit anti-human; Thermo Fisher Scientific; 1:1,000 WB), β_3 -integrin (2C9.G3; Armenian hamster anti-human/anti-mouse; eBioscience; 1:300 IF), β_5 -integrin (AST-3T; mouse anti-human; BioLegend; 1:150 IF; and KN-52; mouse anti-mouse/human; eBioscience; 1:300 IF), carcinoembryonic antigen-related cell adhesion molecule (CEACAM) 1,3,4,5,6 (D14HD11; Aldevron; 1:6,000 WB, 1:200 IF), Ezrin (MAB3822; mouse anti-human; Millipore; 1:200 WB), FAK (77; mouse anti-human; BD Biosciences; 1:250 WB), ILK (EP1593Y; rabbit anti-human; Epitomics; 1:800 WB), Kindlin-2 (3A3; mouse anti-human; Millipore; 1:200 WB, 1:250 IF), paxillin (5H11; mouse monoclonal; Thermo Fisher Scientific; 1:1,000 WB), hPPM1F (17020-1-AP; rabbit anti-human; Protein-Tech; 1:1,000 WB), mPPM1F (1147; rabbit anti-mouse PPM1F; generated at the Tierforschungsanlage, University of Konstanz [see below]; 1:200 WB), filaminA (EP2405Y; IgG, rabbit anti-human; Epitomics; 1:125,000 WB; and PM6/317; mouse anti-human, Millipore; 1:100 IF), Tubulin (E7, IgG1, mouse anti-human, DSHB; 1:1000), Talin (8d4, mouse anti-human; Thermo Fisher Scientific; 1:800 WB, 1:40 IF), vinculin (hVIN-1; mouse anti-human; Sigma-Aldrich; 1:2,000 WB, 1:200 IF), Zyxin (Zol301; mouse anti-human; Abcam; 1:1,000 WB), GFP (J1-8; Clontech; 1:3,000 WB), GST (B-14 sc-138; Santa Cruz; 1:1,000 WB, 1:500 ELISA), 6x His (H8; Thermo Fisher Scientific; 1:1,000 WB and ELISA), Dylight488-conjugated goat anti-mouse IgG (Jackson; 1:200), Cy3-conjugated goat anti-rabbit IgG (Jackson; 1:200), Cy3-conjugated goat anti-mouse IgG (Jackson; 1:200), Cy5-conjugated goat anti-mouse IgG (Jackson; 1:200), RhodamineRed-conjugated goat anti-rat IgG (Jackson; 1:200), RhodamineRed-conjugated goat anti-Armenian hamster IgG (Jackson; 1:200), Cy5-conjugated phalloidin (A22287; Molecular Probes; 1:100), HRP-conjugated goat anti-mouse IgG (Jackson;

1:10,000 WB), HRP-conjugated goat anti-rat IgG (Santa Cruz; 1:250), HRP-conjugated goat anti-rabbit IgG (Jackson; 1:3,000 WB), streptactin-HRP (IBA Lifesciences; 1:10,000 WB, 1:1,000 ELISA), murine endoglin (CD105; rat anti-mouse, MJ7/18; DSHB), and unspecific control IgG (anti-mouse 96/1; generated at the Tierforschungsanlage, University of Konstanz).

Recombinant DNA

For the construction of His-Sumo-tagged talin F3 subdomain of the FERM domain (residues 309–411), the murine talin1 cDNA (kindly provided by R. Fässler, Max-Planck-Institut Biochemie, Martinsried, Germany) was amplified with the following primers: mTalin1 F3-forward: 5'-GACGGTCTCAAGGTGGTGTCTCCTTCTTCTAGTC-3' and mTalin1 F3-reverse: 5'-GTCTCTAGATTACAGCCCAAATGGTCTTGGCTG-3'. The resulting PCR fragment was cloned into pET24a His-Sumo bacterial expression vector (Andréasson et al., 2008) via BsaI and XhoI restriction sites. For construction of GFP-tagged talin, cDNA of human talin-1 (kindly provided by R. Fässler) was cloned into pDNR Dual (Clontech) using the following primers and restriction digest with Sall/AgeI: hTalin1_Sall_sense: 5'-GAAGTTATCAGT CGACACCATGGTTGCACTTTCAGTGAAG-3' and hTalin1_AgeI_anti: 5'-GTCATACCGGTTTGTAGTCTCATCTCGAAGCTCTG-3'. Cre/LoxP recombination was used to move sequences from pDNR Dual into pEGFP-C1-loxP for eukaryotic expression.

Human kindlin2 cDNA (ID4547604 in pOTB7; Source Bioscience) was used as a template for PCR amplification with the following primers: hKindlin-2_Sall_sense: 5'-ATCAGTCGACGC TCTGGACGGGATAAGGATG-3' and hKindlin-2_BamHI_anti: 5'-TACCGGATCCTCACACCCAACCACTGGTAAG-3'. The product cloned into pDNR Dual via Sall/BamHI restriction digest. The kindlin2 cDNA was transferred to pEGFP-C1-loxP vector by Cre-recombination. Mouse kindlin2 cDNA (pCMV-SPORT6; Source Bioscience) was used as a template for PCR amplification with the following primers: mKindlin2_LIC_sense: 5'-ACTCCTCCC CCGCCATGGCTCTGGACGGGATAAGGATG-3' and mKindlin2_LIC_anti: 5'-CCCCACTAACCCGTCACACCCAACCACTGGTGAG-3'. The product was cloned into pDNR Dual-LIC vector by ligation-independent cloning (LIC; Adrian et al., 2019). The mKindlin-2 insert was cloned into pET24a-His-SUMO by PCR amplification with the following primers: mKindlin-2_BamHI_sense: 5'-TAT AGGATCCCATGGCTCTGGACGGGATAAG-3' and mKindlin-2_XhoI_anti: 5'-TATACTCGAGTCACACCCAACCACTGGTGAG-3' and by restriction digest with BamHI and XhoI enzymes.

The integrin-binding part of filaminA (filaminA Ig19-21 [FLNIg19-21]) was generated by amplifying human filaminA (plasmid 8982; Addgene) with the following primers: FLNIg19-forward 5'-ACTCCTCCCCCGCATGATCAGCCAGTCGGAAATT G-3' and FLNIg21-reverse 5'-CCCCACTAACCCGAGCCACAGGCA CCACGAAG-3'. It was cloned into pDNR-Dual-LIC. FLNIg19-21 cDNA was subsequently transferred to pEGFP-C1-loxP by Cre-mediated recombination, generating GFP-FLNIg19-21 for mammalian expression, and to pGEX4T1 loxP (Schmitter et al., 2007) for bacterial expression of GST-FLNIg19-21.

For His-Sumo-tagged FLNIg19-21, the respective filaminA sequence was amplified by PCR with the primer pair FLNIg19-forward: 5'-GACGGTCTCAGGTGGGGATGCCAGTCTGT

TCGGCTCTCTG-3' and FLN1g21-reverse: 5'-CTGATGCTCGAGTTA AGACGGAGAAGCCACAG-3'. The resulting PCR fragment was cloned into pET24aHis-Sumo via BsaI and XhoI restriction sites.

cDNA of control protein yeast enolase-1 was obtained by genomic DNA extraction (PureLink Genomic DNA Mini Kit; Thermo Fisher Scientific) from *Candida albicans* SC5314 (generous gift of J. Morschhäuser, University of Würzburg, Würzburg, Germany) and PCR amplification using the following primers: enolase-1 BamHI sense: 5'-ATAGGATCCGATGTCTTA CGCCACTAAAATCC-3' and enolase-1 XhoI NEF anti: 5'-ATACTC GAGTTATTTAAAGTATTCGGGCCCAATTGAGAAGCCTTTTGG-3'. The resulting PCR fragment was cloned into pET24aHis-Sumo via BamHI and XhoI restriction sites.

For the production of recombinant GST-tagged cytoplasmic tail of integrin β 1, the human integrin β 1 cDNA (plasmid 54129; Addgene) was amplified by PCR with the following primer pair: h β 1Integrin-cyto-EcoRI-sense: 5'-ATAGAATTCTGGAAGCTT TTAATGATAATTC-3' and h β 1Integrin-cyto-XhoI-anti: 5'-ATA CTGAGTCATTTCCCTCATACTTCG-3'. The cDNAs of human integrin β 1 T788A/T789A, T788D, and T788D/T789D cytoplasmic domains were custom synthesized (Eurofins Genomics GmbH) and amplified using the same primer pair as for WT β 1 integrin. PCR products of integrin β 1 WT and T788A/T789A were cloned into pGEX-4T1 via EcoRI/XhoI restriction sites to yield an N-terminal GST-tagged fusion protein, respectively. The Y795A mutation was inserted by using integrin β 1 WT cDNA as a template and the following primers: integrin β 1 Y795A BamHI sense: 5'-GCTATGGATCCCATGACAGAAGGGAGTTTG-3' and integrin β 1 Y795A XhoI anti: 5'-ATATCTCGAGTCATTTCCCT CCGCCTTCGGATTG-3'.

The Strep-tag vector for bacterial expression of Strep-tagged integrin cytoplasmic domains was produced by custom gene synthesis (pEX-A128 Strep-integrin β ; Eurofins Genomics GmbH) according to Pfaff et al. (1998). Briefly, the *E. coli* codon-optimized cDNA encompasses an N-terminal Twin-StrepII-tag and a coiled-coil domain encoding a heptad-repeat coiled-coil-forming region followed by in-frame BamHI/XhoI restriction sites for insertion of integrin cytoplasmic tails. Using NcoI/XhoI restriction sites, the Strep-tag and coiled-coil sequence of pEX-A128 Strep-integrin β was ligated into the pET28a(+) vector (Novagen; Merck Millipore). Strep-tagged integrin β 1 WT, T788D, T788D/T789D, T788A/T789A, and Y795A constructs were produced by BamHI/XhoI restriction digest of corresponding pGEX-4T1 vectors and subcloning of the integrin β 1 tail cDNA into the Strep-tag vector. For the generation of Strep-tagged integrin β 1 Y783A, Strep-integrin β 1 WT cDNA containing vector was used as a template for site-directed mutagenesis with the following primers: integrin β 1 Y783A sense: 5'-CACGGG TGAAAATCCTATTGCTAAGAGTGCCGTAACAACATG-3' and integrin β 1 Y783A anti: 5'-CACAGTTGTTACGGCACTCTTAGCAATAGG ATTTTCACCCGTGTCCC-3'. To generate Strep-tagged β 1 integrin Y783A + T788D/T789D, Strep-tagged integrin β 1 T788D/T789D vector was used as a template for site-directed mutagenesis with the following primers: integrin β 1 Y783A DD sense: 5'-GGTGAA AATCCTATTGCTAAGAGTGCCGTAGAC-3' and integrin β 1 Y783A DD anti: 5'-GTCTACGGCACTCTTAGCAATAGGATTTTCACC-3'.

CEACAM3-integrin β 1 fusion constructs were generated via PCR amplification using the cDNA of human integrin β 1 WT, T788/789D, or T788/789A synthetic sequences as a template with following primers: integrin β 1_E762-K798_BamHI sense: 5'-GCGGCTATGGATCCGAGTTTGCTAAATTTGAAAAGGAGA AAATG-3' and integrin β 1_E762-K798_XhoI anti: 5'-TATCTC GAGTCATTTTCCCTCATACTTCGG-3'. PCR products were cloned into pcDNA3.1 CEACAM3 Δ ACT using BamHI/XhoI restriction sites (Baade et al., 2019; Schmitter et al., 2004). For the β 1 integrin Y783A construct, pcDNA3.1 CEA3- β 1 WT integrin-containing plasmid was used to perform site-directed mutagenesis using the following primers: integrin β 1 Y783A sense: 5'-CACGGGTGAAAATCCTATTGCTAAGAGTGCCGTAACAAC TG-3' and integrin β 1 Y783A anti: 5'-CACAGTTGTTACGGCACT CTTAGCAATAGGATTTTCACCCGTGTCCC-3'. CEACAM3-integrin β 1 Y783A + T788D/T789D fusion construct was generated via PCR amplification using Strep-tagged β 1 integrin Y783A + T788D/T789D as a template with the following primers: integrin β 1_E762-K798_BamHI sense: 5'-GCGGCTATGGATCCG AGTTTGCTAAATTTGAAAAGGAGAAAATG-3' and integrin β 1_E762-K798_XhoI anti: 5'-TATCTCGAGTCATTTTCCCTC ATACTTCGG-3'. The PCR product was cloned into pcDNA3.1 CEACAM3 Δ ACT using BamHI/XhoI restriction sites (Baade et al., 2019; Schmitter et al., 2004).

For the generation of mCherry- and GST-tagged PPM1F, the cDNA of human PPM1F (I.M.A.G.E. cDNA clone IRAUp969F10111D) was obtained from Source BioScience. The following primers were used for amplification: hPPM1F-IF-sense: 5'-GAAGTTATCAGT CGACACCATGTCTCTGGAGCCCC-3' and hPPM1F-IF-anti: 5'-ATG GTCTAGAAAAGCTTGCCTAGCTTCTTGGTGGAGC-3'. The resulting PCR fragment was cloned into pDNR-CMV using the In-Fusion dry-down PCR Cloning Kit (Clontech). The sequence-verified pDNR-CMV hPPM1F was used as donor vector, and the insert was transferred by Cre-mediated recombination into the acceptor vector pmCherry-C1-loxP (mammalian expression) and pGEX-4T1-loxP (bacterial expression) generating N-terminal-tagged pmCherry-hPPM1F and pGEX GST-hPPM1F. For the generation of mCherry- or GST-tagged hPPM1F D360A, the phosphatase dead mutant of PPM1F (Harvey et al., 2004), site-directed mutagenesis was performed with the hPPM1F-containing vectors using primers PPM1F-D360A-forward: 5'-GACTACCTG CTGCTAGCCTGTGCTGGCTTCTTTGACGTGC-3' and PPM1F-D360A-reverse: 5'-GTCAAAGAAGCCAGCACAGGCTAGCAGCAG GTAGTCCTC-3'.

For expression of PTP1B (a kind gift from W. Hofer, University of Konstanz, Konstanz, Germany), the cDNA was cloned into pDNR-Dual-LIC after PCR amplification using the primers PTP1B LIC sense: 5'-ACTCCTCCCCGCCATGGAGATGGAAAAGG AGTTCCG-3' and PTP1B LIC anti: 5'-CCCCACTAACCCGCTATG TGTTCGTGTTGAACAGG-3', followed by Cre-lox recombination into pGEX4T1 loxP vector for bacterial expression. All recombinant constructs were verified by sequencing.

Expression of recombinant proteins

Strep-tagged or GST-tagged integrin β 1 cytoplasmic domains and 6xHis-SUMO-tagged or GST-tagged TalinF3, Kindlin-2, FLN1g19-21, enolase-1, human 7xHis-TEV ILKAP (plasmid 34817;

Addgene; pQTEV vector by K. Buessow, Protein Structure Factory, Berlin, Germany), GST-tagged human PTP1B and human Trx-His-S-PP5 (a kind gift of D. Dietrich, University of Konstanz, Konstanz, Germany), and GST-tagged fibronectin type III repeats 9–11 (FN_{III9–11}; gift of M.A. Schwartz, Yale University, New Haven, CT) were expressed in *E. coli* as described for PPM1F. Proteins were purified using His- or GST-Trap FF column (GE Healthcare) or Streptactin Superflow column (IBA Lifesciences) depending on the protein and dialyzed against appropriate buffers.

Pulldown assays with integrin cytoplasmic domains

2.5 µg of Strep-tagged integrins or 10 µg of biotin-integrin phospho-peptide β1-762-798 pTpT (Biotin-EFAKFEKEKMNAKWDTGENPIYKSAV[pT][pT]VVNPKYEGK-OH) or biotin-integrin peptide β1-762-798 (Biotin-EFAKFEKEKMNAKWDTGENPIYKSAVTTVVNPKYEGK-OH; Novopep Limited) were loaded onto Strep-Tactin Sepharose beads (50% suspension; IBA Lifesciences) or streptavidin agarose beads (50% suspension; 16-126; Merck) in immunoprecipitation (IP) buffer (50 mM Tris, pH 7.5, 100 mM NaCl, 10% glycerol, and 0.05% Tween) with freshly added Na₃VO₄ (200 mM) and Na₄P₂O₇ (200 mM) for 30 min at RT under continuous rotation. After centrifugation (2,700 g, 2 min, 4°C), samples were washed three times with IP buffer. Then integrin-loaded beads were suspended in bait protein solution (corresponding amount of protein diluted in IP buffer) and incubated 2 h at 4°C under constant rotation. Samples were centrifuged (2,700 g, 2 min, 4°C) and washed again three times with IP buffer. Strep-Tactin samples were eluted under native conditions by adding 30 µl of buffer BXT (50 mM Tris, pH 8, 150 mM NaCl, 50 mM biotin; IBA Lifesciences). After 10 min incubation at RT under constant rotation, samples were centrifuged. Supernatants were mixed with 4× SDS and boiled for 5 min at 95°C before they were subjected to WB. Streptavidin agarose beads were directly mixed with 2× SDS and boiled for 10 min at 95°C to elute proteins from biotin-integrin peptides before they were subjected to WB.

Solid phase binding assay

96 wells (high-binding; 655061; Greiner Bio-One) were coated with 1 µM of His-Sumo-tagged or GST-tagged proteins in PBS (1.37 M NaCl, 26.8 mM KCl, 14.7 mM KH₂PO₄, and 78.1 mM Na₂PO₄) overnight at 4°C in triplicate. Wells were washed three times with PBS and blocked with 200 µl/well PBS plus 2% BSA for 1 h at RT before incubation with 0.5 µM of Strep-tagged integrin β1 proteins in PBS plus 0.05% Tween overnight at 4°C. For competitive assays with FLN19-21 and TalinF3 domain, Strep-tagged integrin β1 cytoplasmic domains were immobilized first before incubation with FLN19-21 and/or TalinF3. Wells were washed three times with PBS plus 0.05% Tween and blocked again for 1 h at RT. Streptactin-HRP (IBA Lifesciences) or mouse-α-His antibodies followed by HRP-conjugated goat α-mouse IgG antibodies for competitive assays were added in blocking buffer for 1 h at RT, respectively. Finally, wells were intensively washed with PBS plus 0.05% Tween, and 100 µl/well of tetramethylbenzidine (TMB) solution was added (9.5 ml of 2.4 mg/ml TMB in 1:9 acetone:ethanol plus 20 µl/10 ml H₂O₂ plus 0.5 ml 30mM potassium citrate, pH 4.1). The reaction was

stopped after 20 min by adding 100 µl/well 2 M H₂SO₄, and samples were measured at 450 nm in a microplate reader (Varioscan; Thermo Fisher Scientific).

Cell culture and transient transfection

Human embryonic kidney 293T cells (293T; American Type Culture Collection CRL-3216) and A172 glioblastoma cells (American Type Culture Collection CRL-1620) were grown in DMEM supplemented with 10% calf serum. NHDFs were obtained from PromoCell and cultured in PromoCell fibroblast growth medium. All cells were maintained at 37°C, 5% CO₂, and subcultured every 2–3 d.

For transient transfection of 293T cells, cells were seeded at 25% confluence the day before and transfected using the standard calcium phosphate method with a total amount of 5 µg plasmid DNA/dish. For transient transfection of A172 cells, Lipofectamine 3000 was used (Thermo Fisher Scientific) according to the provided protocol after seeding 2.5 × 10⁵ cells for 2 h into six-well plates.

OPTIC

The detailed OPTIC protocol, fluorescence microscopy, and evaluation of protein recruitment were described elsewhere (Baade et al., 2019). Briefly, HEK293T cells were transfected with pcDNA3.1 CEACAM3-integrin β1 fusion constructs together with GFP, GFP-FLN19-21, GFP-talin-1, or GFP-kindlin-2 and optionally mCherry-PPM1F or mCherry-PPM1FD360A. 48 h after transfection, cells were seeded onto 10 µg/ml poly-L-lysine-coated coverslips in suspension medium (DMEM plus 0.25% BSA). After 2 h, adherent cells were infected with Pacific Blue-stained *Ngo* (Opa₅₂-expressing, nonpiliated *Neisseria gonorrhoeae* MS11; Baade et al., 2019) at MOI 20 for 1 h in DMEM plus 0.25% BSA. Infection medium was aspirated, and cells were immediately fixed with 4% PFA for 15 min, permeabilized with 0.1% Triton X-100 in PBS for 5 min, and stained with α-CEACAM antibody (clone D14HD11; Aldevron) in blocking solution (10% calf serum [CS] in PBS) after washing with PBS and blocking. Wells were again washed with PBS and blocked followed by a second antibody staining. Coverslips were mounted on glass slides using Dako mounting medium (Dako). Samples were imaged at RT on a Leica SP5 confocal microscope equipped with a 63.0×/1.40 NA oil HX PL APO CS UV objective and analyzed using LAS AF Lite software. Protein recruitment at one bacterial infection site was quantified per cell (*n* = 60 cells per sample).

Whole cell lysates (WCLs) and WB

To obtain WCLs, equal cell numbers were lysed by treatment with radioimmunoprecipitation assay buffer (1% Triton X-100, 50 mM Hepes, 150 mM NaCl, 10% glycerol, 1.5 mM MgCl₂, 1 mM EGTA, 0.1% wt/vol SDS, and 1% vol/vol deoxycholic acid) supplemented with freshly added protease and phosphatase inhibitors (10 mM sodium pyrophosphate, 100 mM NaF, 1 mM sodium orthovanadate, 5 µg/ml leupeptin, 10 µg/ml aprotinin, 10 µg/ml Pefabloc, 5 µg/ml pepstatin, and 10 µM benzamide) and phosphatase saturating substrate (para-nitrophenolphosphate [pNPP]; Sigma-Aldrich; 10 mM). Chromosomal DNA and cell debris were pelleted by addition of Sepharose beads and

Table 1. **Lentiviral plasmids encoding desired shRNA for stable protein knock-down**

Vector	shRNA	Primer
pLKO.1	hANKRD28	hANKRD28_shRNA_sense 5'-ccggaaGCCTTAGGTCCTATTCATActcgagTATGAATAGGACCTAAGGCTttttttg-3' hANKRD28_shRNA_anti 5'-aattcaaaaaaGCCTTAGGTCCTATTCATActcgagTATGAATAGGACCTAAGGCTt-3'
pLKO.1	hβ1 Integrin	hβ1 Integrin_shRNA_sense 5'-ccggaaTGCAGCACAGATGAAGTActcgagTAACTTCATCTGTGCTGCAtttttttg-3' hβ1 Integrin_shRNA_anti 5'-aattcaaaaaaTGCAGCACAGATGAAGTActcgagTAACTTCATCTGTGCTGCAtt-3'
pLKO.1	hFilaminA	hFilaminA_shRNA_sense 5'-ccggaaGACCACCTACTTTGAGATCctcgagGATCTCAAAGTAGGTGGTctttttttg-3' hFilaminA_shRNA_anti 5'-aattcaaaaaaGACCACCTACTTTGAGATCctcgagGATCTCAAAGTAGGTGGTctt-3'
pLKO.1	hILKAP	hILKAP_shRNA_sense 5'-ccggaaAGAAAGTTTGTAAAGCCTCctcgagGAGGCTTTACAAACTTTCTttttttg-3' hILKAP_shRNA_anti 5'-aattcaaaaaaAGAAAGTTTGTAAAGCCTCctcgagGAGGCTTTACAAACTTTCTt-3'
pLKO.1	hPPM1F	hPPM1F_shRNA_sense 5'-ccggaaCCAGCTCTTCGGCTTGCTctcgagAGACAAGCCGAAGAGCTGgtttttttg-3' hPPM1F_shRNA_anti 5'-aattcaaaaaaCCAGCTCTTCGGCTTGCTctcgagAGACAAGCCGAAGAGCTGgtt-3'
pLKO.1	hPP2A	hPP2A_shRNA_sense 5'-ccggaaTGGGAAGAGCAACAGTAACTcctcgagGTTACTGTTGCTCTTCCCAtttttttg-3' hPP2A_shRNA_anti 5'-aattcaaaaaaTGGGAAGAGCAACAGTAACTcctcgagGTTACTGTTGCTCTTCCCAtt-3'
pLKO.1	hPTP1B	hPTP1B_shRNA_sense 5'-ccggaaCTCTCCACTCCATTTTATctcgagATAAATATGGAGTGGAGAGttttttg-3' hPTP1B_shRNA_anti 5'-aattcaaaaaaCTCTCCACTCCATTTTATctcgagATAAATATGGAGTGGAGAGtt-3'
pLKO.1	hPTP-PEST	hPTP_PEST_shRNA_sense 5'-ccggaaGCCAGATTTATAGTATTCCctcgagGGAATACTATAAATCTGGCttttttg-3' hPTP-PEST_shRNA_anti 5'-aattcaaaaaaGCCAGATTTATAGTATTCCctcgagGGAATACTATAAATCTGGCtt-3'
pLKO.1	hPTPRF	hPTPRF_shRNA_sense 5'-ccggaaTCAGAGAGCCTAGAACATCctcgagGATGTTCTAGGCTCTCTGAtttttttg-3' hPTPRF_shRNA_anti 5'-aattcaaaaaaTCAGAGAGCCTAGAACATCctcgagGATGTTCTAGGCTCTCTGAtt-3'
pLKO.1	hPTPRO	hPTPRO_shRNA_sense 5'-ccggaaGAAATGGTCATTCTACTTCctcgagGAAGTAGAATGACCATTTctttttttg-3' hPTPRO_shRNA_anti 5'-aattcaaaaaaGAAATGGTCATTCTACTTCctcgagGAAGTAGAATGACCATTTctt-3'
pLKO.1	hRPTPα	hRPTPα_shRNA_sense 5'-ccggaaTGGATGATGCAGTTCAAATctcgagATTTGAACTGCATCATCCAtttttttg-3' hRPTPα_shRNA_anti 5'-aattcaaaaaaTGGATGATGCAGTTCAAATctcgagATTTGAACTGCATCATCCAtt-3'

Table 1. **Lentiviral plasmids encoding desired shRNA for stable protein knock-down (Continued)**

Vector	shRNA	Primer
pLKO.1	hSHP1	hSHP1_shRNA_sense 5'-ccggaaCCCTTCTCCTCTTGAAATctcgagATTTACAAGAGGAGAAGGGTttttttg-3' hSHP1_shRNA_anti 5'-aattcaaaaaaCCCTTCTCCTCTTGAAATctcgagATTTACAAGAGGAGAAGGGtt-3'
pLKO.1	hSHP2	hSHP2_shRNA_sense 5'-ccggaaCAGACGCAAGAAAGTTTATctcgagATAAACTTTCTGCGTCTGttttttg-3' hSHP2_shRNA_anti 5'-aattcaaaaaaCAGACGCAAGAAAGTTTATctcgagATAAACTTTCTGCGTCTGtt-3'
pLKO.1	hTCPTP	hTCPTP_shRNA_sense 5'-ccggaaCCTGCACTTGATATAAGCActcgagTGCTTATATCAAGTGCAGGttttttg-3' hTCPTP_shRNA_anti 5'-aattcaaaaaaCCTGCACTTGATATAAGCActcgagTGCTTATATCAAGTGCAGGtt-3'

GTGCCCCAGTTTGCTAGG-3'. The resulting mKate-encoding PCR fragment was cloned into pLL3.7 (plasmid 11795; Addgene) via AgeI/EcoRI restriction digest to replace the GFP cDNA to yield the pLL3.7-mKate2 vector. Subsequently, pLL3.7-LIC-mKate2 vector was created by replacing the multiple cloning site with a LIC sequence (primers 5'-CTAGCGACTCTCCCCGGGTTAGTGGGGCA-3' and 5'-CCGGTGCCCCACTAACCGGGGGAGAGTCG-3') via NheI/AgeI. Then, hPPM1F and hPPM1F D360A cDNA in pmCherry were modified by site-directed mutagenesis with primers Rescue_sgRNA-hPPM1F_for: 5'-CGAACAGATCAAATGTTCCTGAGGAAAGCCAAGCGAGAGCG-3' and Rescue_sgRNA-hPPM1F_rev: 5'-CCTCAGGAACATTTGATCTGTTCCGCCGGAAGGCTTCTGAGGG-3' to inactivate the sgRNA-hPPM1F target sequence by silent mutations. The resulting sgRNA-resistant cDNAs of hPPM1F and hPPM1F D360A were amplified with primers PPM1F_LIC_for: 5'-CGAACAGATCAAATGTTCTGAGGAAAGCCAAGCGAGAGCG-3' and PPM1F_LIC_rev: 5'-CCTCAGGAACATTTGATCTGTTCCGCCGGAAGGCTTCTGAGGG-3' and inserted via LIC (Aslanidis and de Jong, 1990) into pLL3.7-LIC-mKate2 to result in pLL3.7 mKate2-hPPM1F and pLL3.7 mKate2-hPPM1F D360A.

IF staining for confocal microscopy and cell spreading analysis

Sterile coverslips were coated with 0.4–10 µg/ml FN_{III9-11} in PBS overnight at 4°C in a 24-well plate, and cells were starved with DMEM plus 0.5% FCS for 15 h. The next day, coating solution was removed, and wells were blocked with suspension medium (DMEM plus 0.25% BSA). In parallel, cells were trypsinized, trypsin-inactivated with soybean trypsin inhibitor (12.5 mg in 50 ml DMEM, sterile filtered; AppliChem), counted, and kept in suspension medium for 45 min at 37°C. 2.5×10^4 cells were seeded onto coverslips and allowed to adhere for corresponding time periods. Cells were fixed with 4% PFA supplemented with 0.1% Triton X-100 for 5 min at RT and again without Triton X-100 for 20 min. Coverslips were washed thrice with PBS²⁺ (0.9 mM CaCl₂ and 0.5 mM MgCl₂ in 1× PBS) and blocked for 20 min with blocking solution (10% CS in PBS). Primary

antibody solution was added for 1 h at RT. After washing thrice with PBS²⁺ and blocking for another 20 min, coverslips were treated with secondary antibody in blocking solution and optionally with phalloidin-Cy5 or DAPI for 1 h at RT in the dark. Finally, cells were washed thrice with PBS²⁺ and mounted with Dako fluorescent mounting medium (Dako). Samples were imaged on a Leica SP5 confocal microscope equipped with a 63.0×/1.40 NA oil HCX PL APO CS UV objective and acquired in xyz mode with a 1,024 × 1,024 pixel format and 100 Hz scanning speed at 8-bit resolution. All images were analyzed in ImageJ Software. For spreading assays, a macro was set up together with the Bioimaging Center at the University of Konstanz and used for quantitative picture analysis. Unrecognized cells were analyzed manually in the Leica LAS AF Lite software.

IF staining for FACS analysis

Cells were detached with trypsin/EDTA, pelleted, and suspended in FACS buffer (0.1% NaAzide and 5% FCS in PBS). After centrifugation (800 rpm, 3 min), cells were washed with FACS buffer, and 3×10^5 cells were transferred into Eppendorf tubes, centrifuged (2,500 rpm, 2 min, 4°C), and incubated with primary antibody in FACS buffer at the desired concentration for 1 h at 4°C under constant rotation. Cells were washed thrice with FACS buffer and incubated with secondary antibody in FACS buffer at desired concentrations for 30 min at 4°C under constant rotation in the dark. After washing thrice with FACS buffer, cells were suspended in 1 ml of FACS buffer containing 2 mM EDTA. Finally, cells were analyzed by flow cytometry (BD LSRII, FACSDiva software; BD Biosciences).

Replating assay for pT788/pT789 β1 integrin analysis in intact cells

10-cm dishes were coated with 2 µg/ml FN_{III9-11} in PBS overnight at 4°C. Cells were starved with DMEM plus 0.5% FCS overnight at 37°C. The next day, dishes were blocked with DMEM plus 0.25% BSA for 1 h at 37°C. In parallel, cells were trypsinized, trypsin-inactivated with soybean inhibitor, counted, and kept in

suspension medium for 45 min at 37°C. Afterward, the same cell numbers were seeded onto coated dishes and allowed to adhere for corresponding time periods at 37°C. Dishes were washed with PBS. WCLs were prepared and subjected to WB analysis. Phosphorylation of proteins was detected by phospho-specific antibodies. Densitometric analysis was performed by ImageJ software. The amount of phosphorylated $\beta 1$ integrin was normalized to total $\beta 1$ integrin expression levels.

Cell adhesion assay

96-well plates were coated with PBS containing corresponding concentrations of collagen I (Sigma-Aldrich), FN_{III9-11}, or poly-L lysine (SERVA) as an integrin-independent control overnight at 4°C. Wells were blocked with DMEM plus 0.25% BSA for 1 h at 37°C. In parallel, cells were trypsinized and kept in suspension medium for 45 min. 2×10^4 cells/well were seeded and allowed to adhere for the indicated time periods at 37°C. After incubation, nonadherent cells were removed by gently washing with PBS²⁺ thrice. Adherent cells were fixed with 4% PFA in PBS for 15 min, washed with PBS, and stained with 0.1% crystal violet in 0.2 M borate buffer (pH 8.5) for 30 min. After intense washing, the color was unhinged from cells with 10 mM acetic acid, and the absorption was measured at 590 nm using a spectrophotometer.

IA

For ELISA, 96-well plates were coated with 0.1 $\mu\text{g/ml}$ FN_{III9-11} in PBS overnight at 4°C. The next day, wells were blocked with 0.25% BSA in DMEM. In parallel, cells were trypsinized and kept in suspension for 1 h. Then, 5×10^4 cells were seeded in triplicate and allowed to adhere for 40 min. Then cells were transferred onto ice, fixed with 4% PFA, washed with PBS, and permeabilized with 0.15% Triton X-100 for 15 min. Afterward, cells were blocked with 2% BSA in PBS for 20 min and stained with 9EG7 or AIIB2 antibodies. After incubation with the primary antibody, cells were washed with PBS, blocked for 20 min, and incubated with the secondary HRP-conjugated goat anti-rat IgG antibody for 1 h at RT. Finally, cells were intensively washed, and 100 μl of substrate solution was added (10 ml of 2.4 mg/ml TMB in 10% acetone/90% ethanol with 0.5 ml of 30 mM potassium citrate, pH 4.1). The enzymatic color reaction was stopped by adding 100 $\mu\text{l/well}$ 2 M H₂SO₄, and the absorption was detected via spectrophotometric measurement at 450 nm. Controls were stained with secondary antibody only.

For FACS, starved cells were trypsinized and kept in suspension (2% BSA and 5 mM glucose in PBS) for 45 min before they were stimulated with 10 $\mu\text{g/ml}$ FN_{III9-12} for 15 min at 37°C or kept unstimulated by adding double-distilled H₂O. Cells were put on ice and split into two fractions, which were stained for either active integrin $\beta 1$ (9EG7; 1:600) or total integrin $\beta 1$ (HM $\beta 1$ -1; 1:300, or AIIB2; 1:600) for 1 h on ice in PBS plus 2% BSA. Cells were washed thrice with PBS and incubated with Rhodamine-Red conjugated secondary antibody for 45 min on ice in the dark. Cells were washed, and fluorescence intensity was measured by flow cytometry (BD LSRII, FACSDiva software; BD Biosciences).

Expression and purification of GST-tagged hPPM1F and hPPM1F D360A in 293T cells and *E. coli*

293T cells were transfected by standard calcium phosphate coprecipitation using plasmid DNA encoding for either GST-hPPM1F or GST-hPPM1F D360A. 48 h after transfection, cells were lysed in lysis buffer (50 mM Tris, pH 8, 1% Triton X-100, 1 mM EDTA, and 0.1% β -mercaptoethanol). Cleared lysates were incubated with glutathione-Sepharose beads for 3 h under constant rotation at 4°C. Beads were pelleted via centrifugation and washed three times in lysis buffer and once in GST buffer (50 mM Tris-HCl, pH 8, 150 mM NaCl, 1 mM DTT, and 5 mM MgCl₂). For the elution of the GST-fusion proteins, beads were incubated in GST buffer supplemented with 10 mM reduced L-glutathione twice for 20 min at 4°C under constant rotation. Aliquots were transferred to liquid nitrogen, and long-term storage occurred at -80°C .

For the production of recombinant GST-tagged hPPM1F or GST-hPPM1F D360A, the corresponding sequence-verified construct was transformed into competent *E. coli* BL21 Rosetta (DE3). Bacteria were cultured in lysogeny broth medium containing appropriate antibiotics at 37°C with constant shaking at 200 rpm. Expression was induced at OD₅₈₀ = 0.6 with 0.5 mM IPTG at 30°C and 220 rpm for 3 h, and bacteria were pelleted by centrifugation at 4,700 rpm, 20 min, RT. Afterward, bacteria were resuspended in PBS (pH 7.4) supplemented with 5 mM EDTA, protease inhibitors (10 $\mu\text{g/ml}$ Pefabloc, 10 $\mu\text{g/ml}$ aprotinin, 1 μM PMSF, and 5 $\mu\text{g/ml}$ leupeptin) and 2.5 mM DTT and sonicated at 4°C three times for 2 min. Cleared lysates were put onto a GST-Trap FF column (GE Healthcare) and washed with PBS, pH 7.4. Finally, GST-tagged proteins were eluted with 50 mM Tris, pH 8.0, supplemented with 10 mM reduced L-glutathione and dialyzed against 25 mM sodium phosphate, pH 8.0, supplemented with 150 mM NaCl and 1 mM EDTA or against 50 mM Tris pH 8.0 supplemented with 150 mM NaCl and 1 mM Tris(2-carboxyethyl)phosphine (TCEP). The amount and the purity of proteins were analyzed via SDS-gel electrophoresis and aliquots supplemented with 10% glycerol frozen at -80°C .

In vitro phosphorylation and phosphatase assays

Human recombinant CaMKII β (PV4205; Thermo Fisher Scientific) was resuspended in kinase buffer (50 mM Tris-HCl, pH 7.7, 10 mM MgCl₂, 5 mM MnCl₂, 1 mM TCEP, and 0.05% Triton X-100) either supplemented with 200 μM ATP, 1.2 μM calmodulin (Sigma-Aldrich), and 2 mM CaCl₂ or without supplementation and incubated for 10 min at 30°C. The kinase assay was started by adding 2 μg of purified GST-fusion protein and incubated for 60 min at 30°C under constant shaking at 750 rpm. The reaction was stopped via the addition of SDS sample buffer.

For the in vitro phosphatase assay, the CaMKII β phosphorylated cytoplasmic tail of $\beta 1$ integrin was incubated with 2 μg of recombinant GST-PPM1F or PPM1F D360A or corresponding amounts of ILKAP in phosphatase buffer (50 mM Tris-HCl, pH 8, 10 mM MnCl₂, and 0.01% Tween 20) for 1 h at 30°C under constant shaking at 750 rpm. The reaction was stopped by the addition of either SDS sample buffer or the same volume of malachite green solution (54 mM NH₄Mo and 0.9 mM malachite

green in 1 M HCl) and analyzed by WB or photometric measurement with OD_{615nm}.

Phosphatase assays with phospho-peptides were conducted using peptides synthesized by Pepsican: β 1-22pT788pT789: (Biotin-Ahx-TGENPIYKSAV[pT][pT]VVNPKYEGK-OH), β 1-22pT788: (H-TG ENPIYKSAV[pT]TVVNPKEGK-OH), β 1-22pT789: (H-TGENPIYKSAVT[pT]VVNPKYEGK-OH), and MLC2-20pT10: (H-MSSKRAKAK [pT]TKKRPQRATS-OH). Depending on the assay, recombinant, *E. coli*-expressed GST-tagged PPM1F, PPM1FD360A, PTP1B, 7xHis-TEV ILKAP, Trx-His-S-PP5, or GST-PPM1F and GST-PPM1F D360A expressed in 293 cells were incubated with 100 μ M phospho-peptides in phosphatase buffer for 1 h at 30°C. The reaction was stopped by adding the same volume of malachite green solution, and OD_{615nm} was measured. To determine PPM1F kinetics, GST-tagged PPM1F or PPM1FD360A was expressed in 293 cells and purified by glutathione agarose. Proteins were incubated with different concentrations of the double phosphorylated β 1 integrin TpTp788/789 peptide or with 4-methylumbelliferone phosphate (Sigma-Aldrich). A standard curve for either K₂HPO₄ or 4-methylumbelliferone was measured in parallel and used to determine the kinetic parameters K_m and V_{max} by directly fitting the data to the Michaelis-Menten equation $v = \frac{V_{max} [S]}{K_m + [S]}$ with reaction rate v , maximum velocity V_{max} , substrate concentration $[S]$, and Michaelis constant K_m . Activity of ILKAP, PP5, and PTP1B was determined by 4-MUP assay using same molar amounts of each phosphatase. As negative controls, phosphatases were inhibited by 100 mM EDTA, 20 mM NaF, or 250 μ M PTP1B specific inhibitor (CAS765317-72-4; Merck Millipore), and activity was determined by measuring fluorescence over 30 min (excitation/emission 386/448 nm). PPM1F WT was used as the reference.

Husbandry and genotyping of mice

Mice were kept in accordance with relevant institutional and national guidelines and regulations in the central animal care facility of University of Konstanz. The B6.129P2-PPM1Ftm1Dgen/J (PPM1F^{+/-}) mouse strain was obtained from The Jackson Laboratory. The targeted *ppm1f* gene was created by Deltagen by inserting a LacO-SA-IRES-lacZ-Neo555G/Kan cassette via homologous recombination into the *ppm1f* locus, allowing the endogenous promoter to drive expression of β -galactosidase. The PPM1F^{+/-} mice have been backcrossed at least 20 generations to C57BL/6 mice. 3-wk-old mice or embryos were genotyped by amplification of DNA extracted from tissue biopsies or isolated from mouse embryonic fibroblast. The following PCR primers were used: primer 1, WT forward: 5'-CAACTCTCCATCATGCCCATCAG-3'; primer 2, common reverse: 5'-AAGCAGGAAGGACACGTGTCGGTC-3'; and primer 3, targeted allele forward: 5'-GGGTGGGATTAGATAAATGCCTGCTCT-3'.

For genotyping, a PCR with 32 cycles was performed with an annealing temperature of 59°C and an elongation time of 40 s at 72°C, yielding a 200-bps and 450-bps PCR fragment for the WT and the targeted allele, respectively (see also Fig. 9 A).

Derivation of MEFs

For the generation of *ppm1f*^{+/-} MEFs, heterozygous mice were mated, and 10.5 d after coitus, the female mice were anesthetized and sacrificed. The uterus was dissected and cut between the implantation sites along the uterine horns into pieces

containing single embryos. The embryos were isolated by removing the enveloping tissue, washed in sterile fibroblast growth medium (Promocell) supplemented with penicillin, streptomycin, and ciprofloxacin, and minced via up and down pipetting. The tissue homogenates were plated onto gelatin (0.1%) and human fibronectin (2 μ g/ml)-coated dishes. After the second passage, primary fibroblasts were immortalized via transduction with pBabeZeo SV40 largeT (plasmid 1779; Addgene; Hahn et al., 2002). MEFs were cultured in DMEM supplemented with 10% FCS, nonessential amino acids, and sodium pyruvate.

Generation of polyclonal anti-mPPM1F antibody

The cDNA of mPPM1F was obtained from Source BioScience (I.M.A.G.E. Full Length cDNA clone IRVp968A0987D; sequence accession BC042570) and was amplified with primers mPPM1F-BamHI-forward: 5'-GCTTTAGGATCCAATGGCCTCTGGAGCCGCACAGAAC-3' and mPPM1F-HindIII-reverse: 5'-CGCCCGTCAAGCTTCTTAGCTTCTCTGTGAGGTATTAC-3'. The resulting PCR fragment was cloned into the pET24aHis-Sumo bacterial expression vector (Andréasson et al., 2008) via BamHI and HindIII restriction sites. The sequence-verified construct was transformed into competent *E. coli* BL21 (DE3), and expression of the recombinant protein was induced at OD₅₈₀ = 0.67 with 0.5 mM IPTG at 30°C for 4.5 h. His-Sumo-tagged mPPM1F was purified on a HisTrap FF column and eluted with 50 mM sodium phosphate buffer, pH 8, 0.5 M NaCl, and 0.5 M imidazole before removal of the His-Sumo tag by Ulp1 protease (Andréasson et al., 2008). 100 μ g of purified recombinant mPPM1F were used for immunization of a New Zealand White rabbit in accordance with relevant institutional and national guidelines and regulations in the central animal care facility of University of Konstanz.

Single cell tracking

MEFs were seeded in 24-well plates and incubated for 24 h. Cells were starved in DMEM supplemented with 0.5% BSA for 12 h, and afterward stimulated with serum-containing growth medium and imaged for 12 h (30 min/frame). Single cells were tracked manually using the ImageJ particle tracking plugin and analyzed using the chemotaxis and migration tool (Ibidi GmbH).

Statistics

All data are presented as mean \pm SEM or mean \pm SD as indicated. All statistical significances were determined using a two-tailed Student's *t* test or one-way ANOVA followed by Bonferroni post hoc test with Prism5 (GraphPad). Significance is indicated with *, $P < 0.05$; **, $P < 0.01$; ***, $P < 0.001$; or ns, not significant.

Online supplemental material

Fig. S1 shows that the T788/T789 motif in the integrin β 1 cytoplasmic tail is evolutionary conserved and that its pseudo-phosphorylation regulates the association with talin and filamin. Fig. S2 demonstrates that knock-down of PPM1F in 293T cells or NHDFs does not alter expression of core focal adhesion proteins and does not affect integrin surface levels. Fig. S3 shows that PPM1F KO in A172 cells does not alter integrin

surface levels or expression of core focal adhesion proteins, but strongly affects integrin-dependent processes. Fig. S4 shows that filaminA knock-down phenocopies integrin-dependent effects of PPM1F depletion in A172 cells. Fig. S5 shows that PPM1F purified from 293T cells dephosphorylates the conserved T788/T789 motif in the integrin β 1 cytoplasmic domain.

Acknowledgments

The authors thank W. Hofer, D. Dietrich, R. Fässler, J. Morschhäuser, D.W. Piston, M.A. Schwartz, and D. Vestweber for valuable reagents. We are indebted to S. Feindler-Boeckh and the Flow Cytometry Facility Konstanz (FlowKon) for expert technical support. We also thank S. Helfrich and M. Stöckl for help in image analysis (Bioimaging Center, University of Konstanz).

T.M. Grimm and N.I. Dierdorf acknowledge support by the Konstanz Research School Chemical Biology. This study was supported by funds from the Deutsche Forschungsgemeinschaft (CRC969 project B06) to C.R. Hauck.

The authors declare no competing financial interests.

Author contributions: T.M. Grimm, N.I. Dierdorf, and C.R. Hauck conceived the study and designed the experiments; T.M. Grimm and N.I. Dierdorf conducted the experiments and evaluated the data; C. Paone conducted cell migration assays; K. Betz performed structure modeling; T.M. Grimm and C.R. Hauck wrote the paper. All authors read and approved the final manuscript.

Submitted: 9 January 2020

Revised: 20 July 2020

Accepted: 11 September 2020

References

Adrian, J., P. Bonsignore, S. Hammer, T. Frickey, and C.R. Hauck. 2019. Adaptation to host-specific bacterial pathogens drives rapid evolution of a human innate immune receptor. *Curr. Biol.* 29:616–630.e5. <https://doi.org/10.1016/j.cub.2019.01.058>

Andréasson, C., J. Fiaux, H. Rampelt, M.P. Mayer, and B. Bukau. 2008. Hsp110 is a nucleotide-activated exchange factor for Hsp70. *J. Biol. Chem.* 283: 8877–8884. <https://doi.org/10.1074/jbc.M710063200>

Anthis, N.J., J.R. Haling, C.L. Oxley, M. Memo, K.L. Wegener, C.J. Lim, M.H. Ginsberg, and I.D. Campbell. 2009. Beta integrin tyrosine phosphorylation is a conserved mechanism for regulating talin-induced integrin activation. *J. Biol. Chem.* 284:36700–36710. <https://doi.org/10.1074/jbc.M109.061275>

Arias-Salgado, E.G., F. Haj, C. Dubois, B. Moran, A. Kasirer-Friede, B.C. Furie, B. Furie, B.G. Neel, and S.J. Shattil. 2005. PTP-1B is an essential positive regulator of platelet integrin signaling. *J. Cell Biol.* 170:837–845. <https://doi.org/10.1083/jcb.200503125>

Aslanidis, C., and P.J. de Jong. 1990. Ligation-independent cloning of PCR products (LIC-PCR). *Nucleic Acids Res.* 18:6069–6074. <https://doi.org/10.1093/nar/18.20.6069>

Baade, T., C. Paone, A. Baldrich, and C.R. Hauck. 2019. Clustering of integrin β cytoplasmic domains triggers nascent adhesion formation and reveals a protozoan origin of the integrin-talin interaction. *Sci. Rep.* 9:5728. <https://doi.org/10.1038/s41598-019-42002-6>

Bledzka, K., J. Liu, Z. Xu, H.D. Perera, S.P. Yadav, K. Bialkowska, J. Qin, Y.Q. Ma, and E.F. Plow. 2012. Spatial coordination of kindlin-2 with talin head domain in interaction with integrin β cytoplasmic tails. *J. Biol. Chem.* 287:24585–24594. <https://doi.org/10.1074/jbc.M111.336743>

Bökel, C., and N.H. Brown. 2002. Integrins in development: moving on, responding to, and sticking to the extracellular matrix. *Dev. Cell.* 3:311–321. [https://doi.org/10.1016/S1534-5807\(02\)00265-4](https://doi.org/10.1016/S1534-5807(02)00265-4)

Böttcher, R.T., M. Veelders, P. Rombaut, J. Faix, M. Theodosiou, T.E. Stradal, K. Rottner, R. Zent, F. Herzog, and R. Fässler. 2017. Kindlin-2 recruits paxillin and Arp2/3 to promote membrane protrusions during initial cell spreading. *J. Cell Biol.* 216:3785–3798. <https://doi.org/10.1083/jcb.201701176>

Bouvard, D., L. Vignoud, S. Dupé-Manet, N. Abed, H.N. Fournier, C. Vincent-Monegat, S.F. Retta, R. Fassler, and M.R. Block. 2003. Disruption of focal adhesions by integrin cytoplasmic domain-associated protein-1 α . *J. Biol. Chem.* 278:6567–6574. <https://doi.org/10.1074/jbc.M211258200>

Bunch, T.A. 2010. Integrin α IIb β 3 activation in Chinese hamster ovary cells and platelets increases clustering rather than affinity. *J. Biol. Chem.* 285:1841–1849. <https://doi.org/10.1074/jbc.M109.057349>

Buyon, J.P., S.G. Slade, J. Reibman, S.B. Abramson, M.R. Philips, G. Weissmann, and R. Winchester. 1990. Constitutive and induced phosphorylation of the α - and β -chains of the CD11/CD18 leukocyte integrin family. Relationship to adhesion-dependent functions. *J. Immunol.* 144:191–197.

Calderwood, D.A. 2004. Integrin activation. *J. Cell Sci.* 117:657–666. <https://doi.org/10.1242/jcs.01014>

Calderwood, D.A., R. Zent, R. Grant, D.J. Rees, R.O. Hynes, and M.H. Ginsberg. 1999. The Talin head domain binds to integrin beta subunit cytoplasmic tails and regulates integrin activation. *J. Biol. Chem.* 274:28071–28074. <https://doi.org/10.1074/jbc.274.40.28071>

Calderwood, D.A., B. Yan, J.M. de Pereda, B.G. Alvarez, Y. Fujioka, R.C. Liddington, and M.H. Ginsberg. 2002. The phosphotyrosine binding-like domain of talin activates integrins. *J. Biol. Chem.* 277:21749–21758. <https://doi.org/10.1074/jbc.M111996200>

Chatila, T.A., R.S. Geha, and M.A. Arnaout. 1989. Constitutive and stimulus-induced phosphorylation of CD11/CD18 leukocyte adhesion molecules. *J. Cell Biol.* 109:3435–3444. <https://doi.org/10.1083/jcb.109.6.3435>

Cluzel, C., F. Saltel, J. Lussi, F. Paulhe, B.A. Imhof, and B. Wehrle-Haller. 2005. The mechanisms and dynamics of α (α) ν (β) β 3 integrin clustering in living cells. *J. Cell Biol.* 171:383–392. <https://doi.org/10.1083/jcb.200503017>

Craig, D.H., C.P. Gayer, K.L. Schaubert, Y. Wei, J. Li, Y. Laouar, and M.D. Basson. 2009. Increased extracellular pressure enhances cancer cell integrin-binding affinity through phosphorylation of β 1-integrin at threonine 788/789. *Am. J. Physiol.* 296:C193–C204. <https://doi.org/10.1152/ajpcell.00355.2008>

Fagerholm, S., N. Morrice, C.G. Gahmberg, and P. Cohen. 2002. Phosphorylation of the cytoplasmic domain of the integrin CD18 chain by protein kinase C isoforms in leukocytes. *J. Biol. Chem.* 277:1728–1738. <https://doi.org/10.1074/jbc.M106856200>

Czuchra, A., H. Meyer, K.R. Legate, C. Brakebusch, and R. Fässler. 2006. Genetic analysis of β 1 integrin “activation motifs” in mice. *J. Cell Biol.* 174(6):889–899. <https://doi.org/10.1083/jcb.200604060>

Fagerholm, S.C., T.J. Hilden, S.M. Nurmi, and C.G. Gahmberg. 2005. Specific integrin α and β chain phosphorylations regulate LFA-1 activation through affinity-dependent and -independent mechanisms. *J. Cell Biol.* 171:705–715. <https://doi.org/10.1083/jcb.200504016>

Fässler, R., and M. Meyer. 1995. Consequences of lack of β 1 integrin gene expression in mice. *Genes Dev.* 9(15):1896–1908. <https://doi.org/10.1101/gad.9.15.1896>

Feng, Y., M.H. Chen, I.P. Moskowitz, A.M. Mendonza, L. Vidali, F. Nakamura, D.J. Kwiatkowski, and C.A. Walsh. 2006. Filamin A (FLNA) is required for cell-cell contact in vascular development and cardiac morphogenesis. *Proc. Natl. Acad. Sci. U.S.A.* 103(52):19836–19841. <https://doi.org/10.1073/pnas.0609628104>

Gahmberg, C.G., S.C. Fagerholm, S.M. Nurmi, T. Chavakis, S. Marchesan, and M. Grönholm. 2009. Regulation of integrin activity and signalling. *Biochim. Biophys. Acta.* 1790:431–444. <https://doi.org/10.1016/j.bbagen.2009.03.007>

Gahmberg, C.G., M. Grönholm, and L.M. Uotila. 2014. Regulation of integrin activity by phosphorylation. *Adv. Exp. Med. Biol.* 819:85–96. https://doi.org/10.1007/978-94-017-9153-3_6

García-Alvarez, B., J.M. de Pereda, D.A. Calderwood, T.S. Ulmer, D. Critchley, I.D. Campbell, M.H. Ginsberg, and R.C. Liddington. 2003. Structural determinants of integrin recognition by talin. *Mol. Cell.* 11:49–58. [https://doi.org/10.1016/S1097-2765\(02\)00823-7](https://doi.org/10.1016/S1097-2765(02)00823-7)

Garton, A.J., A.J. Flint, and N.K. Tonks. 1996. Identification of p130(cas) as a substrate for the cytosolic protein tyrosine phosphatase PTP-PEST. *Mol. Cell. Biol.* 16:6408–6418. <https://doi.org/10.1128/MCB.16.11.6408>

Gee, K.R., W.C. Sun, M.K. Bhalgat, R.H. Upson, D.H. Klauert, K.A. Latham, and R.P. Haugland. 1999. Fluorogenic substrates based on fluorinated

- umbelliferones for continuous assays of phosphatases and beta-galactosidases. *Anal. Biochem.* 273:41–48. <https://doi.org/10.1006/abio.1999.4202>
- Gringras, A.R., W.H. Ziegler, A.A. Bobkov, M.G. Joyce, D. Fasci, M. Himmel, S. Rothmund, A. Ritter, J.G. Grossmann, B. Patel, et al. 2009. Structural determinants of integrin binding to the talin rod. *J. Biol. Chem.* 284: 8866–8876. <https://doi.org/10.1074/jbc.M805937200>
- Hagel, M., E.L. George, A. Kim, R. Tamimi, S.L. Opitz, C.E. Turner, A. Imamoto, and S.M. Thomas. 2002. The adaptor protein paxillin is essential for normal development in the mouse and is a critical transducer of fibronectin signaling. *Mol. Cell Biol.* 22(3):901–915. <https://doi.org/10.1128/mcb.22.3.901-915.2002>
- Hahn, W.C., S.K. Dessain, M.W. Brooks, J.E. King, B. Elenbaas, D.M. Sabatini, J.A. DeCaprio, and R.A. Weinberg. 2002. Enumeration of the simian virus 40 early region elements necessary for human cell transformation. *Mol. Cell Biol.* 22:2111–2123. <https://doi.org/10.1128/MCB.22.7.2111-2123.2002>
- Hamidi, H., and J. Ivaska. 2018. Every step of the way: integrins in cancer progression and metastasis. *Nat. Rev. Cancer.* 18:533–548. <https://doi.org/10.1038/s41568-018-0038-z>
- Harburger, D.S., and D.A. Calderwood. 2009. Integrin signalling at a glance. *J. Cell Sci.* 122:159–163. <https://doi.org/10.1242/jcs.018093>
- Harburger, D.S., M. Bouaouina, and D.A. Calderwood. 2009. Kindlin-1 and -2 directly bind the C-terminal region of beta integrin cytoplasmic tails and exert integrin-specific activation effects. *J. Biol. Chem.* 284: 11485–11497. <https://doi.org/10.1074/jbc.M809233200>
- Harvey, B.P., S.S. Banga, and H.L. Ozer. 2004. Regulation of the multifunctional Ca²⁺/calmodulin-dependent protein kinase II by the PP2C phosphatase PPM1F in fibroblasts. *J. Biol. Chem.* 279:24889–24898. <https://doi.org/10.1074/jbc.M400656200>
- Hibbs, M.L., S. Jakes, S.A. Stacker, R.W. Wallace, and T.A. Springer. 1991. The cytoplasmic domain of the integrin lymphocyte function-associated antigen 1 beta subunit: sites required for binding to intercellular adhesion molecule 1 and the phorbol ester-stimulated phosphorylation site. *J. Exp. Med.* 174:1227–1238. <https://doi.org/10.1084/jem.174.5.1227>
- Hilden, T.J., L. Valmu, S. Kärkkäinen, and C.G. Gahmberg. 2003. Threonine phosphorylation sites in the beta 2 and beta 7 leukocyte integrin polypeptides. *J. Immunol.* 170:4170–4177. <https://doi.org/10.4049/jimmunol.170.8.4170>
- Horton, E.R., A. Byron, J.A. Askari, D.H.J. Ng, A. Millon-Frémillon, J. Robertson, E.J. Koper, N.R. Paul, S. Warwood, D. Knight, et al. 2015. Definition of a consensus integrin adhesome and its dynamics during adhesion complex assembly and disassembly. *Nat. Cell Biol.* 17: 1577–1587. <https://doi.org/10.1038/ncb3257>
- Hughes, P.E., F. Diaz-Gonzalez, L. Leong, C. Wu, J.A. McDonald, S.J. Shattil, and M.H. Ginsberg. 1996. Breaking the integrin hinge. A defined structural constraint regulates integrin signaling. *J. Biol. Chem.* 271: 6571–6574. <https://doi.org/10.1074/jbc.271.12.6571>
- Hynes, R.O. 2002. Integrins: bidirectional, allosteric signaling machines. *Cell.* 110:673–687. [https://doi.org/10.1016/S0092-8674\(02\)00971-6](https://doi.org/10.1016/S0092-8674(02)00971-6)
- Ilić, D., Y. Furuta, S. Kanazawa, N. Takeda, K. Sobue, N. Nakatsuji, S. Nomura, J. Fujimoto, M. Okada, and T. Yamamoto. 1995. Reduced cell motility and enhanced focal adhesion contact formation in cells from FAK-deficient mice. *Nature.* 377(6549):539–544. <https://doi.org/10.1038/377539a0>
- Ishida, A., I. Kameshita, and H. Fujisawa. 1998. A novel protein phosphatase that dephosphorylates and regulates Ca²⁺/calmodulin-dependent protein kinase II. *J. Biol. Chem.* 273:1904–1910. <https://doi.org/10.1074/jbc.273.4.1904>
- Ishida, A., N. Sueyoshi, Y. Shigeri, and I. Kameshita. 2008. Negative regulation of multifunctional Ca²⁺/calmodulin-dependent protein kinases: physiological and pharmacological significance of protein phosphatases. *Br. J. Pharmacol.* 154:729–740. <https://doi.org/10.1038/bjp.2008.127>
- Ishida, A., N. Sueyoshi, and I. Kameshita. 2018. Functions and dysfunctions of Ca²⁺/calmodulin-dependent protein kinase phosphatase (CaMKP/PPM1F) and CaMKP-N/PPM1E. *Arch. Biochem. Biophys.* 640:83–92. <https://doi.org/10.1016/j.abb.2018.01.001>
- Kiema, T., Y. Lad, P. Jiang, C.L. Oxley, M. Baldassarre, K.L. Wegener, I.D. Campbell, J. Ylänne, and D.A. Calderwood. 2006. The molecular basis of filamin binding to integrins and competition with talin. *Mol. Cell.* 21: 337–347. <https://doi.org/10.1016/j.molcel.2006.01.011>
- Kim, S.M., M.S. Kwon, C.S. Park, K.R. Choi, J.S. Chun, J. Ahn, and W.K. Song. 2004. Modulation of Thr phosphorylation of integrin beta1 during muscle differentiation. *J. Biol. Chem.* 279:7082–7090. <https://doi.org/10.1074/jbc.M311581200>
- Koh, C.G., E.J. Tan, E. Manser, and L. Lim. 2002. The p21-activated kinase PAK is negatively regulated by POPX1 and POPX2, a pair of serine/threonine phosphatases of the PP2C family. *Curr. Biol.* 12:317–321. [https://doi.org/10.1016/S0960-9822\(02\)00652-8](https://doi.org/10.1016/S0960-9822(02)00652-8)
- Leung-Hageteijn, C., A. Mahendra, I. Naruszewicz, and G.E. Hannigan. 2001. Modulation of integrin signal transduction by ILKAP, a protein phosphatase 2C associating with the integrin-linked kinase, ILK1. *EMBO J.* 20:2160–2170. <https://doi.org/10.1093/emboj/20.9.2160>
- Li, H., Y. Deng, K. Sun, H. Yang, J. Liu, M. Wang, Z. Zhang, J. Lin, C. Wu, Z. Wei, and C. Yu. 2017. Structural basis of kindlin-mediated integrin recognition and activation. *Proc. Natl. Acad. Sci. USA.* 114:9349–9354. <https://doi.org/10.1073/pnas.1703064114>
- Liu, J., M. Das, J. Yang, S.S. Ithychanda, V.P. Yakubenko, E.F. Plow, and J. Qin. 2015. Structural mechanism of integrin inactivation by filamin. *Nat. Struct. Mol. Biol.* 22:383–389. <https://doi.org/10.1038/nsmb.2999>
- Ma, Y.Q., J. Qin, C. Wu, and E.F. Plow. 2008. Kindlin-2 (Mig-2): a co-activator of beta3 integrins. *J. Cell Biol.* 181:439–446. <https://doi.org/10.1083/jcb.200710196>
- Meves, A., C. Stremmel, R.T. Böttcher, and R. Fässler. 2013. β 1 integrins with individually disrupted cytoplasmic NPXY motifs are embryonic lethal but partially active in the epidermis. *J. Invest. Dermatol.* 133(12): 2722–2731. <https://doi.org/10.1038/jid.2013.232>
- Monkley, S.J., X.H. Zhou, S.J. Kinston, S.M. Giblett, L. Hemmings, H. Priddle, J.E. Brown, C.A. Pritchard, D.R. Critchley, and R. Fässler. 2000. Disruption of the talin gene arrests mouse development at the gastrulation stage. *Dev. Dyn.* 219(4):560–574. [https://doi.org/10.1002/1097-0177\(2000\)9999:9999<:AID-DVDY1079>3.0.CO;2-Y](https://doi.org/10.1002/1097-0177(2000)9999:9999<:AID-DVDY1079>3.0.CO;2-Y)
- Montague, T.G., J.M. Cruz, J.A. Gagnon, G.M. Church, and E. Valen. 2014. CHOPCHOP: a CRISPR/Cas9 and TALEN web tool for genome editing. *Nucleic Acids Res.* 42(W1):W401–7. <https://doi.org/10.1093/nar/gku410>
- Montanez, E., S. Ussar, M. Schifferer, M. Bösl, R. Zent, M. Moser, and R. Fässler. 2008. Kindlin-2 controls bidirectional signaling of integrins. *Genes Dev.* 22:1325–1330. <https://doi.org/10.1101/gad.469408>
- Moorhead, G.B., V. De Wever, G. Templeton, and D. Kerk. 2009. Evolution of protein phosphatases in plants and animals. *Biochem. J.* 417:401–409. <https://doi.org/10.1042/BJ20081986>
- Morse, E.M., N.N. Brahme, and D.A. Calderwood. 2014. Integrin cytoplasmic tail interactions. *Biochemistry.* 53:810–820. <https://doi.org/10.1021/bi401596q>
- Moser, M., K.R. Legate, R. Zent, and R. Fässler. 2009. The tail of integrins, talin, and kindlins. *Science.* 324:895–899. <https://doi.org/10.1126/science.1163865>
- Muenzner, P., V. Bachmann, W. Zimmermann, J. Hentschel, and C.R. Hauck. 2010. Human-restricted bacterial pathogens block shedding of epithelial cells by stimulating integrin activation. *Science.* 329:1197–1201. <https://doi.org/10.1126/science.1190892>
- Nieswandt, B., D. Varga-Szabó, and M. Elvers. 2009. Integrins in platelet activation. *J. Thromb. Haemost.* 7(Suppl 1):206–209. <https://doi.org/10.1111/j.1538-7836.2009.03370.x>
- Nilsson, S., D. Kaniowska, C. Brakebusch, R. Fässler, and S. Johansson. 2006. Threonine 788 in integrin subunit beta1 regulates integrin activation. *Exp. Cell Res.* 312:844–853. <https://doi.org/10.1016/j.yexcr.2005.12.001>
- O'Toole, T.E., J. Ylänne, and B.M. Cullley. 1995. Regulation of integrin affinity states through an NPXY motif in the beta subunit cytoplasmic domain. *J. Biol. Chem.* 270:8553–8558. <https://doi.org/10.1074/jbc.270.15.8553>
- Oxley, C.L., N.J. Anthis, E.D. Lowe, I. Vakonakis, I.D. Campbell, and K.L. Wegener. 2008. An integrin phosphorylation switch: the effect of β 3 integrin tail phosphorylation on Dok1 and talin binding. *J. Biol. Chem.* 283:5420–5426. <https://doi.org/10.1074/jbc.M709435200>
- Parrini, M.C., J. Camonis, M. Matsuda, and J. de Gunzburg. 2009. Dissecting activation of the PAK1 kinase at protrusions in living cells. *J. Biol. Chem.* 284:24133–24143. <https://doi.org/10.1074/jbc.M109.015271>
- Pfaff, M., S. Liu, D.J. Erle, and M.H. Ginsberg. 1998. Integrin beta cytoplasmic domains differentially bind to cytoskeletal proteins. *J. Biol. Chem.* 273: 6104–6109. <https://doi.org/10.1074/jbc.273.11.6104>
- Rantala, J.K., J. Pouwels, T. Pellinen, S. Veltel, P. Laasola, E. Mattila, C.S. Potter, T. Duffy, J.P. Sundberg, O. Kallioniemi, et al. 2011. SHARPIN is an endogenous inhibitor of β 1-integrin activation. *Nat. Cell Biol.* 13: 1315–1324. <https://doi.org/10.1038/ncb2340>
- Rehberg, K., S. Kliche, D.A. Madencioglu, M. Thiere, B. Müller, B.M. Meineke, C. Freund, E. Budinger, and O. Stork. 2014. The serine/threonine kinase Ndr2 controls integrin trafficking and integrin-dependent neurite growth. *J. Neurosci.* 34:5342–5354. <https://doi.org/10.1523/JNEUROSCI.2728-13.2014>

- Schiller, H.B., C.C. Friedel, C. Boulegue, and R. Fässler. 2011. Quantitative proteomics of the integrin adhesome show a myosin II-dependent recruitment of LIM domain proteins. *EMBO Rep.* 12:259–266. <https://doi.org/10.1038/embor.2011.5>
- Schmitter, T., F. Agerer, L. Peterson, P. Munzner, and C.R. Hauck. 2004. Granulocyte CEACAM3 is a phagocytic receptor of the innate immune system that mediates recognition and elimination of human-specific pathogens. *J. Exp. Med.* 199:35–46. <https://doi.org/10.1084/jem.20030204>
- Schmitter, T., S. Pils, V. Sakk, R. Frank, K.D. Fischer, and C.R. Hauck. 2007. The granulocyte receptor CEACAM3 directly associates with Vav to promote phagocytosis of human pathogens. *J. Immunol.* 178:3797–3805. <https://doi.org/10.4049/jimmunol.178.6.3797>
- Sekine, K., T. Kawauchi, K. Kubo, T. Honda, J. Herz, M. Hattori, T. Kinashi, and K. Nakajima. 2012. Reelin controls neuronal positioning by promoting cell-matrix adhesion via inside-out activation of integrin $\alpha 5 \beta 1$. *Neuron* 76:353–369. <https://doi.org/10.1016/j.neuron.2012.07.020>
- Shattil, S.J., C. Kim, and M.H. Ginsberg. 2010. The final steps of integrin activation: the end game. *Nat. Rev. Mol. Cell Biol.* 11:288–300. <https://doi.org/10.1038/nrm2871>
- Shen, Y., P. Lyons, M. Cooley, D. Davidson, A. Veillette, R. Salgia, J.D. Griffin, and M.D. Schaller. 2000. The noncatalytic domain of protein-tyrosine phosphatase-PEST targets paxillin for dephosphorylation in vivo. *J. Biol. Chem.* 275:1405–1413. <https://doi.org/10.1074/jbc.275.2.1405>
- Sims, P.J., M.H. Ginsberg, E.F. Plow, and S.J. Shattil. 1991. Effect of platelet activation on the conformation of the plasma membrane glycoprotein IIb-IIIa complex. *J. Biol. Chem.* 266:7345–7352.
- Stephens, L.E., A.E. Sutherland, I.V. Klimanskaya, A. Andrieux, J. Meneses, R.A. Pedersen, and C.H. Damsky. 1995. Deletion of beta 1 integrins in mice results in inner cell mass failure and peri-implantation lethality. *Genes Dev.* 9(15):1883–1895. <https://doi.org/10.1101/gad.9.15.1883>
- Stern, A., E. Privman, M. Rasis, S. Lavi, and T. Pupko. 2007. Evolution of the metazoan protein phosphatase 2C superfamily. *J. Mol. Evol.* 64:61–70. <https://doi.org/10.1007/s00239-006-0033-y>
- Stewart, S.A., D.M. Dykxhoorn, D. Palliser, H. Mizuno, E.Y. Yu, D.S. An, D.M. Sabatini, I.S. Chen, W.C. Hahn, P.A. Sharp, et al. 2003. Lentivirus-delivered stable gene silencing by RNAi in primary cells. *RNA* 9: 493–501. <https://doi.org/10.1261/rna.2192803>
- Suzuki, K., and K. Takahashi. 2003. Reduced cell adhesion during mitosis by threonine phosphorylation of beta1 integrin. *J. Cell. Physiol.* 197:297–305. <https://doi.org/10.1002/jcp.10354>
- Tadokoro, S., S.J. Shattil, K. Eto, V. Tai, R.C. Liddington, J.M. de Pereda, M.H. Ginsberg, and D.A. Calderwood. 2003. Talin binding to integrin beta tails: a final common step in integrin activation. *Science* 302:103–106. <https://doi.org/10.1126/science.1086652>
- Takahashi, K. 2001. The linkage between beta1 integrin and the actin cytoskeleton is differentially regulated by tyrosine and serine/threonine phosphorylation of beta1 integrin in normal and cancerous human breast cells. *BMC Cell Biol.* 2:23. <https://doi.org/10.1186/1471-2121-2-23>
- Takala, H., E. Nurminen, S.M. Nurmi, M. Aatonen, T. Strandin, M. Takatalo, T. Kiema, C.G. Gahmberg, J. Ylännä, and S.C. Fagerholm. 2008. Beta2 integrin phosphorylation on Thr758 acts as a molecular switch to regulate 14-3-3 and filamin binding. *Blood* 112:1853–1862. <https://doi.org/10.1182/blood-2007-12-127795>
- Tan, K.M., S.L. Chan, K.O. Tan, and V.C. Yu. 2001. The *Caenorhabditis elegans* sex-determining protein FEM-2 and its human homologue, hFEM-2, are Ca²⁺/calmodulin-dependent protein kinase phosphatases that promote apoptosis. *J. Biol. Chem.* 276:44193–44202. <https://doi.org/10.1074/jbc.M105880200>
- Theodosiou, M., M. Widmaier, R.T. Böttcher, E. Rognoni, M. Veelders, M. Bharadwaj, A. Lambacher, K. Austen, D.J. Müller, R. Zent, and R. Fässler. 2016. Kindlin-2 cooperates with talin to activate integrins and induces cell spreading by directly binding paxillin. *eLife* 5:e10130. <https://doi.org/10.7554/eLife.10130>
- Uotila, L.M., F. Jahan, L. Soto Hinojosa, E. Melandri, M. Grönholm, and C.G. Gahmberg. 2014. Specific phosphorylations transmit signals from leukocyte $\beta 2$ to $\beta 1$ integrins and regulate adhesion. *J. Biol. Chem.* 289: 32230–32242. <https://doi.org/10.1074/jbc.M114.588111>
- Valmu, L., M. Autero, P. Siljander, M. Patarroyo, and C.G. Gahmberg. 1991. Phosphorylation of the beta-subunit of CD11/CD18 integrins by protein kinase C correlates with leukocyte adhesion. *Eur. J. Immunol.* 21: 2857–2862. <https://doi.org/10.1002/eji.1830211130>
- van Kooyk, Y., and C.G. Figdor. 2000. Avidity regulation of integrins: the driving force in leukocyte adhesion. *Curr. Opin. Cell Biol.* 12:542–547. [https://doi.org/10.1016/S0955-0674\(00\)00129-0](https://doi.org/10.1016/S0955-0674(00)00129-0)
- Vestweber, D. 2002. Regulation of endothelial cell contacts during leukocyte extravasation. *Curr. Opin. Cell Biol.* 14:587–593. [https://doi.org/10.1016/S0955-0674\(02\)00372-1](https://doi.org/10.1016/S0955-0674(02)00372-1)
- Vinogradova, O., A. Velyvis, A. Velyviene, B. Hu, T. Haas, E. Plow, and J. Qin. 2002. A structural mechanism of integrin alpha (IIb)beta (3) “inside-out” activation as regulated by its cytoplasmic face. *Cell* 110:587–597. [https://doi.org/10.1016/S0092-8674\(02\)00906-6](https://doi.org/10.1016/S0092-8674(02)00906-6)
- Waldt, N., A. Seifert, Y.E. Demiray, E. Devroe, B.E. Turk, P. Reichardt, C. Mix, A. Reinhold, C. Freund, A.J. Müller, et al. 2018. Filamin A Phosphorylation at Serine 2152 by the Serine/Threonine Kinase Ndr2 Controls TCR-Induced LFA-1 Activation in T Cells. *Front. Immunol.* 9:2852. <https://doi.org/10.3389/fimmu.2018.02852>
- Wegener, K.L., A.W. Partridge, J. Han, A.R. Pickford, R.C. Liddington, M.H. Ginsberg, and I.D. Campbell. 2007. Structural basis of integrin activation by talin. *Cell* 128:171–182. <https://doi.org/10.1016/j.cell.2006.10.048>
- Wennerberg, K., R. Fässler, B. Wärmegård, and S. Johansson. 1998. Mutational analysis of the potential phosphorylation sites in the cytoplasmic domain of integrin beta1A. Requirement for threonines 788–789 in receptor activation. *J. Cell Sci.* 111:1117–1126.
- Winograd-Katz, S.E., R. Fässler, B. Geiger, and K.R. Legate. 2014. The integrin adhesome: from genes and proteins to human disease. *Nat. Rev. Mol. Cell Biol.* 15:273–288. <https://doi.org/10.1038/nrm3769>
- Xie, Y., E.J. Tan, S. Wee, E. Manser, L. Lim, and C.G. Koh. 2008. Functional interactions between phosphatase POPX2 and mDia modulate RhoA pathways. *J. Cell Sci.* 121:514–521. <https://doi.org/10.1242/jcs.013557>
- Ye, F., G. Hu, D. Taylor, B. Ratnikov, A.A. Bobkov, M.A. McLean, S.G. Sligar, K.A. Taylor, and M.H. Ginsberg. 2010. Recreation of the terminal events in physiological integrin activation. *J. Cell Biol.* 188:157–173. <https://doi.org/10.1083/jcb.200908045>
- Ye, F., B.G. Petrich, P. Anekal, C.T. Lefort, A. Kasirer-Friede, S.J. Shattil, R. Ruppert, M. Moser, R. Fässler, and M.H. Ginsberg. 2013. The mechanism of kindlin-mediated activation of integrin $\alpha \text{IIb} \beta 3$. *Curr. Biol.* 23: 2288–2295. <https://doi.org/10.1016/j.cub.2013.09.050>
- Zaidel-Bar, R., and B. Geiger. 2010. The switchable integrin adhesome. *J. Cell Sci.* 123:1385–1388. <https://doi.org/10.1242/jcs.066183>
- Zaidel-Bar, R., S. Itzkovitz, A. Ma’ayan, R. Iyengar, and B. Geiger. 2007. Functional atlas of the integrin adhesome. *Nat. Cell Biol.* 9:858–867. <https://doi.org/10.1038/ncb0807-858>
- Zhang, S., T. Guo, H. Chan, S.K. Sze, and C-G. Koh. 2013. Integrative transcriptome and proteome study to identify the signaling network regulated by POPX2 phosphatase. *J. Proteome Res.* 12:2525–2536. <https://doi.org/10.1021/pr301113c>
- Zhang, Y., H. Zhao, J. Wang, J. Ge, Y. Li, J. Gu, P. Li, Y. Feng, and M. Yang. 2013. Structural insight into *Caenorhabditis elegans* sex-determining protein FEM-2. *J. Biol. Chem.* 288:22058–22066. <https://doi.org/10.1074/jbc.M113.464339>

Supplemental material

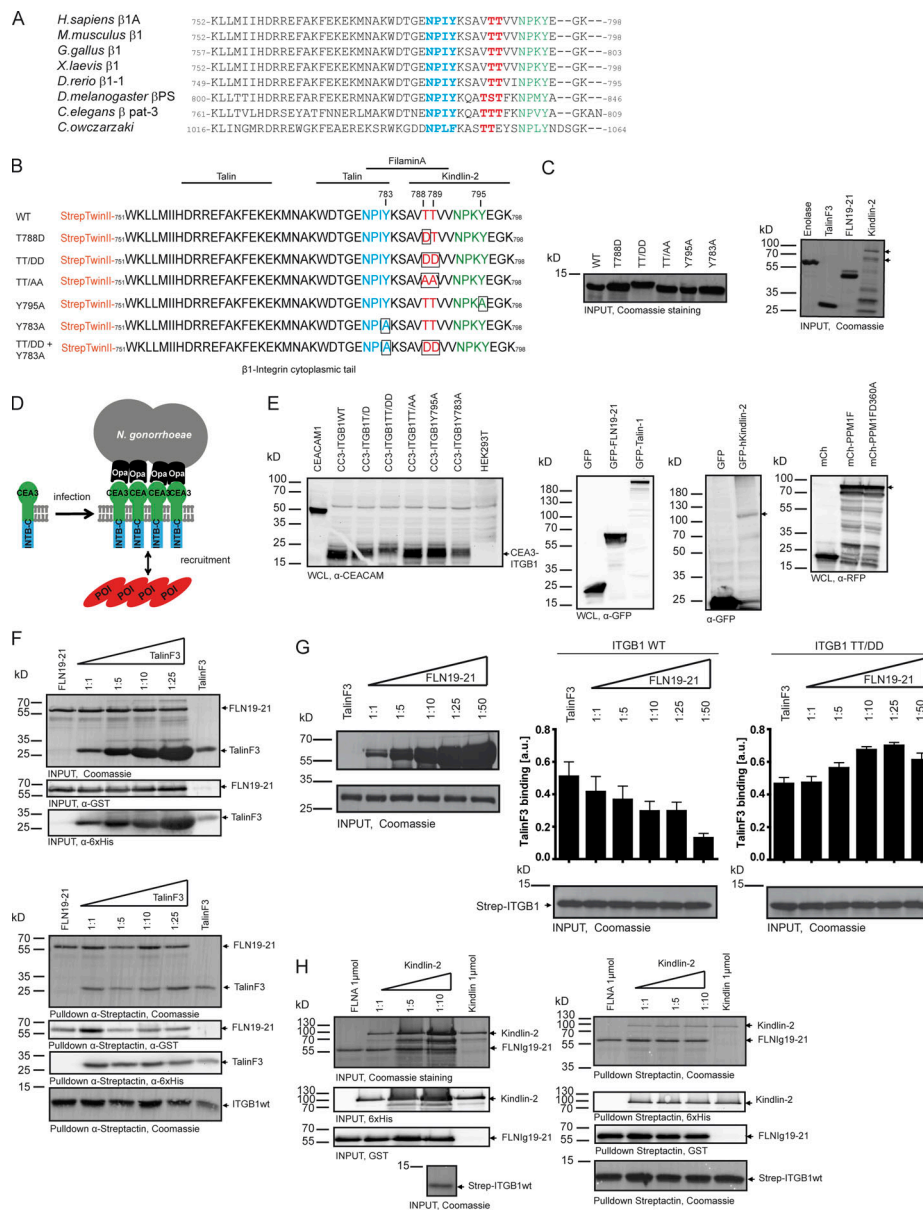


Figure S1. Related to Fig. 1, Fig. 2, Fig. 7, Fig. 8, and Fig. 9: The T788/T789 motif in the integrin β1 cytoplasmic tail is evolutionarily conserved, and its phosphorylation regulates association with filaminA and talin. (A) Alignment of cytoplasmic amino acid residues of integrin β subunits derived from different species. The conserved threonine residues (red), the proximal NPxY motif (blue), and the distal NPxY motif (green) are marked. (B) Alignment of amino acid residues of strep-tagged integrin β1 cytoplasmic tails with indicated binding sites of talin, filaminA, and kindlin-2. The threonine residues (red) and the proximal (blue) and distal (green) NPxY motifs are marked. Point mutations are marked by black boxes. (C) The indicated strep-tag-integrin β1 (Strep-ITGB1) cytoplasmic domains and His-tagged enolase, talinF3 domain, FLN19-21, or kindlin-2 were expressed as soluble proteins in BL21 DE3 bacteria and equal amounts detected by WB and Coomassie staining. (D) Schematic model of the OPTIC principle. OPTIC fusion constructs consist of integrin β1 cytoplasmic domains (ITGB-C) and the transmembrane and extracellular domain of CEACAM3 (CEA3). Receptor clustering is triggered by binding of Opa₅₂ protein expressing *Neisseria gonorrhoeae* (*N. gonorrhoeae*) to CEACAM3, thereby potentially recruiting an intracellular protein of interest (POI). (E) 293T cells were transiently transfected with the indicated expression constructs and WCL subjected to WB; CEACAM1 protein served as positive control for the CEACAM antibody, and nontransfected 293T cell lysate served as negative control. (F) GST-FLN19-21 and Strep-ITGB1 WT were incubated with increasing amounts of His-talinF3. Upper panels show the input proteins. Upon streptactin pulldown, proteins bound to ITGB1 WT were visualized by Coomassie staining (bottom part; top panel), WB with α-GST antibody to detect FLN19-21 (second panel), or with α-His to detect talinF3 (third panel). Coomassie staining also verified similar amounts of precipitated Strep-ITGB1 WT (lowest panel). (G) Strep-ITGB1 WT or the T788D/T789D variant was immobilized in triplicate wells and incubated with His-tagged talinF3 and increasing amounts of GST-FLN19-21 at 4°C. After washing, talinF3 binding was detected by incubation with α-6xHis antibody and secondary HRP-coupled antibody. Bars represent mean ± SEM of triplicates from a representative experiment. Coomassie staining verified similar amounts of input FLN19-21 (upper panel), talinF3 (middle panel), and Strep-ITGB1 WT and TT/DD (lowest panel). (H) GST-FLN19-21 and Strep-ITGB1 WT were incubated with increasing amounts of His-kindlin-2. Left panels show the input proteins. Upon streptactin pulldown, proteins bound to ITGB1 WT were visualized by Coomassie staining (right; top panel), WB with α-His to detect kindlin-2 (second panel), or α-GST antibody to detect FLN19-21 (third panel). Coomassie staining also verified similar amounts of precipitated Strep-ITGB1 WT (lowest panel). *C. owczarzi*, *Capsaspora owczarzi*; *D. melanogaster*, *Drosophila melanogaster*; *D. rerio*, *Danio rerio*; *G. gallus*, *Gallus gallus*; *H. sapiens*, *Homo sapiens*; *M. musculus*, *Mus musculus*; *X. laevis*, *Xenopus laevis*; mCh, mCherry.

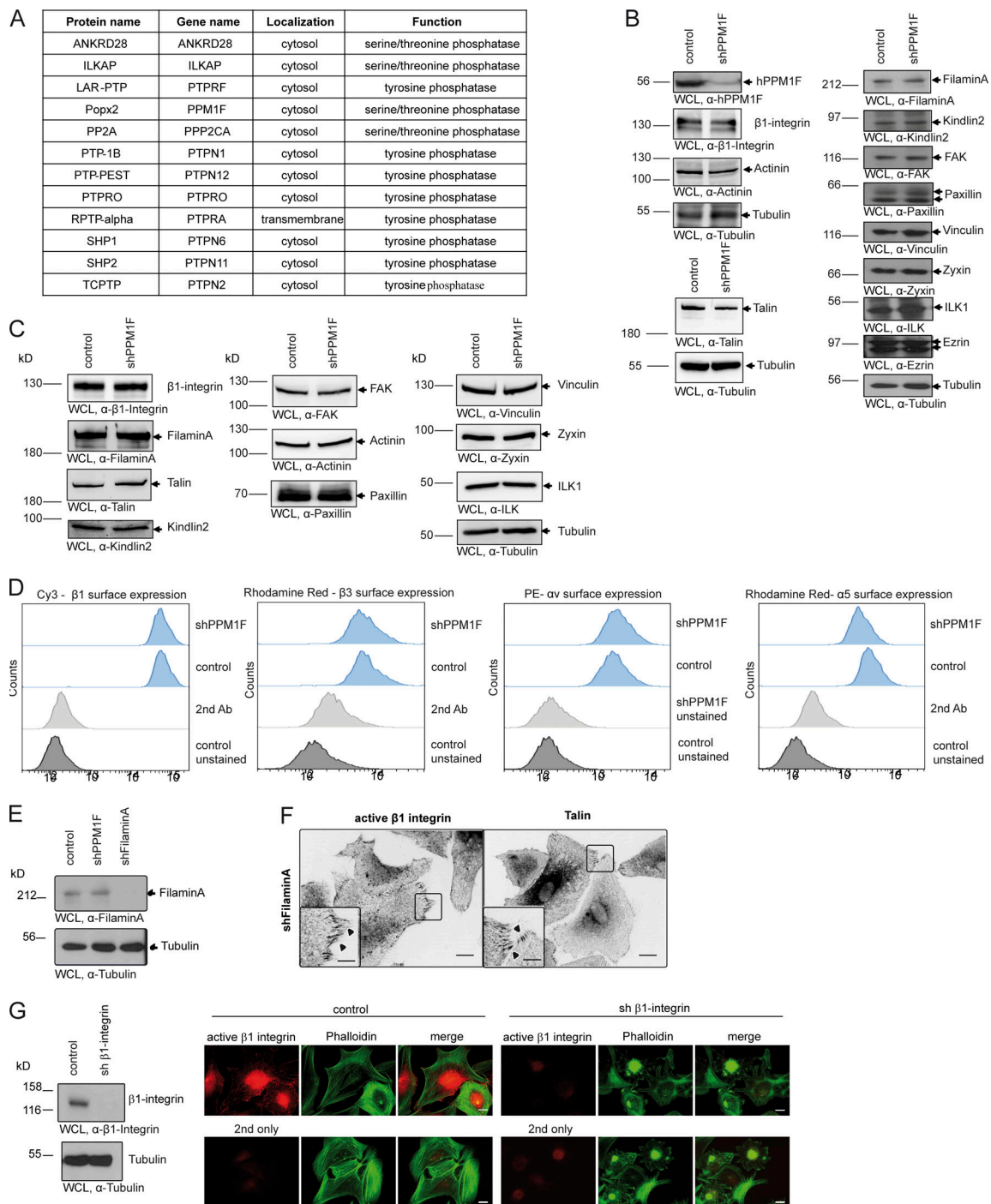


Figure S2. **Related to Fig. 3: knock-down of PPM1F in 293T cells or NHDFs does not alter expression of core focal adhesion proteins and does not affect integrin surface levels.** (A) Overview of protein phosphatases present in the human integrin adhesome (Zaidel-Bar et al., 2007). These enzymes have been targeted individually by specific shRNA-encoding lentiviral particles. Control cells were treated with lentiviral particles lacking shRNA. (B) Immunoblotting of WCL from PPM1F knock-down (shPPM1F) and control 293T cells probed with antibodies against the indicated focal adhesion proteins. Monoclonal α -tubulin antibody was used as loading control. (C) Immunoblotting of WCLs from control and PPM1F knock-down (shPPM1F) NHDF probed with antibodies against core focal adhesion proteins. Probing with monoclonal α -tubulin antibody confirmed equal loading of WCLs. (D) Integrin surface expression levels of control and shPPM1F NHDF were analyzed by flow cytometry. Cells were stained with the indicated monoclonal integrin-specific antibodies. As a comparison, cells were stained the fluorescent labeled second antibody only (second Ab), or remained unstained; count $\geq 10,000$ cells. (E) FilaminA was depleted in NHDF with a shRNA encoding lentivirus. WCLs were analyzed by WB with α -filaminA (upper panel) and α -tubulin (lower panel) antibodies. (F) FilaminA-depleted NHDFs were seeded for 1.5 h onto $1 \mu\text{g/ml}$ FN_{III9-11}-coated coverslips. After fixation, cells were stained with indicated antibodies and analyzed by confocal microscopy; scale bar, $20 \mu\text{m}$. Insets: Higher magnification of boxed areas; arrowheads point to enrichment of active integrin $\beta 1$ and filaminA; scale bar, $10 \mu\text{m}$. (G) Integrin $\beta 1$ was depleted in NHDF with a shRNA encoding lentivirus. WCLs were analyzed by WB with α -integrin $\beta 1$ (upper panel) and α -tubulin (lower panel) antibodies. Control and integrin $\beta 1$ -depleted NHDF were seeded for 1.5 h onto $1 \mu\text{g/ml}$ FN_{III9-11}-coated coverslips. After fixation, cells were stained with a monoclonal antibody against active integrin $\beta 1$ (9EG7) and phalloidin. Additional samples were stained with the second antibody only; scale bar, $20 \mu\text{m}$.

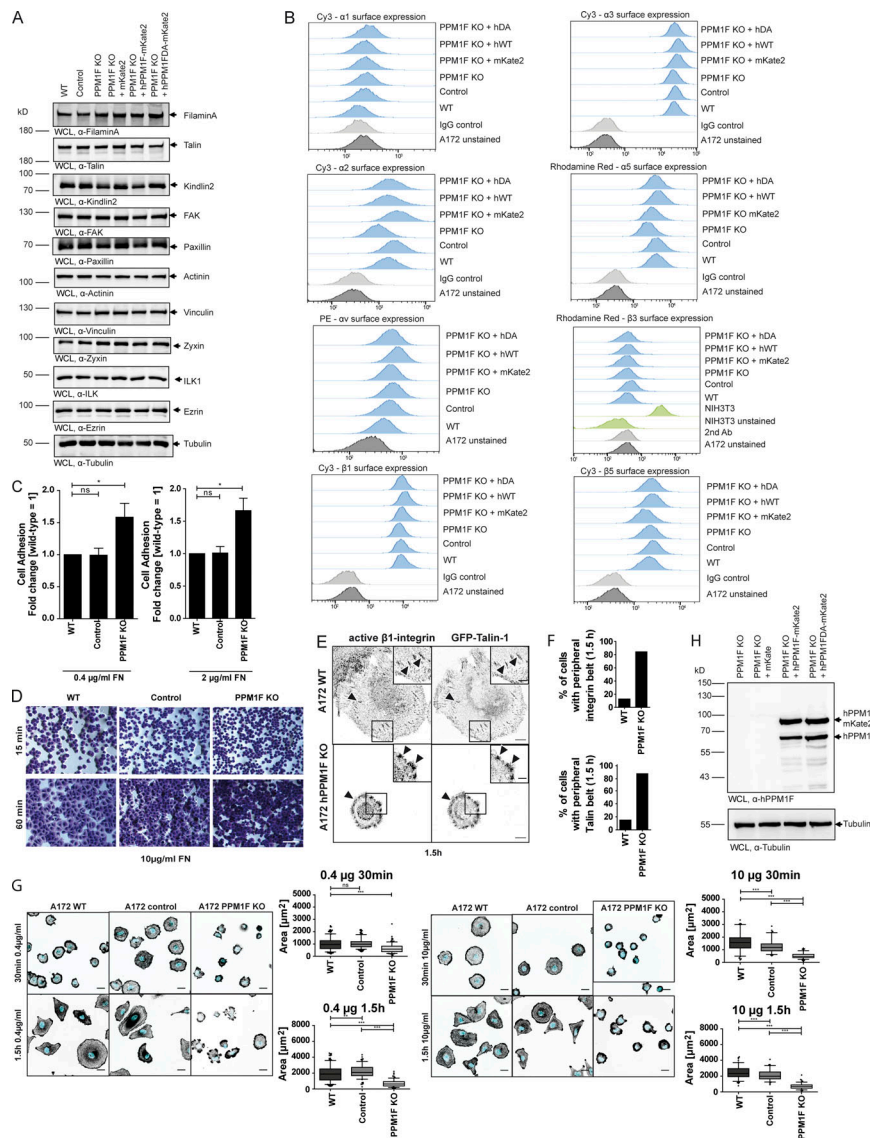


Figure S3. Related to Fig. 4: PPM1F KO in A172 cells does not increase integrin surface levels or alter expression of core focal adhesion proteins, but strongly affects integrin-dependent processes. (A) A172 cells expressing Cerulean (WT) were treated with sgRNA against Cerulean combined with Cas9 or with sgRNAs against Cerulean and PPM1F combined with Cas9. Clonal Cerulean-negative (Control) and clonal Cerulean/PPM1F-negative cell lines (hPPM1F KO) were derived. The hPPM1F KO cells were stably transduced with mKate2 encoding lentivirus (hPPM1F KO plus mKate2), or lentivirus encoding hPPM1F WT (PPM1F KO plus hPPM1F-mKate2), or lentivirus encoding PPM1F D360A (PPM1F KO plus hPPM1F DA-mKate2). WCL from the different cell lines were analyzed by WB with antibodies against indicated core focal adhesion proteins. Monoclonal α -tubulin antibody was used as loading control. (B) A172 cell lines as in A were analyzed by flow cytometry for surface expression levels of indicated integrins by staining with integrin-specific antibodies. IgG control: WT cells receiving an isotype-matched control antibody. In the case of integrin β 3, NIH3T3 cells served as positive controls. Count $\geq 10,000$ cells. WT, hPPM1F-mKate2; DA, hPPM1F D360A-mKate2. (C) A172 WT, control, or hPPM1F KO cells were seeded onto 0.4 or 2 μ g/ml FN₁₁₉₋₁₂ for 30 min in triplicate. Cells were washed, fixed, and stained with crystal violet. Crystal violet staining was quantified and normalized to A172 WT cells. Bars represent mean \pm SEM from three independent experiments. Significance was calculated using one-way ANOVA, followed by Bonferroni post hoc test (*, $P < 0.05$). For cell adhesion on 10 μ g/ml FN, see Fig. 2 H. (D) A172 WT, control, or PPM1F KO cells were seeded onto 10 μ g/ml FN for 15 and 60 min and processed as in C. Representative pictures of crystal violet-stained wells; scale bar, 150 μ m. (E) A172 WT or hPPM1F KO cells were transiently transfected with GFP-talin-1 before seeding onto 2 μ g/ml FN₁₁₉₋₁₁ for 1.5 h. Fixed cells were stained with antibodies against active integrin β 1 (9EG7) and analyzed by confocal microscopy. Scale bars, 10 μ m. Arrowheads point to clusters of active integrin β 1/talin. Insets: Higher magnification of boxed area; scale bar, 5 μ m. (F) Quantification of cells from E showing a peripheral active integrin belt (upper graph) or peripheral talin-1 clustering (lower graph). Data are shown in percentages of all cells analyzed by confocal microscopy; $n \geq 30$ derived from two or more independent experiments. (G) A172 WT, control, or PPM1F KO cells were seeded onto 0.4 μ g/ml FN₁₁₉₋₁₂-coated coverslips (left side) or onto 10 μ g/ml FN₁₁₉₋₁₁-coated coverslips (right side) for 30 min (upper panels) or 1.5 h (lower panels) before fixation and staining with DAPI and phalloidin. Cells were analyzed by confocal microscopy. Representative pictures are shown; scale bar, 25 μ m. Quantification of cell areas was done in ImageJ using a custom plugin. Cells not recognized by the plugin were manually analyzed with Leica LAS AF Lite software; $n \geq 100$ cells from two or more independent experiments; box plots depict means with 95% CIs (whiskers) and outliers (dots). Significance was determined using one-way ANOVA with post hoc Bonferroni test (**, $P < 0.01$; ***, $P < 0.001$). (H) A172 hPPM1F KO and derived reconstituted cell lines were lysed and subjected to WB with α -PPM1F (upper panel) and α -tubulin (lower panel) antibodies to test for PPM1F expression levels. The two bands correspond to the hPPM1F-mKate2 fusion protein and the hPPM1F protein, which results from proteolytic separation of the mKate tag. FN, FN₁₁₉₋₁₁.

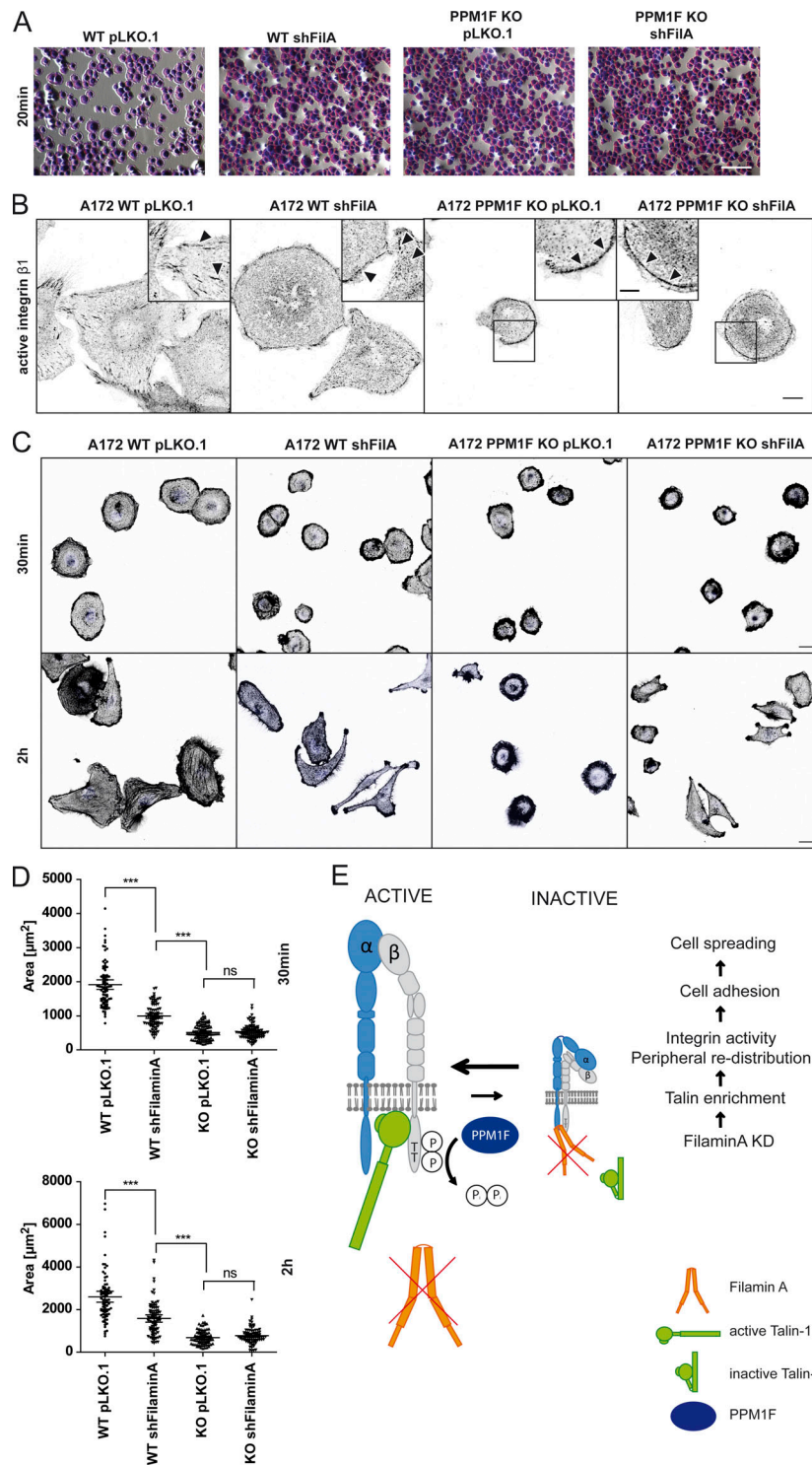


Figure S4. **Related to Fig. 4: filaminA knock-down in A172 cells phenocopies integrin-dependent effects of PPM1F depleted cells.** (A) Cell adhesion assays were performed with indicated A172 cell lines using 10 $\mu\text{g}/\text{ml}$ FN_{III9-11}. Shown are representative pictures of crystal violet stained wells after 20 min adhesion; scale bar, 150 μm . (B) Indicated cell lines were seeded onto 5 $\mu\text{g}/\text{ml}$ FN_{III9-11} for 2 h, fixed, and stained against active integrin $\beta 1$ before analysis by confocal microscopy; scale bar, 10 μm . Insets show higher magnification of boxed areas. Arrowheads point to active integrin $\beta 1$, which accumulates at the cell periphery in PPM1F KO and filaminA knock-down cells; scale bar, 5 μm . (C and D) Indicated cell lines were seeded onto 10 $\mu\text{g}/\text{ml}$ FN_{III9-11} for 30 min or 2 h, fixed, and stained with DAPI and phalloidin-Cy5. Samples were imaged using confocal microscopy. (C) Representative images from cells at indicated time points; scale bar, 25 μm . Cell spreading was quantified in D. Bars show mean with 95% CIs from two independent experiments; $n \geq 80$ cells. Statistics was performed using one-way ANOVA, followed by Bonferroni post hoc test (***, $P < 0.001$). (E) Model summarizing effects of filaminA knock-down on integrin activity. In filaminA knock-down cells, the balance between active and inactive integrins is shifted toward the active conformation. Talin-integrin association is increased due to the lack of the counterregulator filaminA, thereby promoting cell adhesion, reducing cell spreading and phenocopying effects of PPM1F KO cells. FilaminA KD, filaminA knock-down; P, phospho-; shFilA, short-hairpin RNA targeting filaminA; T, threonine.

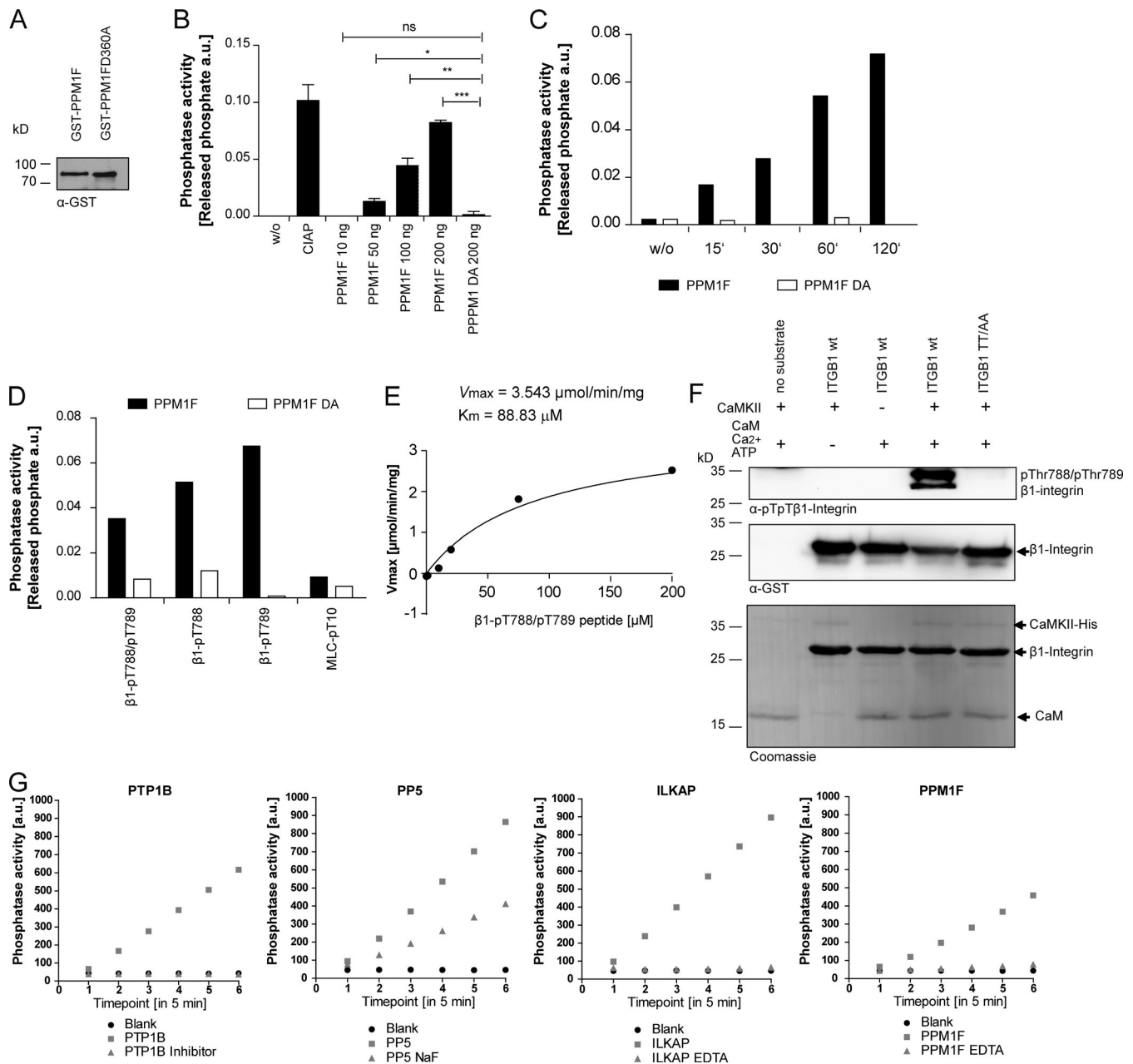


Figure S5. **Related to Fig. 6: PPM1F purified from 293T cells dephosphorylates the conserved T788/T789 motif in the integrin β 1 cytoplasmic domain.** (A) GST-tagged PPM1F or PPM1FD360A was expressed in 293 cells and affinity-purified from lysates with glutathione-coupled beads. Equal amounts of beads were subjected to WB analysis using α -GST antibody. (B) The integrin β 1 derived synthetic peptide β 1-pT788/pT789 was incubated with increasing amounts of cell-purified GST-PPM1F, with 200 ng GST-PPM1F D360A (PPM1F DA), or 100 ng calf intestine alkaline phosphatase (CIAP) for 1 h at 30°C. Released phosphate was detected by malachite green solution. Background values (buffer plus malachite green) were subtracted; w/o, peptide without phosphatase. Shown are mean \pm SD of three independent experiments; unpaired *t* test, *, *P* < 0.05; **, *P* < 0.01; ***, *P* < 0.001. (C) β 1-pT788/pT789 was incubated with 100 ng of cell-purified GST-PPM1F or GST-PPM1F DA for indicated time periods at 30°C. Released phosphate was detected as in B. (D) 50 ng PPM1F or PPM1F DA were incubated with the indicated phospho-peptides for 60 min and released phosphate measured as in B. (E) Dephosphorylation of increasing β 1-pT788/pT789 peptide concentrations by 150 ng cell-purified PPM1F was analyzed after 60 min incubation at 30°C as in B. The indicated curve was obtained by direct fit of the data to the Michaelis–Menten equation, and V_{max} and K_m values were determined. (F) 120 ng His-tagged CaMKII β was incubated with recombinant GST-tagged WT β 1 integrin cytoplasmic domain, the nonphosphorylatable integrin β 1 TT/AA mutant, or without any substrate. As indicated, samples received calmodulin (CaM), Ca²⁺, and ATP. After 60 min, reactions were stopped via addition of SDS sample buffer and subjected to WB using the indicated antibodies. Samples without kinase or ATP/Ca²⁺/calmodulin served as additional controls. (G) 200 ng of the indicated recombinant phosphatases were employed in enzyme assays using the fluorogenic substrate 4-MUP. The increase in fluorescence of 4-MU was recorded over 30 min for each enzyme (green squares), while samples without phosphatase (black dots) or including the phosphatase together with a phosphatase inhibitor (orange triangles) served as controls. Depicted is a representative experiment.